**The Dissertation Committee for Ye Hu Certifies that this is the approved version of the following dissertation:**

# MESOPOROUS SILICA CHIPS FOR HARVESTING THE LOW MOLECULAR WEIGHT PROTEOME FROM HUMAN SERUM

**Committee:**

Mauro Ferrari, Supervisor

Xuewu Liu

David G. Gorenstein

Xiaojing John Zhang

Pengyu Ren

# MESOPOROUS SILICA CHIPS FOR HARVESTING THE LOW MOLECULAR WEIGHT PROTEOME FROM HUMAN SERUM

**by**

Ye Hu, B.S., M.A.

**Dissertation**

Presented to the Faculty of the Graduate School of

The University of Texas at Austin

in Partial Fulfillment

of the Requirements

for the Degree of

**Doctor of Philosophy**

**The University of Texas at Austin**

**December, 2009**

# Dedication

This thesis is dedicated to my wife Jinghua Kuang, my parents Yushan Hu, Xiaohua Sun and my children Abigail C. Hu and Logan E. Hu, for their love and support.

## Acknowledgements

The printed pages of this dissertation reflect the relationships with many generous and inspiring people I have met since beginning my graduate work. I could never have reached the heights or explored the depths without their help, support, guidance and efforts. My sincere gratitude goes to all of them.

First and foremost, I wish to thank Dr. Mauro Ferrari, my doctoral advisor. His infectious enthusiasm, unlimited passion, constant trust and inspiration have been major driving forces through my graduate career at the University of Texas at Austin. My graduate studies would not have been the same without the social and academic challenges and diversions provided by Dr. Ferrari. He is one of the rare advisors that students dream that they will find. I also thank Dr. Xuewu Liu. As my secondary advisor, Dr. Liu offered his intelligent, insightful and generous support throughout this research effort, which enabled me to finish this thesis. In that same vein, I want to thank my doctoral committee Dr. David G. Gorenstein, Dr. John Zhang and Dr. Pengyu Ren for their encouraging words, thoughtful comments, and time and attention during busy semester. This dissertation would not have been possible without their expert guidance.

My thanks go out to my Proteomic team members: Dr. Ennio Tasciotti, Dr. Ali Bouamrani and Li Li, whom I work with on a daily basis. They are all talented individuals who jointly put together high-quality research products. I enjoyed working with them and look forward to more co operations.

I wish to thank my friends and colleagues in Austin who also work in Dr. Ferrari's group: Dr. Dan Fine, Ciro Chiappini, Zongxing Wang, Jean Raymond Fakhoury, Jeff Schmulen, Donald Erm, Haiyu Huang, and Kevin Lin. These people built for me an invaluable network of support and friendship, without which I could not have survived the process.

I am also grateful to all my teachers and professors. Without them, I can never get to where I am right now. They've built the ladder for my academic advancement.

Ultimately, of course, it all comes down to family, and here I have been blessed with good fortune beyond the normal measure. My parents, Xiaohua Sun and Yushan Hu, have continually expressed both confidences in my abilities as well as a belief in the value of education for its own sake. Their endless supports and understanding over all these years have provided tremendous power and motivation for me. I would like to mention also my grandma Siqin Yu, who passed away in 2005. She has been an invisible presence during the composition of these pages. In addition, I thank my two young children, Abigail (age 4) and Logan (age 1), for being like angels and serving as a reminder that I have to work as efficiently as possible to complete this highest endeavor in my education. Last, but most importantly, I have had the unflagging devotion of a wonderful wife. Jinghua Kuang has been with me through it all, with patience and love. There is no way to express how much this has meant to me every day. This PhD belongs to my family.

# MESOPOROUS SILICA CHIPS FOR HARVESTING THE LOW MOLECULAR WEIGHT PROTEOME FROM HUMAN SERUM

Publication No._____

Ye Hu, Ph.D.

The University of Texas at Austin, 2009

Supervisor: Mauro Ferrari

Abstract

In this dissertation, mesoporous silica thin films with tunable features at the nanoscale were fabricated using the triblock copolymer template pathway, with the aim of specifically harvesting the low molecular weight peptides and proteins from human serum, which has been regarded as a potential source of diagnostic biomarkers for the early detection of disease. The superior properties of mesoporous silica have been demonstrated in applications which include chemical sensing, filtration, catalysis, drug-delivery and selective biomolecular uptake. These properties depend on the architectural, physical and chemical properties of the materials, which in turn are determined by the processing parameters in evaporation-induced self-assembly (EISA). Using the different polymer templates and polymer concentration in the precursor solution, various pore size

distributions, pore structures and surface hydrophilicities were obtained and applied for nanotexture-selective recovery of low mass proteins. With the assistance of mass spectrometry and statistic analysis, we demonstrated the correlation between the nanophase characteristics of the mesoporous silica thin film and the specificity and efficacy of low mass proteome harvesting. In addition, to overcome the limitations of the pre-functionalization method in polymer selection, plasma ashing was used for the first time for the treatment of the mesoporous silica surface prior to chemical modification. Opposite surface charges due to the different functional groups used, resulted in a distinctive selectivity of the low molecular weight proteins from the serum sample. The mesoporous silica chips operate with extraordinary rapidity, high reproducibility, no sample pre-processing, and substantial independence from sample acquisition and storage temperature.In conclusion our study demonstrates that the ability to tune the physico-chemical properties of mesoporous silica surfaces has the potential to promote the use of this material as a tool for the selective separation and concentration of the low molecular weight proteome from complex biological fluids.

# Table of Contents

# List of Tables

# List of Figures

# CHAPTER 1

# NANOTECHNOLOGY AND EARLY DIAGNOSTICS

## 1.1 Overview

Many diseases, including cancer, originate from mutations and alterations to normal cellular regulatory and metabolic pathways at a molecular level. [1, 2] Accurate and sensitive diagnosis (e.g. early diagnostics) has been constrained by the lack of biosensors and molecular probes capable of rapidly recognizing the distinct molecular features of these diseases. Nanomaterials are defined as materials comprised of basic components which have at least one dimension in the nanoscale (less than 100 nm.) They have had an impact on the field of biomedical research even before the term nanomedicine was coined. [3] The ability of nanomaterials and nanopatterned devices to directly interact with biologically significant molecules and to convert those interactions into transduced or significantly amplified electrical or electromagnetic signals has ushered in a new generation of early stage diagnostic techniques.

The interface between nanosystems and biosystems is emerging as one of the broadest and most dynamic areas of science and technology, bringing together biology, chemistry, physics and many areas of engineering, biotechnology and medicine. The combination of these diverse areas of research promises to yield revolutionary advances in healthcare, medicine and the life sciences through, for example, the creation of powerful tools that enable direct, sensitive and rapid analysis of biological and chemical species for the diagnosis and treatment of diseases. The greater the detail with which the

molecular components of a specific disease can be determined, the more specifically the therapeutic regimen can be tailored to the individual. [4] These nanoscale structures represent powerful diagnostic tools as they can be surface functionalized with a range of specific targeting agents or amplification modalities and then systemically circulated to locate and monitor specific biological components. The development of microfluidics and "lab on a chip" systems with specifically designed nanoscale features allows for the combination of multiple complex diagnostic procedures into one simple device for point-of-care diagnosis. Many products have emerged for laboratory clinical and diagnostic uses including separation technologies for blood into its components, the fractionation of complex biofluidic mixtures into, e.g., its protein and nucleic acid digest sub-populations, DNA amplification strategies via PCR-on-chip, precise fluidic dispensation technologies for automated high-throughput analyses, multiplexed analyte sensors for point-of-care diagnostics, and many more. Despite the enormous potential of nanotechnology as it relates to diagnosis, many important concerns must still be addressed including the toxicological effects of the *in vivo* use of the relevant nanomaterials, the identification of appropriate target molecules and biomarkers to be screened for, the proper protocols for sample preparation, and the complete interpretation of diagnostic results obtained from both animal models and human trials. The ability to address these concerns will ultimately determine how extensively nanotechnology driven diagnostic techniques can percolate into the clinic.

Presently, conventional radiological diagnostic techniques focus on detecting the physical manifestations of disease. Given the high correlation between survival rate and

early detection [5], it is highly advantageous to identify abnormal cellular function before significant physiological modifications become apparent. Mammography is the process of using low energy x-rays to examine the human breast for characteristics masses or microcalcifications. It is a widely used technique because its relatively low cost and operational simplicity allow for population-wide screening. Regular mammographic screening can detect between 80 and 90% of breast cancers in asymptotic individuals, resulting in reduced breast cancer mortality. [4] However, for women with dense breasts the sensitivity of mammography is low (45.8%-55%). [6] Furthermore, successful screening and diagnosis rely too heavily on the skill and experience of the radiological practitioner. Finally, this imaging-based technology requires a critical mass of localized accumulated tumor cells for effective neoplasm identification and is therefore not capable of detecting tumors with masses or densities below this critical dimension. The diagnosis of breast cancer can be also accomplished by directly analyzing tumor cells through techniques such as the cytomorphology of exfoliated cells. [7] However, due to the subjective nature of tumor cell identification and the labor-intensiveness of the process, direct visualization of tumor cells does not lend itself to regular population-wide screening of asymptomatic women. Several studies have recognized that diagnostic biomarkers isolated from blood, such as circulating proteins and nucleic acids, may offer the greatest potential for the earliest and most reliable screening of diseases. [8-10] Without the assistant of nanomaterials and nanotechnologies, the identification and screening of potential biomarkers is unlikely to overcome the inherent requirements of high throughput and sensitivity. For example, the breakthrough in utilizing inorganic

nanoparticles for contrast enhancement in imaging biomarkers provides a robust framework for biomedical application. [11-15] The marriage of biology and micro-/nanofabrication has revolutionized biosensing by allowing for the integration of biological recognition elements into devices that will significantly impact the commercial availability of detection and diagnostic technologies at the genome, proteome and metabolome levels. This should dramatically decrease the time between disease onset and the initiation of tailored medical intervention and thus greatly increase the likelihood of a positive clinical outcome.

In this chapter we will discuss disease diagnosis by means of molecular recognition, genomic analysis, and proteomic analysis. Several of the most promising and advanced nanotechnologies relevant to achieving the goal of the earliest possible detection of abnormal cellular function will be summarized. First we will give an introduction about the study in this dissertation: using mesoporous silica chips for rapid proteomic and genomic screening of blood and plasma, as compared to conventional proteomic technologies. Next we will briefly cover some other nanopatterned devices and nanomaterials used in diagnostics, including nanowire biosensors, micro- and nanocantilevers, single electron transistors, the DNA-based nanobarcodes, quantum dots, and gold nanoparticles. We will also discuss magnetic nanoparticles, predominantly as contrast agents for magnetic resonance imaging.

## 1.2 Molecular Recognition in Diagnostics

### 1.2.1 Origin of Biomarkers

Understanding how a normal cell transforms into a diseased cell is crucial for developing diagnostic technologies. A large component in the regulation of normal cellular function occurs through the interaction of extracellular components with receptors on the cell membrane surface which trigger specific signaling pathways within the cell. Both the cell surface receptors and the subsequently triggered signaling pathways are composed of specific evolutionarily designed molecules. These cellular structures and signaling pathways also allow the cell to respond to changes in its external physiological environment. The molecular processes in one pathway then trigger other pathways in precise sequence. These propagated signals may cause a change in cell behavior or in gene expression, resulting in a response at the cellular or molecular level. Understanding how these specific pathways malfunction can provide scientists, pharmacists, and clinicians with possible molecular targets that can be used to generate new diagnostic strategies. In the case of tumor progression, Hanahan and Weinberg have defined six important subcellular regulatory systems whose malfunctioning is required for most cancers (See Figure 1). These malfunctions include the acquisition of self-sufficiency in growth signals, insensitivity to anti-growth signals, limitless replication, evading apoptosis, sustained angiogenesis, and tissue invasion and metastasis. [16] Cancer represents a class of diseases containing over 100 subtypes whose distinguishing characteristics are related to the tissue of origin and the type and nature of the malfunction of specific molecular pathways. Molecular diagnostics is based on the

detection of abnormal nucleic acids sequences, proteins, and other biomolecules derived from biological fluids (serum, urine, saliva, cerebrospinal fluid), which comprise the machinery, or in some cases the by-products, of these regulatory signaling pathways and can therefore be indicative of diseased states. [17]

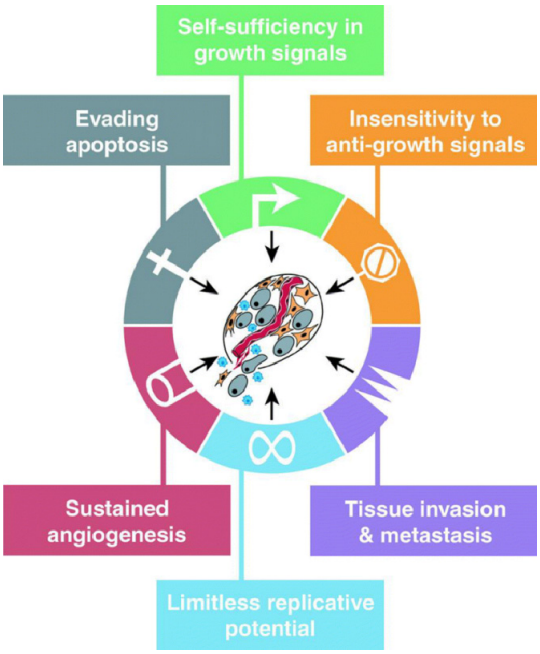


Figure 1.1: The six hallmarkers of cancer. It was suggested that most if not all cancers have acquired the same set of functional capabilities during their development, albeit through various mechanistic strategies. (Reprinted, with permission from Ref. [16] Copyright 2000 Cell.)

### 1.2.2 Genomics and Proteomics in Disease Diagnosis

As we introduced above, cancer is a diverse disease. Current diagnostics modalities have obvious limitations to provide an accurate prediction based on the

varying situation between individual patients, even when they are at the same clinical stage. Therefore, the next level of molecular diagnostics is needed: diagnostics that are focused on the personalization of medicine.

A gene is a segment of DNA that encodes for a specific protein, including the mechanisms for gene expression and protein synthesis. Therefore, human disease is thought to be largely genetic in etiology. Genomics is the study of the structure and function of genetic material in chromosomes and regulates the gene expression patterns to correlate with the classification and prediction of diseases. The spectacular success in sequencing the complete human genomes has dramatically advanced the possibility of realizing personalized medicine. With the development of gene chips, microarrays and bioinformatics, genomics has moved to a functional phase where gene expression can be determined by detecting gene-specific mRNA sequences. Fully understanding the molecular processes leading from health to disease, however, is considerably more involved than identifying active gene sequences. Increasingly, Attention has being focused on proteins and enzymes and their interactions which determine cellular architecture and function. [18-20]

For many diseases, such as cancer, protein function is altered in the context of key signaling pathways that regulate critical cellular functions including proliferation, apoptosis, differentiation, survival, immunity, metabolism, invasion and metastasis. Understanding which combinations of protein regulatory networks are dysfunctional, and which specific nodes in the cell circuitry are dysfunctional may be critical to the development of effective combinations of pharmacologic inhibitors. [21] Proteomics, in

contrast to genomics, refers to the systematic study of the total protein complement expressed by the genome of particular cells or tissues, both healthy and diseased. [22, 23] Proteomic studies to determine the structure and function of each protein and the complexities of protein-protein interactions will be important for developing accurate, effective, and timely diagnostic and therapeutic modalities. Currently, a number of techniques, including western blots [24], immunohistochemical analysis [25], enzyme-linked immunosorbent assays (ELISA) [26] and mass spectrometry [27], allow us to test for specific proteins and thus diagnose a particular disease. There is no doubt, however, that completely defining the human proteome is going to involve a very different set of challenges than the sequencing the human genome. As an example, it is essential to know the concentration of a particular protein and not just its presence in order to determine its functional activity. Therefore, the accurate quantification of low abundance proteins is one of the biggest challenges in the study of proteomics. Proteomic biomarkers are important tools for cancer detection and monitoring. They serve as hallmarks for the physiological status of a cell at a given time and change during the disease process. Fortunately with the aid of advanced protein-based nanotechnology methods capable of detecting zeptogram quantities, this problem can be overcome and will be of great use for specific and sensitive diagnosis. [28-30] By linking genomic or proteomic biomarkers and clinic-pathological parameters, scientists and physicians will be able to identify protein information for features of clinical relevance to individual cancer patients.

### 1.2.3 Low Molecular Weight Proteome in Human Serum

Discovering the novel specific biomarkers for early disease detection is the key to develop medicine to combat complex diseases such as cancer. The identification of circulating biomarkers holds great potential for non invasive approaches in early diagnosis and prognosis, as well as for the monitoring of therapeutic efficiency. [31, 32] Scientists presume upon the characterization of the thousands of individual serum proteins/peptides to enable the discovery of an increasing number of reliable disease biomarkers. Because of its high protein content (i.e. 60-80 mg/ml), human serum is expected to provide valuable information for proteomic investigation. [33, 34] Mounting evidence confirms that the circulating low molecular weight proteome (LMWP), composed of small proteins shed from tissues and cells or peptide fragments derived from the proteolytic degradation of larger proteins has been associated with the pathological condition in patients and likely reflects the state of disease. [35-37]

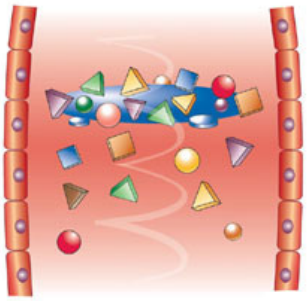

Figure 1.2: the low-molecular-weight region of the blood proteome is a treasure trove of diagnostic information ready to be harvested by nanotechnology. (Reprinted, with permission, from Ref. [35]. Copyright 2003 Nature.)

Despite these potential clinical applications, the use of Mass Spectrometry (MS) to profile the LMWP from biological fluids has proven to be very challenging due to the large range of protein and peptide concentrations in serum, spanning more than 10 orders of magnitude. In addition, the protein content of serum is dominated by a handful of proteins such as albumin, haptoglobulin, immunoglobulins, and lipoproteins. As exhibited in Figure 1.3, 10 proteins make up 90% of the protein content of serum. 12 other proteins constitute the majority of the remaining 10%. In fact, only 1% of the entire protein content of human serum is made up of LMW proteins that are considered to be of great interest in proteomic studies in search of potential biomarkers. [38]

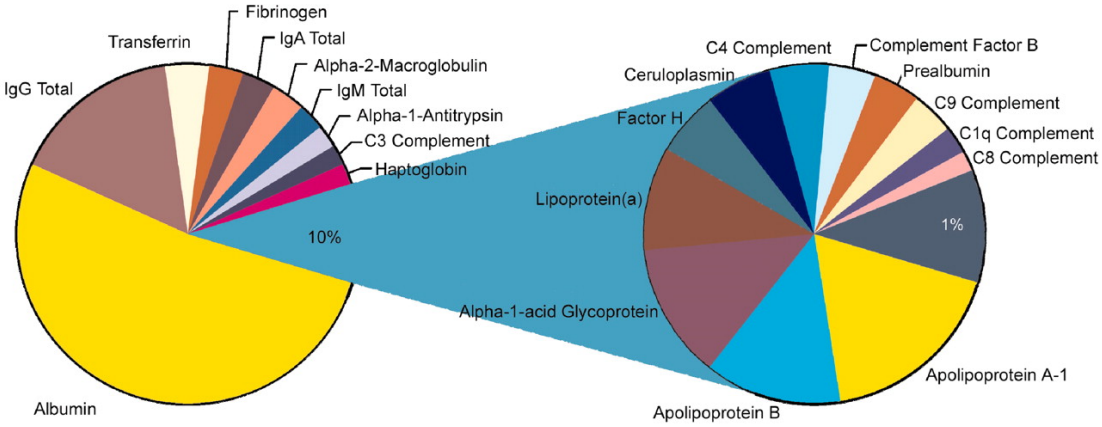


Figure 1.3: Pie chart representing the relative contribution of proteins within plasma. Twenty-two proteins constitute ~99% of the protein content of plasma. (Reprinted, with permission, from Ref. [38] Copyright 2003 The American Society for Biochemistry and Molecular Biology, Inc.)

Without sample pre-treatment, some of the more bundant proteins obscure the detection of low-abundance species in serum/plasma**.** This ultimately limits the resolution of most protein screening methodologies in the range of protein sizes of diagnostic interest. Furthermore, many common enzymes (i.e. thrombin, plasmin and complement proteins) also circulate in the blood that may initialize endoprotolytic cleavage and cause the LMWP signature to be altered during sample processing. For this reason sample collection, storage, and processing must be carefully standardized and documented and occur within a specifically controlled duration.

### 1.2.4 Conventional Proteomics-based Approaches

The introduction of proteomic tools, especially development in mass spectrometry (MS) [39, 40] has allowed for the investigation of complex proteomes and the identification of proteins in cells, tissues and body fluids, increasing the interest of proteomic biomarker research. [41] Now there are several different proteomic based approaches that can be used to attempt to discover novel biomarkers. Three of the most popular techniques are discussed herein. Two-dimentional polyacrylamide gel electrophoresis (2D-PAGE) is widely used to separate the mixtures of proteins in two dimensions by two properties, such as isoelectric point, protein complex mass in the native state, and protein mass. In their application in proteomic study, they primarily analyze bio-markers by identifying individual proteins, and showing the separation between one or more protein "spots" on a scanned image of a 2D electrophoresis gel. Furthermore, spots matched between gels of similar samples are able to show proteomic

differences between early and advanced stages of an illness. However, 2D-PAGE requires a large amount of protein as starting material, and the technique cannot be reliably used to detect and identify low-abundance proteins because of their poor fluidity in gel. These disadvantages, in addition to weak spots/noise and unmatched/undetected spots leading to missing values, represent a significant obstacle to search for biomarkers in early-stage cancers. Surface enhanced laser desorption and ionization time-of-flight (SELDI-TOF) MS is a method to use on-chip protein fractionation, which is dependent on the type of chromatographic matrix used, such as weak cation, strong anion or immobilized metal affinity. As a result of the interaction occurring on the chip surface, a subset of the proteins in the sample binds to the substrate. This interaction is specific as the chromatographic binding is based on the inherent amino-acid sequence of any given protein, as well as on the pH, detergent and salt concentration in the binding reaction buffer. Although SELDI-TOF technology has a clear advantage in that just a minuscule amount of input material is required, a caveat to its efficacy is that substantial upfront fractionation of protein mixtures and down-stream purification methods are required to obtain absolute protein identification, ultimately resulting in a lack of reproducibility. A number of studies have used SELDI technology to identify specific disease-related biomarkers for several types of cancer. Protein array is another very active research program that studies the abundance or the extent of modification of particular proteins through their interaction with specific affinity reagents such as antibodies or aptamers. But it is limited by antibody sensitivity and specificity. These proteomic-based approaches for serum fractionation are labor-intensive, low throughput and offer limited

suitability for clinical applications, especially for those based on the identification of LMWP. Therefore, a more effective strategy is needed to isolate LMWP from blood and allow the high throughput screening of clinical samples.

## 1.3 Objective of the Dissertation

LMWP extracted from serum has the potential to reflect ongoing pathological conditions. However, in order to profile the LMWP, there are significant technical challenges that must be overcome. Specifically, progress must be made regarding the development of fast, reliable, and highly sensitive and specific sample analysis methods. The main objective of this research is to develop a nanotechnology-based strategy using nanoporous silica chips for the efficient removal of the high molecular weight proteins and for the specific isolation and enrichment of LMW species present in complex biological mixtures.

These nanoporous silica chips were synthesized using a process that began with the self-assembly of a mixture of a triblock copolymer (poly(ethylene oxide) (PEO)-poly(propylene oxide) (PPO)- poly(ethylene oxide) (PEO)) and hydrolyzed silicate precursors. [42, 43] The preferential evaporation of the solvent after dip or spin coating drives the self assembly of this mixture into a uniform thin-film nanophase by increasing the concentration of polymer in the solution until it exceeds the critical micelle concentration. Nanoporous silica thin films with narrow nanoscale pore size distributions and high surface area to pore volume ratios were formed after removing the organic template through calcination. In Nanoporous Silica Chip Technology, tunable pore sizes,

structure and surface chemistries act as integrated “processors” for the selective depletion of the high molecular weight protein content in serum samples and for the enrichment of LMW peptides and proteins. [44-46] The detailed synthesis mechanism of mesoporous silica thin film will be discussed in the next chapter.

Serum fractionation using the mesoporous silica thin films was carried out by a rapid 4-step on-chip strategy shown in Figure 1.4. The sample is first spotted on the chip surface (step 1) and incubated to allow the low molecular weight (LMW) proteins to be trapped in the pores (step 2). Next the chip surface is washed to remove the larger protein species which remained outside the pores. The enriched small molecules are then eluted from the nanopores (step 3) and subjected to further mass spectrometry (MS) analysis (step 4). To validate this approach in the context of complex biological samples, the MS profiles of human serum before and after fractionation using the mesoporous chips were compared, shown in Figure 1.5. After washing using deionized water the larger proteins were shown to have been thoroughly removed as demonstrated by a dramatic reduction in signal intensity compared to that of the LMW proteins and peptides. The proteomic profiles depicted in Figure 1.5 (e, f) clearly demonstrate the efficiency of this fractionation strategy in eliminating most of the abundant high molecular weight (HMW) proteins and enriching the otherwise undetectable LMW species present in the serum. This added sensitivity in the LMW portion of the spectrum is crucial for biomarker identification and screening and ultimately for successful disease detection.

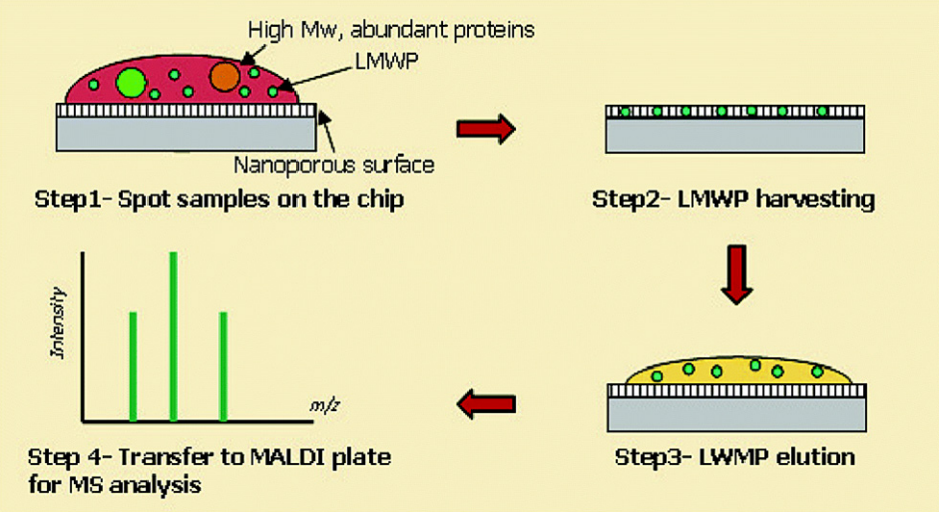


Figure 1.4: Schematic of the harvesting protocol consisting of (1) deposition of plasma directly onto the chip surface; (2) washing of unbound substances; (3) extraction of bound molecules; and (4) MS analysis. (Reprinted, with permission, from Ref.[46]. Copyright 2006. *American Chemical Society*)

By tuning the chemo-physical properties of nanoporous silica surfaces we demonstrated for the first time the correlation between pore size and molecular cut-off. Reproducibility, sensitivity and protein profiles were assessed in relation to the physical (pore size, pore connectivity and structure) and chemical (surface charge, hydrophobicity, hydrophilicity) properties of nanoporous silica. Finally, we applied the Nanoporous Silica Chip Technology to the analysis of human serum and developed different proteomic chips to specifically target regions of the human LMW circulating peptidome. Harvested peptides were subjected to MALDI analysis and profiles consisting of more than 300 peaks in the range 800-20 000 m/z were generated. Our results demonstrate that

nanoporous silicon chips are valuable tools for the detection of low abundance LMW peptides in complex solutions such as serum. Furthermore, the evaluation of the differential recovery of peptides and proteins from human serum is performed from statistical analysis of spectrographic profiles obtained using mass spectrometry, a well established technique. We envision that screenings based on our nanoporous silica chip technology may serve as a complement to histopathology, molecular imaging, and other state of the art diagnostic techniques. This approach may help in the selection of individualized therapeutic combinations that target the entire disease-specific protein network, in the real-time assessment of therapeutic efficacy and toxicity, and in the rational modulation of therapy based on changes in the protein network associated with prognosis and drug resistance.

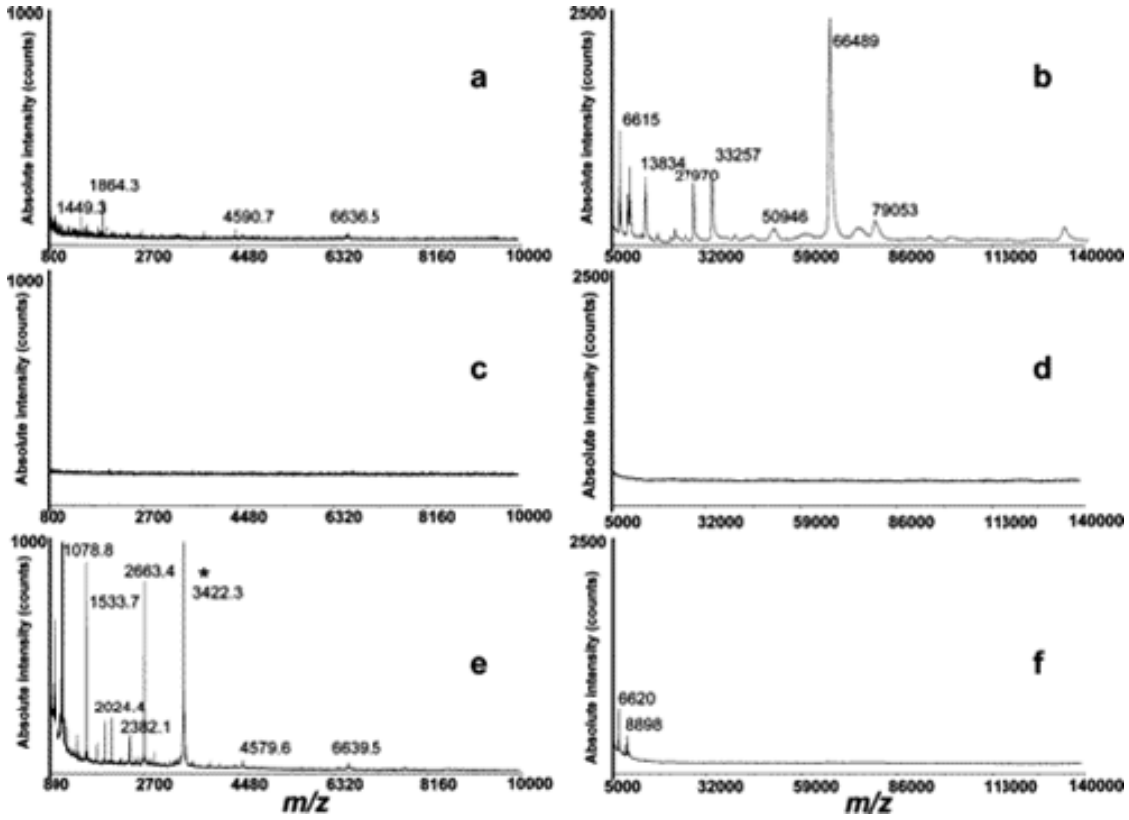


Figure 1.5: MALDI-TOF profiles of human plasma using as matrixes CHCA (left panels) and SA (right panels). a, b: control experiment without chip incubation (direct MS analysis with no pretreatment); a plasma aliquot was diluted 100-fold with matrix for MS analysis analysis. c, d: control experiment using a solid silica surface (nonporous). e, f: analysis of human plasma proteins after exposure to a nanoporous silica chip. All experiments used 5 μL of human plasma spiked with calcitonin at a concentration of 1 μg/mL. For obtaining spectra c and e, chip surfaces were extracted directly with matrix solution; for spectra d and f, the extract was instead mixed with matrix in a subsequent step (matrix/extract ratio 3:1). The calcitonin peak, only visible in panel "e", is marked with a star. (Reprinted, with permission, from Ref.[46]. Copyright 2006. *American Chemical Society*)

## 1.4 Literature Review - Other Nanodevices and Nanomaterials in Diagnostics

Realizing the full potential of nanotechnology as it pertains to genomic and proteomic diagnosis requires the ability to fabricate nanoscale devices and materials with a high degree of precision and accuracy. Reproducibility is of crucial importance to insure that device and material variation can be eliminated as a source of diagnostic variability. All of the nanoscale biosensing devices and nanomaterials in this section are included based on their potential to significantly impact point-of-care diagnosis due to their high sensitivity and capacity for high throughput screening of biological samples.

### 1.4.1 Nanowire Biosensors

The field effect transistor (FET), the basic three terminal logic device found in almost all integrated circuits and which has been in development for over 50 years, can be fabricated using a number of different semiconductor materials, such as silicon, germanium, and gallium arsenide to name a few. This device can be configured as a sensor by eliminating the metal gating electrode and directly modifying the gate oxide with molecular receptors capable of binding to charged species of interest resulting in a direct change to the channel conductance. [47] The FET channel conductance indicates the amount of current that can flow through the channel for a given bias voltage. Boron-doped silicon nanowires have been used to create extremely sensitive, real-time, electrically based sensors for the quantitative detection of biological species. [48] The

sensitivity of FETs whose active areas are comprised of nanowires is greatly enhanced over conventional bulk semiconductor FETs because of their small diameter, between 10 nm and 20 nm, and high surface area to volume ratios, which allow for binding of target molecules, causing accumulation or depletion of carriers throughout a much larger percentage of the channel cross-section. Furthermore, a very large percentage of the nanowire surface is available for functionalization with chemical or biological molecular recognition units that provide selective analyte detection. [49-51] Devices based on chemically functionalized or antigen-conjugated silicon nanowire have been demonstrated to successfully transduce biological binding events in real-time at sensitivities approaching 0.9 pg/mL.

An interesting approach was based on the real-time, label-free, electrical detection of vascular endothelial growth factor (VEGF) for cancer diagnosis using an anti-VEGF aptamer-modified Si nanowire field-effect transistors (SiNW-FETs). In this system, the target VEGF molecules consistently act on the gate dielectrics and their recognition to the anti-VEGF aptamers induces changes in the detection currents. The detection limit for VEGFs in this study was determined as 104pM, a sensitivity threshold compatible with the natural concentration of this protein in blood. [52] To realize the considerable potential of sensors based on electrical detection, arrays of independent nanodevices must be fully integrated with on-chip computation and wireless communication. Nanowire assemblies with microchip technology is emphasized as a key step toward the ultimate goal of multiplexed detection at the point of care using portable, low power, electronic biosensor chips. [53]

### 1.4.2 Micro- and Nanocantilever Arrays

Another promising area in diagnostic research emphasizes specific molecular recognition through the use of micro- and nanocantilevers, with the nomenclature indicating the length scale of the cantilever beam thickness (all other dimensions are usually microscale). One widely investigated architecture to realize this label free strategy is the micro- or nanocantilever, with the nomenclature indicating the length scale of the cantilever beam thickness. These micro- and nanocantilevers, which are usually microfabricated in silicon but can also be produced with piezoelectric material such as quartz, can operate either statically, by measuring absolute cantilever deflection, or dynamically, by measuring resonance frequency shifts. [54] Micro- and nanocantilevers, in addition to quantifying DNA hybridization with single base pair resolution, have used been to detect a variety of biomarkers using both the static [55] and dynamic [56] measurement modes. Through multiplexed testing using arrays of differentially functionalized cantilevers, this device architecture demonstrates great potential for high throughput protein screening, a crucial component for effective proteomic profiling.

### 1.4.3 Magnetic Nanoparticles

Magnetic nanoparticles, typically colloidal superparamagnetic iron oxides (SPIO), have been investigated as magnetic resonance imaging (MRI) contrast agents which have the attractive properties of being able to enhance the proton relaxation times of specific tissues and to be surface functionalized for targeted delivery. [57] The SPIO nanoparticles

are usually synthesized by an aqueous co-precipitation process, in which the pH value in the solution and the presence of surfactant coating materials play a predominant role in tuning the nanoparticle properties. [58] Typically, the magnetic nanoparticles are then chemically coated with various types of polymers to prevent nanoparticle aggregation and to imbue them with greater biological functionality. To significantly improve magnetic nanoparticles' capability to detect and localize tumor, Zhang's group have reported that the specific accumulation of CTX-targeted iron oxide nanoparticles in 9L glioma flank xenografts result in more thorough contrast enhancement of tumors in comparison to non-targeted control nanoparticles. [59]

### 1.4.4 Quantum Dots

Quantum dots consist of a semiconductor coreencapsulated by another semiconductor shell with a typical diameter of 2-10 nm. Due to their tunable nanoscale dimensions, high photostability, broad absorption spectra and narrow emission bands, quantum dots have been used as florescent labels to optically image a host of biological structures and processes ranging from DNA, small organelles, and tumors to cell/cell interactions and cell signaling processes. [60-62] The quantum confinement effect allows for careful control of the emission properties of quantum dots by varying their size and material composition. [63] The fact that multiple quantum dots may be excited by a single excitation wavelength, thanks to their aforementioned broad absorption spectra, allows them to facilitate multiplexed diagnosis. [60, 64, 65]

### 1.4.5 Gold Nanoparticles

Another promising nanomaterial for diagnostic applications is the gold nanoparticle. These nanoscale constructs can be fabricated either as solid gold spherical nanoparticles with diameters in the range of 0.8nm to 250nm or as thin gold shells surrounding a dielectric core (i.e. silica). Au nanoparticles, unlike their quantum dot counter parts, do not emit light but only absorb it in a process called surface plasmon resonance (SPR). [66] This phenomenon describes a coherent oscillation of the surface conduction electrons excited by incident electromagnetic radiation. [67] This oscillation can only be sustained in materials that possess a complex dielectric constant with a negative real part and a slightly positive imaginary. The size and shape of the Au nanoparticles determine their optical resonance and can be tuned to achieve absorption in the mid infrared. [68, 69] The binding of Au nanoparticle-labeled entities to their respective targets leads to aggregation of the nanoparticles, resulting in a color change in the optical signal. [70] Furthermore, adsorption of target molecules on the surface of the Au nanoparticles causes changes to the local refractive index which can be measured as shifts in the plasmon frequency. As a diagnostic tool, Au nanoparticles have been used to label DNA and proteins for detection of biological targets with enhanced sensitivity.

### 1.4.6 Nanoparticle Based Bio-Bar Codes

Methods for increasing the sensitivity and signal-to-noise ratio of clinically relevant assays by either directly amplifying low abundance targets, such as the replication of DNA and RNA sequences using polymerase chain reaction (PCR), or their corresponding optical or electronic signals have garnered considerable attention due to

their promising application towards biomarker screening and proteomic profiling. In 2003, a nanoparticle-based bio-barcode method was developed for the ultrasensitive detection of proteins by Mirkin et al.. [71] This novel technique uses both a magnetic microparticle functionalized with one recognition element, which can be constituted of recognition molecules such as aptamers or antibodies, that specifically bind a target of interest and a gold nanoparticle conjugated by a similar second recognition element as well as large numbers of specific double stranded DNA sequences. The two particles then sandwich and extract a specific target using a magnetic field. Whereas all of the magnetic microparticles are captured, only gold nanoparticles which have bonded to the target are captured. The double-stranded DNA immobilized on the gold nanoparticle surface is then dehybridized to release one of the strands into solution, either chemically (dithiothreitol) [72] or thermally [73-75], and then experimentally detected using chip-based DNA detection. The barcode assay possesses the potential for massive multiplexing through the simultaneous detection of a number of biological components in a single solution. The sensitivity of this methodology exceeds that of ELISA by up to $10^6$, opening up the possibility for the use of low abundance biomarkers in diagnosis whose concentrations were considered too low to be useful with previous technologies.

## 1.5 Conclusion

The real-time, personalized and highly sensitive early stage diagnosis of disease remains an important challenge in modern medicine. With the ability to interact with matter at the nanoscale, the development of nanotechnology architectures and materials

could potentially extend subcellular and molecular detection beyond the limits of conventional diagnostic modalities. At the very least, nanotechnology should be able to dramatically accelerate disease identification and biomarker discovery, as well as facilitate disease monitoring, especially of maladies presenting a high degree of molecular and compositional heterogeneity.

Evidence is mounting that the low molecular-weight region of the circulatory proteome is a rich source of diagnostic biomarkers for the early detection of disease. This dissertation demonstrates that we have successfully fabricated a series of mesoporous silica thin films with a variety of nanophase morphologies and comprehensively explored their use in selectively capturing and enriching LMW peptides and proteins from human serum as well as their potential to provide simple and rapid sample collection, greatly reduced sample thresholds required for analysis and the ability to be produced at low cost. This proteomic profiling platform allows for efficient and flexible collection and analysis of the LMWP from human serum and should therefore prove quite useful in the fields of proteomic biomarker research and clinical proteomic assessment. The details about this study will be thoroughly discussed in the following chapters.

# CHAPTER 2

# AN OVERVIEW OF MESOPOROUS SILICA MATERIALS AND THEIR APPLICATION IN THE IMMOBILIZATION OF BIOMOLECULES

## 2.1 Mesoporous Materials

Porous materials have become attractive due to their ability to interact with atoms, ions and molecules not only at their surfaces, but throughout the bulk of the material. According to IUPAC definition, porous materials are classified into three classes depending on the predominant pore size: (1) microporous with the pore sizes below 2.0 nm, (2) macroporous with pore sizes exceeding 50.0 nm, and (3) mesoporous with pore sizes between 2.0 and 50.0 nm. Since the exciting discovery of the first family of highly ordered mesoporous molecular sieves M41S by Mobil researchers in 1992 [76], many synthetic routes and strategies have been developed to yield a wide variety of porous materials with various chemical compositions and pore structures. Their applications in the fields of adsorption, catalysis, gas sensors, opto-electronic devices and drug delivery have been widely investigated because of their high surface areas, the precise variability of pore size and many other desirable properties.

Long chain cationic surfactants were initially used as the template or pore forming agents to synthesize mesoporous materials with the hydrothermal sol-gel process. [77] However, the relatively small pore size restricts their use in separation, drug delivery and

catalytic process where large molecules are involved. In middle of 1990s, the mesostructures prepared with a nonionic-surfactant-templating approach started attracting considerable attention. It is well known that self-assembly occurs when molecules interact with each other through a balance of attractive and repulsive interactions, such as van der Waals forces or hydrogen bonds. The introduction of nonionic surfactant provided a route to create mesoporous materials with the desired morphology. Hydrogen bonding interaction in self-assembly is significantly complementary to the rigid interaction between ionic surfactants and inorganic species. Depending on the selection of nonionic surfactant used as the template and varying synthesis conditions, this surfactant supermolecular templating approach has led to a breakthrough allowing for the extension of porous materials into the meso-scale with relatively large, uniform and adjustable pore size.

First reported by Pinnavaia and colleagues, mesoporous silicates were synthesized based on hydrogen-bonding interaction between the template of nonionic oligomeric surfactants and triblock copolymers under neutral conditions. In addition, there have been numerous efforts to determine the interaction between the silica surface and biomolecules due to their active saline group on the surface, mechanical strength and chemical inertness. The mesoporous silica combines the intrinsic physical and chemical properties of the inorganic or hybrid matrices with a highly defined nanoporous network which possesses tunable pore size and connectivity, high surface area and accessibility, and a specific orientation with respect to the substrate. In this dissertation, the application of the

mesoporous silica thin films in serum fractionation to selectively enrich the low molecular weight peptides and proteins will be demonstrated.

## 2.2. Sol-gel Process

The sol-gel process, a technique mainly based on inorganic polymerization reactions, has been widely used in the fields of materials science and ceramic engineering of high purity and homogeneity.[77-79] Typical precursors for sol-gel are metal alkoxides or metal chlorides, which undergo different forms of hydrolysis and polycondensation reactions. The formation of a metal oxide starts with connecting the metal centers with oxo (M-O-M) or hydroxo (M-OH-M) crosslink, then metal-oxo or metal-hydroxo polymers is generated in solution through the process of aging, drying, and densification. The general scheme can be represented in Figure 2.1 with silicone alkoxide as the example. [80]

The hydrolysis and condensation reactions in the sol-gel process can be controlled by multiple parameters, such as the hydrolytic properties of the metal alkoxide, the ratio of solvent to metal alkoxide, temperature, the addition of additive, and in particular, solution pH. By changing these experimental conditions, products with different morphologies, structures and surface chemistry can be obtained. In the case of silicon alkoxides, the rate of hydrolysis is higher than the rate of condensation when the experiment is run under an acidic environment. Normally the acid catalysis promotes the development of more linear or polymer-like molecules in the initial stages. On the other hand, base catalysis results in a higher condensation rate, tending to produce a dense-

cluster growth or colloidal particular structure. [80] In addition, the activity of the alkoxy group can also influence the hydrolysis and condensation reactions based on a steric or leaving-group stability effect. For instance, tetramethoxysilane (TMOS) exhibits a more reactivity than tetraethoxysilane (TEOS). To meet the specific request in many applications, thin film can be fabricated by depositing sol-gel solution on a substrate (i.e. glass or silicon wafer) via spin-coating, dip-coating or other deposition techniques. After drying and heat-treatment, the "gel" is converted into dense ceramic or glass particles. In the next section, the detailed mechanism about the formation of mesoporous silica thin film will be discussed.

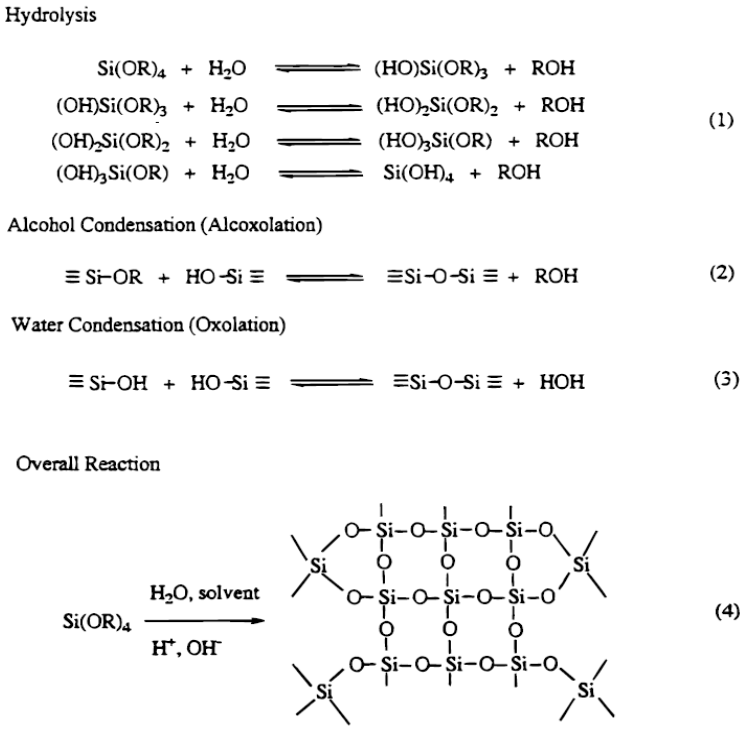


Figure 2.1: The general scheme of sol-gel process of silicone alkoxide. Reprint with permission from Ref [80].

The Sol-gel process is one of the most promising areas of material research. In particular, there is considerable potential for these materials in the fields of Separation and sensor technologies, since they combine mechanical strength, transparency in the visible spectrum, high porosity and surface area of gel-derived oxides. Sol-gel is also an effective method of fabrication and is extensively utilized to design and synthesize inorganic-organic hybrid materials with nanometer-scale architecture. As a result, these hybrid materials can find applications in many fields far beyond the scope of traditional composite materials.

## 2.3 Nonionic Surfactants

In a conventional pathway, sol-gel products synthesized without using a template normally result in microporous materials that are air dried (denoted as xerogels). numerous mesoporous or nanoporous silicate and other metal oxides with narrowly distributed pore diameters of 2-50 nm have been prepared through various synthetic routes and strategies containing a wide variety of materials and displaying various framework chemical compositions and pore structures. As discussed above, mesoporous materials prepared with neutral surfactants usually have improved stability and tunable physical properties. The main classes of nonionic surfactants for use as synthetic templates of mesoporous materials are oligomeric alkyl ethylene oxides, oligomeric alkylphenol ethylene oxides and amphiphilic block copolymers. Selecting a surfactant for the specific purpose is normally based on their hydrophilic/hydrophobic ratio, critical micelle concentration (CMC), hydrophile-lipophile balance (HLB), critical micelle

temperature (CMT) and cloud-point value (CPV). In our study, all triblock copolymers used were gifted from BASF Co.. Figure 2.2 shows a grid profile of triblock copolymers composed by (poly(ethylene oxide) (PEO)-poly(propylene oxide) (PPO)- poly(ethylene oxide) (PEO)) by plotting molecular weight ranges of the hydrophobe (PPO) against the percentage of hydrophile (PEO) of the block copolymer.

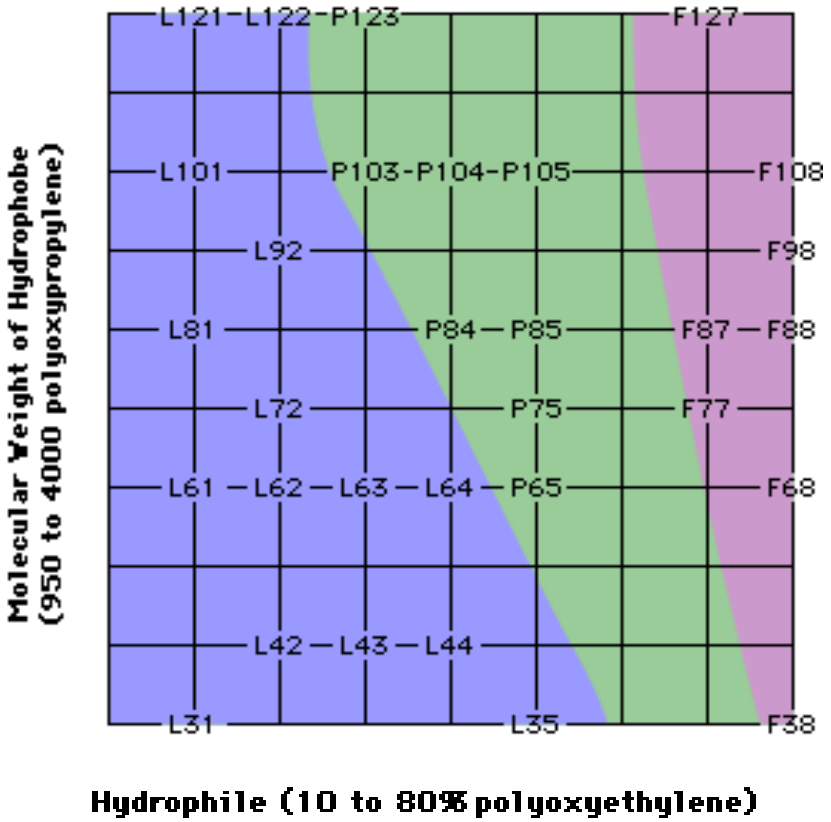


Figure 2.2: Molecular weight ranges of the hydrophobe vs. the percentage of hydrophile of the block copolymer, reprinted with permission from http://www.basf.com/performancechemical/bcperfpluronic_grid.html

Stucky and coworkers utilized commercial PEO-PPO-PEO tri-block copolymers under acidic condition to successfully synthesize a family of meoporous materials with varying ordered structures and a wide range of pore sizes, up to 30 nm. [81, 82] Compared to the conventionally used small molecular surfactants, the PEO-based amphiphilic copolymers exhibit elegantly tunable phase behavior due to their block architecture and the weak hydrogen-bonding interaction between the phases of polymer and solvent, [83, 84] resulting in diverse structural characteristics. Moreover, the PEO surfactants are neutral, nontoxic, and biodegradable. For the family of PEO-PPO-PEO tri-block copolymers, at the given PPO block length, an increase in the PEO block is suitable to stabilize the ordered (e.g. cubic or hexagonal) mesostructures. [85]

In our study, based on the molecular weight of the block copolymer and the ratio of the hydrophilic (PEO) to hydrophobic (PPO) chain length in the amphiphilic polymer, we selected four typical triblock copolymers: $PEO_5$-$PPO_{70}$-$PEO_5$ (Pluronic L121), $PEO_{20}$-$PPO_{70}$-$PEO_{20}$ (Pluronic P123), $PEO_{106}$-$PPO_{70}$-$PEO_{106}$ (Pluronic F127), $PEO_{13}$-$PPO_{30}$-$PEO_{13}$ (Pluronic L64). The hydrophilic/hydrophobic volume ratio ($V_H/V_L$) is suggested especially for nonionic-surfactant-templating systems to account for the formation of different mesophases. [86] The surfactants with high $V_H/V_L$ ratios favor the formation of cage-like cubic mesoporous materials, whose topological curvatures are rather high. Block copolymers with medium hydrophilic/hydrophobic ratios usually direct the synthesis of mesostructures with medium curvatures (e.g. 2D hexagonal structure with space group of p6m or 3D bicontinuous cubic Ia3d). [87]

Furthermore, the advantage of certain high molecular weight block copolymers with is their ability to form a variety of structures by tuning experimental conditions during the synthesis of the mesoporous silica thin film. The concentration of block copolymers which affect the $V_H/V_L$ ratios can also alter mesostructures. Normally, higher concentrations lead to mesostructures with lower mesophase curvature. [43, 88] The structural transformation of the mesoporous arrangement was carried out by tuning the concentration of the template polymer. Increasing the concentration of the template polymer resulted in a reduced interfacial curvature between the phases of the water, the copolymer, and the silicate, consequently initiating the interrelated progression from a spherical to a cylindrical structure. The details about controlling mesostructures will be described in the following section.

## 2.4. Templated Mesoporous Thin Films

### 2.4.1 Synthetic Mechanisms of Mesoporous Materials

Although the synthetic mechanism of mesoporous silica thin films are still under discussion, two popular explanations have been proposed for describing nano-organization of inorganic structures in the presence of nano-segregating surfactants as templating agents. The liquid-crystal templating (LCT) mechanism was first proposed by Beck etc. al. in 1992. [89-91] In this theory, the inorganic precursor condenses around a robust mesoframe formed by self-assembly of polymer surfactants. The second mechanism is cooperative self-assembly, in which surfactant molecules and inorganic species firstly assemble to form hybrid intermediate entities that behave as independent

composite hybrid species. Next these hybrid species, with the amphiphilic component, band together to form oligomeric building blocks with mesostructures. [92-94] However, we prefer to understanding it is a combined effect of both mechanisms that governs the construction of hybrid nanostructure. The starting materials and several critical experimental parameters play key roles in determining which pathway is dominant in the synthetic procedure. This makes understanding the mechanisms of construction very difficult. The different chemical strategies for the synthesis of mesoporous materials are shown in Figure 2.3. [95]

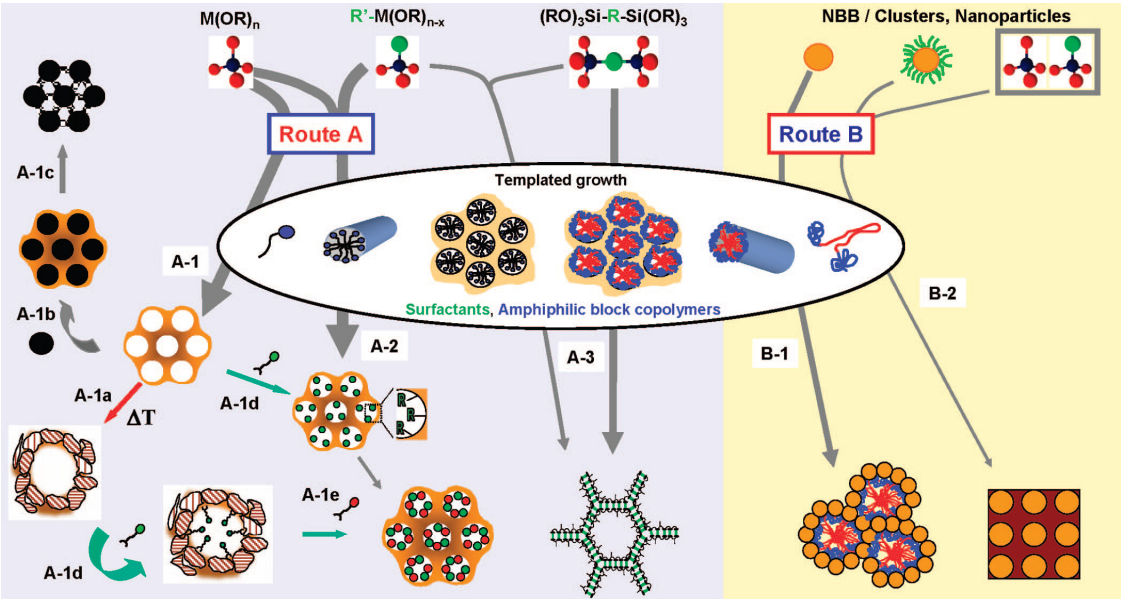


Figure 2.3: Chemical strategies for the synthesis of inorganic and hybrid mesoporous materials. Reprint with permission from Ref [95].

Route A corresponds to the coupling of molecules of sol-gel chemistry with polymer templating. The networks with mesotextures are obtained through the surfactant directed assembling of hydrolyzed inorganic precursors (i.e. silicate). high temperature, UV treatment or solvent extraction is able to achieve complete removal of organic template, as shown in route A1. Based on this pathway, the mesoporous materials can be further used in: 1. consolidation of the inorganic backbone (path A-1a), 2. templates to grow inorganic or organic nano-objects (path A-1b), 3. organic functionalization by alkoxysilanes (R′*n*Si(OR)4-*n*) (path A-2 or path A-1e) or with a post-grafting method (path A-1d), 4. cocondensation with metal alkoxides under surfactant directed assembly conditions (path A-3). On the other hand, strategies that combine surfactant directed assembling of presynthesized well-defined nanobuilding blocks have been also developed (route B).This approach uses precursors based on perfectly calibrated, preformed objects that preserve their integrity in the mesostructured templated hybrid phase (path B-1). The pathway that takes advantage of nanobuilding blocks exhibit several advantages including 1. potentially minimizing collapse problems that may be associated with template removal and crystallization, 2. exhibiting a lower hydrolytic reactivity, 3. possessing perfectly defined structures that facilitate the characterization of mesostructured hybrid phases and 4. allowing for a high control over structure. Alternative approachs based on the combination of path A and path B (path B-2) may be conceived to achieve further control in structure and function of mesoporous materials.

### 2.4.2 Mesoporsous Silica Thin Films

The fabrication of mesoporous silica thin film were reported by Anderson et al., [96] Ogawa, [97] Ozin et al.,[98] and Brinker et al. [99] The application of anionic, cationic, or neutral surfactant led to mesoporous materials with pore dimensions as a function of the chain length of the hydrophobic tail of the template and the headgroup size. The predominant methodology for the synthesis of mesoporous silica thin film is basedon evaporation-induced self-assembly (EISA). [99] Starting with homogeneous, hydro-alcoholic solutions of soluble silicate (i.e. TEOS) and a structure-directing polymer, the preferential evaporation of the solvent after dip or spin coating drives silica/copolymer self assembly into a uniform thin-film nanophase. With dip/spin coating, the precursor solution, strongly adhering to the substrate surface, is deposited in order to construct a homogeneous layer with specific final mesostructure. The solvent is evaporated under a controllable rate to prevent dewetting of the solution. Usually high surface tension solvents, such as water, lead to a nonhomogeneous covering, resulting in good adhesion between the substrate interface and the silica film. With progressive increases in concentration of template and inorganic precursors, the self-assembly is set up to attain a steady state in which the film composition is in equilibrium with its environment. Subsequent polycondensation relies on the consolidation of the inorganic network around the micelles and anchoring of the film at the substrate surface. The spin coating used in our study is slightly different from the other techniques in the sense that a small amount of solution is dropped at the center of the substrate. In order to achieve a uniform coating, the solution is allowed to spread gently for a short time at a relatively slow spin speed. With a faster spin speed, the film is submitted to a shear force applied

between both interfaces of the drying solution layer as it is being formed. Mesoporous silica thin films with a narrow nano-scale pore size distribution and a high ratio of surface area to pore volume were formed after removing the organic template by calcination.

## 2.5 Pore Dimension Control on Mesoporous Silica Thin Film

### 2.5.1. Pore Size Control

The topological design of mesoporous silica thin films with specific pore architecture and pore size has attracted interest from areas such as catalysis, adsorption, and host–guest chemistry. In the case of serum fractionation, the pore structure in mesoporous silica thin films as well as the pore size and porous network connectivity can play an important role in sample diffusion, serum separation and protein extraction. The pathways to control pore size include post-synthesis treatment [100-102] and the use of surfactants of different chain lengths, triblock copolymers, [81, 103-106] and alkyl ethylene oxide as templates or swelling agents [107-110] in the formed micelles.

As introduced in previous section, triblock copolymers were used in our study due to their capability to provide relatively large pore size. With these polymers as the synthetic template, pore characteristics of mesoporous products mainly depend on the molecular weight of copolymer, the ratio of the hydrophilic (PEO) to hydrophobic (PPO) chain length in the amphiphilic polymer and the proportion of the polymer in the starting material. [111] It is easily understood that a polymer template with a higher hydrophobic volume facilitates greater pore size. We selected four typical triblock copolymers with different molecular weights and compositions: $PEO_5$-$PPO_{70}$-$PEO_5$ (Pluronic L121),

$PEO_{20}$-$PPO_{70}$-$PEO_{20}$ (Pluronic P123), $PEO_{106}$-$PPO_{70}$-$PEO_{106}$ (Pluronic F127), $PEO_{13}$-$PPO_{30}$-$PEO_{13}$ (Pluronic L64). These were used as synthetic templates to form the mesoporous silica thin films with diversified structural and morphological properties. L121 is capable of forming the mesoporous silica thin film with the highest porosity and largest pore size as it has the highest hydrophobic to hydrophilic ratio among the pluronic surfactants. Furthermore, the addition of a hydrophobic polymer to the precursor solution modifies this ratio and enlarges the mesoporous silica pore size. In this study, Poly Propylene Glycol (PPG) was used as a swelling agent to extend pore size up to 7 nm and increase porosity to 67% for the thin film prepared with L121.

### 2.5.2 Control of Pore Architecture

#### 2.5.2.1 Tunable Ordered Mesostructures

Selection of the surfactant type and concentration allows for precise control over the resultant mesostructure. Highly ordered mesoporous materials can be synthesized by using nonionic surfactants with high molecular weight under acidic conditions. It is believed that triblock copolymers not only play the role of a template but also insert into the silica framework with PEO blocks and form organic–inorganic hybrid frameworks. [112] In the case of the Pluronic F127 block copolymer, the periodic nanostructure can be transformed from a 3-dimensional (3D) cubic or a honeycomb-like hexagonal to a 2-dimensional (2D) hexagonal framework by tuning the molar ratio of the copolymer to silicate precursor in solution.

The exploration of the range of synthesis parameters reveals a special interplay between the main control variables: silicate/polymer molar ratio, the relative humidity

during and immediately after dip-coating, and the aging time prior to coating. [113, 114] The interaction between these variables is best understood in terms of the interfacial curvature between the hydrophilic and hydrophobic regions. For binary water-surfactant systems, the curvature at the hydrophilic/hydrophobic interface is intimately linked to the lyotropic liquid crystalline phase that self-assembles. A simple geometric theory based on a molecular packing parameter has been developed and is widely used to understand this relationship. The condensation parameter is mainly based on the nature of the amphiphilic copolymer, but the shape of the amphiphile is also very responsive to the environmental conditions such as polymer concentration, temperature, and the presence of other species.

Hillhouse and his colleagues defined a parameter of $g = V/lcAo$, which is inversely related to the interfacial curvature at the hydrophilic/hydrophobic interface. Herein $V$ is the volume of the hydrophobic tail, $lc$ is the critical length of the hydrocarbon chain (which is roughly equal to but less than the fully extended length of the hydrocarbon chain), and $Ao$ is an effective area of the head group at the hydrophilic/hydrophobic interface. For $g = 1/3$, cubic and 3D hexagonal lyotropic liquid crystals composed of packings of spherical micelles are expected. For $g = 1/2$, a 2D hexagonal phase composed of cylindrical micelles is expected. For $g = 1$, lamellar liquid crystals are expected. Estimating the parameter of self-assembly (or the curvature) from the surfactant framework and the environmental conditions in solution is quite complicated even for simple systems. [113, 114] For instance, for ionic surfactants the area of the head group is very dependent on the screening of head group charges, and

thus the area is particularly responsive to the ionic strength of the medium. For nonionic head groups, the area is also difficult to calculate because it depends on how the head group is solvated. It may be expanded or collapsed depending on the temperature and other environmental conditions, as is the case for ethylene oxide head groups. For the silica-nonionic surfactant systems, calculating accurate values of *g* or the curvature a priori is not possible. However, a geometric model which relates curvature with the final structure could be used as a paradigm to understand the systematic changes that occur as a result of altering composition or processing parameters in self-assembled nanostructured films, as shown in Figure 2.4. [115-119]

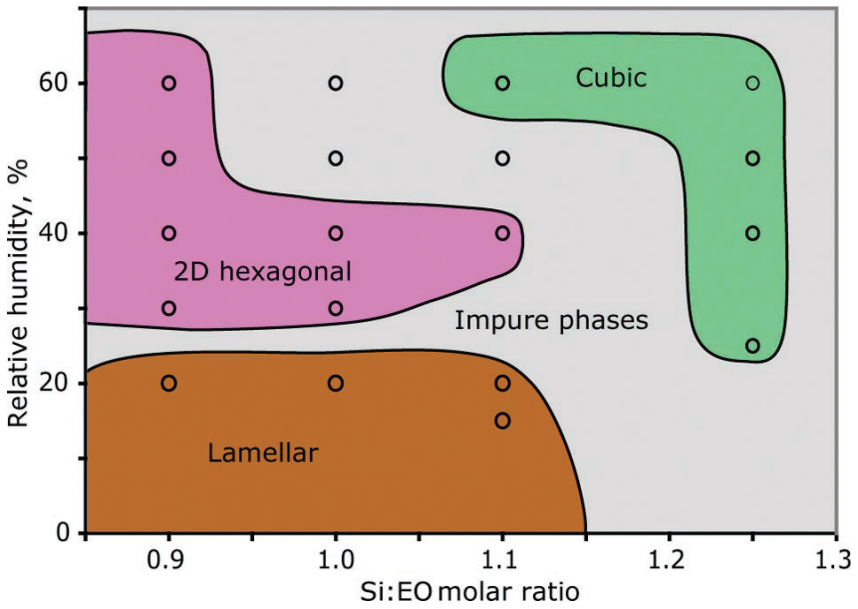


Figure 2.4: EISA processing diagram showing the nanostructures obtained when the solutions are not aged for an extended duration (typically less than 2 h). Note the absence of the double-gyroid phase. Reprint with permission from Ref [113].

It has been shown that the relative volume fractions of the nonvolatile components in the coating solution are closely related to the interfacial curvature of the resulting mesostructure of films formed by EISA from nonionic surfactants. For a given surfactant, the volume fraction corresponding to a given phase was obtained from the binary aqueous-surfactant phase diagram. Alberius and co-workers [116] showed that the concentration of the inorganic precursor in an EISA coating solution needed to synthesize the same phase of the silica-surfactant thin film could be calculated. Thus, this "general predictive" method allows one to connect coating solution composition with the phase of the self-assembled film. However, it has been shown that relative humidity can play a dominant role in determining the phase, [120] and its effects are beyond the scope of the general predictive model as formulated.

#### 2.5.2.2 Disordered Mesostructures

The syntheses of disordered sponge-like or wormhole-like mesoporous silica materials templated by nonionic surfactants have also contributed a great deal to the employment of organization principles in the surfactant-templating approach. Although the mesostructure is disordered, it has uniform mesopores and and a high surface area. In particular, the pore sizes are very dependent on the synthesis temperature because hydrogen bonds between inorganic species and surfactants under neutral conditions are sensitive to temperature. [121] Disordered mesostructures have no unit cell, no symmetry, and no space group. However, characteristics such as uniformly sized pores, high surface area, and easy modulation open up possibilities in catalysis, adsorption,

separation and immobilization. For instance, the mesoporous silica thin films prepared by L121 and L64 exhibit a non-ordered mesostructure but possess a capability for protein recovery in a great mass range.

## 2.6 Immobilization of Biomolecules in Mesoporous Silica

Mesoporous silica materials have been considered to be ideal protein and peptide hosts due to their high adsorption capacity, good dispersibility in aqueous solution, and good compatibility with the surrounding environment. [122-127] Mesoporous structures with tunable pore sizes facilitate the effective size-selective adsorption of protein or peptide with different molecular weights based on the size-exclusion mechanism, [128, 129] by which mesoporous silica is well suited for immobilization of biomolecules under room temperature (or low temperature) . The mesoporous silica showed high adsorption of cytochrome c, lyzozyme, myoglobin and β-lactoglobulin. Yet it had a low adsorption capacity for larger proteins (bovine serum albumin (BSA), ovalbumin and conalbumin) due to the pore exclusion effect. [130]

Compared to other methods of immobilization, mesoporous materials have many advantages. They possess tunable physico-chemical properties, are thermally stable, are not photos-sensitive, have the potential to undergo a wide variety of chemical modifications, enable the stability of the encapsulated molecules, and preventing leaching of proteins due to the effective caging.

Cage-type ordered mesoporous silica patterns are ideal host matrices for immobilizing biomolecules, such as enzymes. For enzyme immobilization inside mesoporous silica, pore size is an important factor. Generally small pores limit the diffusion of enzyme within the network of pores, while large pores increase the capability of mesoporous silica for enzyme immobilization. [130-133] Mesostructure plays another significant role in bioadsorption in terms of mass transfer and pore blocking. [134]

Chemical functionalization on the mesoporous silica surface is necessary for improving the conjugation of biomolecules with supporting material. Modified mesoporous silica has unique characteristics compared to the pure silica and has wider applications including ion exchange, catalysis, and gas separation. [135] In addition, functionalized mesoporous silica shows a higher capacity to immobilize the specific protein compared to pure silica. The organosilanes with amine functionality have received significant attention because of their wide range of applications, such as heterogeneous base catalysis, toxic arsenate ion trapping, support for metallic nanoparticles, sensors, and enzyme immobilization. [136] For the serum fractionation on mesoporous silica thin films investigated in this study, we focus on the recovery of specific proteins affected by the chemical modification on the mesoporous silica surface. Beside amine functionality, carboxyl groups and some other negative functional moieties are also conjugated with mesoporous silica thin films and their effect on harvesting the particular proteins is also explored.

# CHAPTER 3

# PREPARATION OF SURFACTANT-TEMPLATED MESOPOROUS SILICA THIN FILMS FOR ON-CHIP SERUM FRACTIONATION

## 3.1 Introduction

Mesoporous silica thin film made by self-assembly of the triblock copolymer (poly(ethylene oxide) (PEO)-poly(propylene oxide) (PPO)- poly(ethylene oxide) (PEO)) with hydrolyzed silicate precursors has generated substantial interest in the past ten years. [42, 43, 95, 111] With the integration of hydrogen bonding interaction at the organic/inorganic interface, ordered/unordered mesoporous silica thin films with desired and tunable physico-chemical properties have been widely investigated. Different mesoporous materials have been investigated in applications such as high surface area catalysis [137-139], molecular sieves [140, 141], gas sensors [142], opto-electronic devices [143, 144] and drug delivery [124, 145, 146]. As mentioned in the last chapter, mesoporous silica has been extensively studied for the absorption and separation of biological molecules due to their well defined pore network and surface reactivity. [146] The identification of circulating biomarkers holds great potential for non-invasive approaches in early diagnosis and prognosis, as well as for the monitoring of therapeutic efficiency. [31, 32, 40, 41, 147] In Chapter 1, we described that the circulating low molecular weight proteome (LMWP), composed of small proteins shed from tissues and cells or peptide fragments derived from the proteolytic degradation of larger proteins, has

been associated with the pathological condition in patients and likely reflects the state of disease. [35-37]

In previous literature, we have demonstrated the use of mesoporous silica surfaces as substrates for the easy and rapid fractionation of small proteins and peptides. [4, 11, 44, 45] In this dissertation, mesoporous silica thin films with tunable features at the nanoscale were fabricated with the aim of specifically harvesting the low molecular weight peptides and proteins from human serum. Using different polymer templates and polymer concentrations in the precursor solution, various pore size distributions, pore structures and surface hydrophilicities were determined and applied for morphology-selective recovery of low mass proteins. With the assistance of mass spectrometry and statistic analysis, we are able to demonstrate the correlation between the nanophase characteristics of the mesoporous silica thin film and the specificity and efficacy of low mass proteome harvesting. In the present study, we employed advanced materials science and engineering techniques to design and characterize mesoporous silica thin films for efficient and selective harvesting of LMW peptides and proteins from human serum.

The formation mechanism of mesoporous silica thin films has been throughout discussed on Chapter 2. One of the promising characteristics of mesoporous silica thin films is the variety of achievable pore morphologies. Pore structure as well as pore size and porous network connectivity can play an important role in sample diffusion, serum separation and protein extraction. In mesoporous silica, pore characteristics mainly depend on the molecular weight of the block copolymer, the ratio of the hydrophilic (PEO) to hydrophobic (PPO) chain length in the amphiphilic polymer and the proportion

of the polymer in the starting material. Triblock copolymers $PEO_5$-$PPO_{70}$-$PEO_5$ (Pluronic L121), $PEO_{20}$-$PPO_{70}$-$PEO_{20}$ (Pluronic P123), $PEO_{106}$-$PPO_{70}$-$PEO_{106}$ (Pluronic F127), $PEO_{13}$-$PPO_{30}$-$PEO_{13}$ (Pluronic L64) were used as the synthetic templates to form the mesoporous silica thin films with diversified structural and morphological properties. L121 is capable of forming the mesoporous silica thin film with the highest porosity and largest pore size as it has the highest hydrophobic to hydrophilic ratio among the pluronic surfactants. Furthermore, the addition of a hydrophobic polymer to the precursor solution modifies this ratio and thus enlarges the mesoporous silica pore size. In this study, Poly Propylene Glycol (PPG) was used as a swelling agent to extend pore size up to 7 nm and increase porosity to 67% for the thin film prepared with L121. Using Pluronic F127 block copolymer, the periodic nanostructure can be transformed from a 3-dimensional (3D) cubic or a honeycomb-like hexagonal to a 2-dimensional (2D) hexagonal framework by tuning the amount of the copolymer in solution. In addition, ionic surfactant (cetyltrimethylammonium bromide: CTAB) was used to prepare the microporous silica thin film with much smaller pore size (~ 2nm) to study the efficacy of molecular cut-off of protein recovery depending on a wide range of pore size distributions.

## 3.2 Experimental Section

### 3.2.1. Materials

Tetraethyl orthosilicate (TEOS) and cetyl trimethylammonium bromide (CTAB) were purchased from Aldrich Chemicals (Milwaukee, WI). Ethanol and HCl was

purchased from Fisher Scientific (Fair Lawn, NJ). Nonionic surfactants (F127, P123, L121 and L64) were gifted from BASF Co.. All chemicals and reagents were used as received without further purification.

### 3.2.2 Preparation of mesoporous silica thin films

As listed in Table 1, the molar ratios of starting materials are slightly different for various surfactants. The typical preparation of precursor solution is shown in Figure 3.1 and was carried out as follows: 30 ml of TEOS was dissolved in the mixture of 48 ml of ethanol, 20 ml of distilled water, and 3 ml of 2 M HCl and stirred for 1 hour at 75°C to form a clear silicate sol. Separately, a portion of different surfactant (1.0g of CTAB, 1.5g of F127, 1.2g of L64, 1.6g of P123 or 1.2g of L121) was responsively dissolved in 10 ml of ethanol by stirring at room temperature. In the case of using L121 as template, 0.6g or 1.2g of PPG solution was dropped into the L121 solution with vigorous stirring at room temperature. 10 ml of hydrolyzed silicate sol was dropped into the triblock co-polymer solution followed by stirring for 2 hrs at room temperature. The coating sol was spin-coated on a Si (1 0 0) wafter for 25 seconds at the spin rate of 750 rpm for the solution containing CTAB, 1500 rpm for the solution with F127 or P123 and 2500 rpm for the mixture with L64, L121 or L121+PPG. The as-deposited films were heated at 80 °C for 24 hrs to increase the degree of polymerization of the silica framework and to further enhance their thermal stability. The temperature was raised at a rate of 1°C per min, and

the chips was heated at 425°C for 5 h to remove the organic surfactant. The films produced were transparent and crackless.

**a. Formation of Polymer Template**

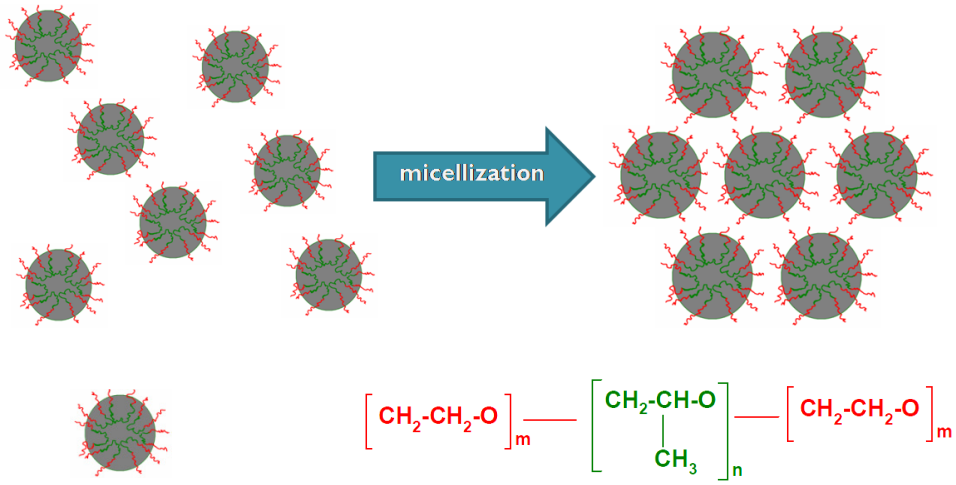


**b. Formation of Mesoporous Silica Thin Films**

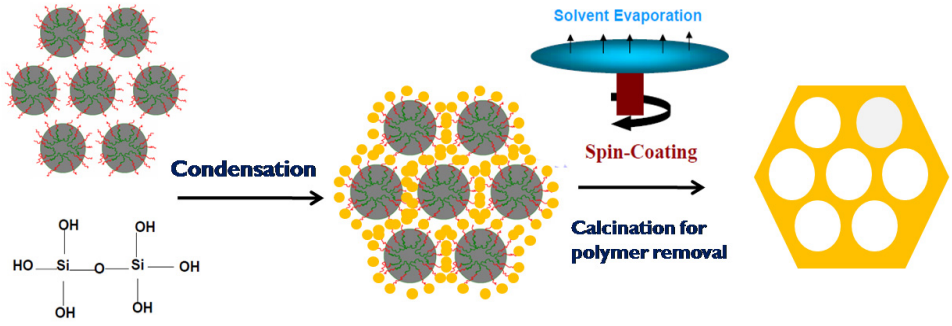


Figure 3.1: The procedure of synthesizing a mesoporous silica thin film. a. The micellization of polymer template in solution, b. the formation of mesoporous silica thin films by spin-coating and calcination.

### 3.2.3 Characterization and instrumentation

Mesostructured thin films are normally composed of a very small amount of matter (usually between 10 and 500 $\mu$g/cm2 of film) spread onto a substrate. This fact makes their characterization more difficult than that of bulk materials and limited to spectroscopic investigations and other common techniques. We utilized several characterization techniques to study the spin-coated mesoporous silica thin fims.

#### 3.2.3.1 Ellipsometry

Ellipsometry measures the change of polarization upon reflection or transmission. The nature of the polarization change is determined by the sample's properties (thickness, complex refractive index or dielectric function tensor). (www.wikipedia.com) In our study, by carrying out with a variable angle spectroscopic ellipsometer (J. A. Woollam Co. M-2000DI) and modeling with WVASE32 software, the thickness of thin films and their porosities were measured respectively in Cauchy model and Effective Medium Approximation (EMA) model. Ellipsometric optical quantities, the phase ($\Delta$), and amplitude ($\psi$) were carried by requiring spectra for 65°, 70°, and 75° incidence angles using wavelengths from 300 to 1800 nm. Ellipsometry is an indirect method, i.e., in general the measured $\psi$ and $\Delta$ cannot be converted directly into the optical constants of the sample. Normally, a layer model must be established, which considers the optical constants (refractive index or dielectric function tensor) and thickness parameters of all individual layers of the sample including the correct layer sequence. The calculated $\psi$ and

Δ values that match the experimental data best provide the optical constants and thickness parameters of the sample.

Therefore, in the Cauchy model, the top layer's thickness, reflective index, and model fit parameters $A_n$, $B_n$ and $C_n$ were determined by fitting experimental data with the model and minimizing the mean square error (usually less than 20). While using the EMA model, the films' porosities were calculated by assuming a certain volume of void in the pure silica and setting the top layer's thickness obtained by the Cauchy model as constant.

#### 3.2.3.2 1D X-ray Diffraction

X-ray diffraction (XRD) is a technique using X-ray scattering on microcrystalline samples for the structural characterization of materials. It is based on the elastic scattering of electromagnetic waves on lattice planes, or more precisely at the electronic shells of regularly arranged atoms. Ideally, every possible crystalline orientation is represented equally in a powdered sample. The Bragg equation is a simple method to determine the distance $d$ of lattice planes. To derive the Bragg equation one considers the lattice planes of a crystal as semitransparent mirrors partly reflecting an incoming beam (Fig. 3.2).

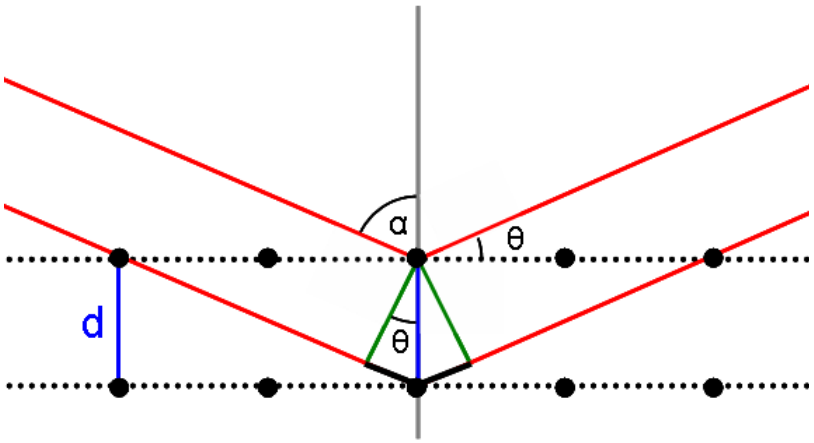


Figure 3.2: Scheme of construct the Bragg equation.

For a monochromatic beam the reflected rays interfere constructively or destructively depending on the angle of incidence $\theta$ and the lattice diameter $d$. Two reflected monochromatic beams interfere if the path difference is an integer multiple of the wavelength $\lambda$. This results in the Bragg equation for constructive interference:

$$n\lambda = 2d\sin\theta \quad \text{with } n = 1, 2, 3, \ldots \qquad \text{Eq. 3.1}$$

When the scattered radiation is collected on a flat plate detector the averaging due to random orientations of the particles leads to smooth diffraction rings around the beam axis rather than the discrete Laue spots as observed for single crystal diffraction. The angle between the beam axis and the ring is called the scattering angle and in x-ray crystallography denoted as $2\theta$.

To investigate the mesostructure of porous silica thin film and determine their periodicity, XRD pattern scanned at small angle range (typically 0.2° to 10°) is carried out. Because this angular range contains information about the shape and size of molecules at nano-scale, characteristic distances of partially ordered materials, pore sizes, and other data. Small angle XRD is capable of delivering structural information of macromolecules between 5 and 25 nm, and of repeat distances in partially ordered systems of up to 150 nm. [148] In this study, X-ray diffraction (XRD) patterns were obtained on Philips X'Pert-MPD system with Cu Kα ray (45 kV, 40mA). *θ-2θ* scanning were recorded from all spin-coated films at 1s/0.001° step over the angle range from 0.2° to 6°.

### 3.2.3.3 X-ray photoelectron spectroscopy (XPS)

XPS is defined as a quantitative spectroscopic technique that measures the elemental composition, empirical formula, chemical state and electronic state of the elements of a material. XPS spectra are obtained by irradiating a material with a beam of X-rays while simultaneously measuring the kinetic energy and number of electrons that escape from the top 1 to 10 nm of the material being analyzed. XPS is a surface chemical analysis technique that can be used to analyze the surface chemistry of a material in its instant state. Its basic components are displayed in Figure 3.3.

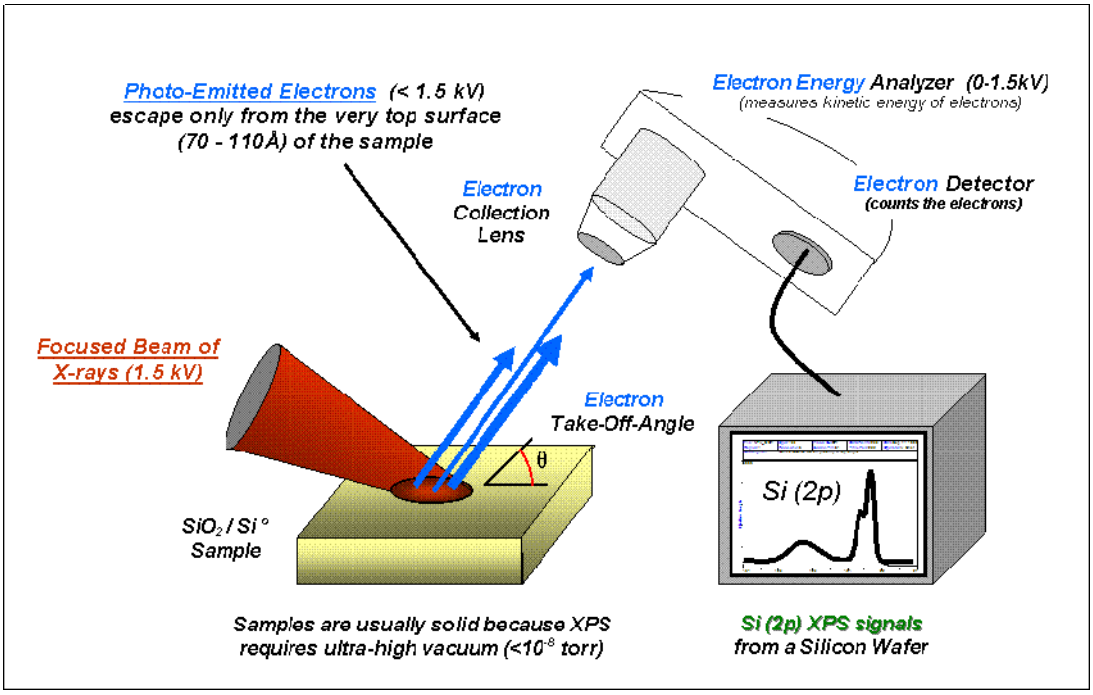


Figure 3.3: Basic components of a monochromatic XPS system. (The Author, the copyright holder of this work, releases it into the public domain. This applies worldwide. He/she grants any entity the right to use this work for any purpose, without any conditions, unless such conditions are required by law. (http://www.wikipedia.com))

In our study, the chemical composition or the purity of mesoporous silica thin film was determined by XPS spectra, which were recorded using a X-ray photoelectron spectrometer (Kratos Axis Ultra), utilizing a monochromated Al-K X-ray source (h = 1486.5 eV), hydrid optics (employing a magnetic and electrostatic lens simultaneously) and a multi-channel plate and delay line detector coupled to a hemispherical analyzer.

The photoelectrons' take off angle was 90 . All spectra were recorded using an aperture slot of 300x700 microns, and high resolution spectra were collected with a pass energy of 20 eV. The pressure in the analysis chamber was typically $2x10^{-9}$ Torr during data acquisition. Kratos XPS analysis software was used to determine the stoichiometry of samples from corrected peak areas and employed Kratos sensitivity factors for each element of interest.

### 3.2.3.4 Transmission Electron Microscopy (TEM)

TEM is a microscopy technique whereby a beam of electrons is transmitted through an ultra thin specimen, interacting with the specimen as it passes through. An image is formed from the interaction of the electrons transmitted through the specimen; the image is magnified and focused onto an imaging device, such as a fluorescent screen, on a layer of photographic film. Transmission electron microscopy (TEM; FEI Technai; FEI Co.) was used in acquiring micrographs of the plant view of mesoporous silica thin films at high tension of 200 kV. The TEM sample was prepared by dipping an ethanol suspension of the finely ground sol-gel onto a Cu grid coated with a holey C film.

### 3.2.3.5 Gas Adsorption/Desorption Isotherm

Porous texture can be described by gas adsorption/desorption isotherms. Many applications involving porous films are critically dependent on accurate knowledge of the pore size distribution (PSD), pore connectivity of the network, and the ability to determine matter exchange and matter adsorption capacities of the porous network and

the film environment. By analyzing the multilayer physisorption and capillary condensation of a gas within the pores, a plot of the adsorbed volume of gas versus the partial pressure $P/P_0$ of gas is obtained. The mono- and multilayer physisorption of the gas observed at low $P/P_0$ can be plotted by the Brunauer-Emmett-Teller (BET) equationEq. 3.2 and allows the determination of the surface area, with $n_m$ being the number of molecules needed to cover the accessible surface with a monolayer of molecules, $n$, the number of molecules adsorbed at the partial pressure $P/P_0$, and $C$, a parameter characteristic of the net heat of adsorption of the molecule at the surface. [149, 150]

$$\frac{P}{n(P_0 - P)} = \frac{1}{n_m C} + \frac{C-1}{n_m C}\frac{P}{P_0} \qquad \text{Eq. 3.2}$$

The gas uptake observed at higher $P/P_0$ values, characteristic of capillary condensation, is used for the determination of the pore size distribution between 2 and 50 nm via the Kelvin equation(Eq. 3.3) that describes the condition of appearance of the capillary condensation at a given value of $P/P_0$, with $\gamma$, the condensed liquid surface tension, $V_L$ the molar volume of the liquid adsorbate, $r_P$ the radius of the pore, and $G$, a geometrical factor characteristic of the liquid-air meniscus curvature. [151]

$$RT \ln\left(\frac{P}{P_0}\right) = -\gamma V_L \frac{G}{r_P} \qquad \text{Eq. 3.3}$$

To determine the pore size distribution, pore volume and surface area of mesoporous silica thin films we prepared, Quantachrome was used to record the $N_2$ adsorption/desorption isotherm at 77 K on the full range of relative $P/P_0$ pressures. BET surface areas were determined over a relative pressure range of 0.05 to 0.3. Nanopore size distributions were calculated from the desorption branch of the isotherms using the Barrett-Joyner-Halenda (BJH) method.

#### 3.2.3.6 Contact Angles

The contact angle is the angle at which the liquid/vapor interface meets the surface. The concept is most often illustrated with a small liquid droplet resting on a flat horizontal solid surface. Contact angle is measured using a contact angle goniometer. If the liquid is very strongly attracted to the solid surface (for example water on a strongly hydrophilic solid) the droplet will completely spread out on the solid surface and the contact angle will be close to 0°. Less strongly hydrophilic solids will have a contact angle up to 90°. On many highly hydrophilic surfaces, water droplets will exhibit contact angles of 0° to 30°. If the solid surface is hydrophobic, the contact angle will be larger than 90°. Highly hydrophobic surfaces have water contact angles as high as 150° or even nearly 180°. On these surfaces, water droplets simply rest on the surface, without actually wetting to any significant extent. In our study, contact angles of film surface were measured by goniometer with captive bubble contact angle measurement.

## 3.3 Results and Discussions

Most of the procedures used for the synthesis of mesoporous silica films are similar to the ones described by Zhao et. al..[43] The primary objective of this study was to tailor mesoporous silica thin film pore morphology and internal structure by adjusting synthetic parameters and to explore their efficacy for the specific harvesting of LMWP species from human serum. A consistent proteomic profiling approach requires that the mesoporous silica-based serum fractionation be performed with a well-defined high purity substrate possessing thermal stability as well as uniform nanostructure and film thickness throughout the entire mesoporous silica layer. Preparation of the precursor solution, which involves the cooperative assembly of a polymer surfactant and soluble silicate species, plays a dominant role in determining the molecular organization of the final product. The molar ratios of starting materials are listed in Table 3.1 for each block copolymer used.

Thickness is the primary characteristic of a thin layer. Parameters controlling the thickness vary with techniques (i.e. dip-coating, spin-coating or spray coating), the time for diffusion, and the quantity and the concentration of the deposited solution. In this study, for a given molar ratio of silicate to polymer in solution, the porous films' thickness was restricted from 700 ~ 900 nm for the purposes of avoiding shrinkage while maintaining enough pore volume in the unit area for sample diffusion by tuning the polymer concentration. This was accomplished by maintaining the molar ratio of ethanol to silicate to between 12 and 14 and water to silicate at less than 6. For all precursor solutions we prepared, the pH was controlled at 1.5 to prevent the precipitation of nanoporous silicate corresponding to the isoelectric point of orthosilicic acid, as well

as to balance the procedure between the silicate hydrolysis and condensation of hydrolyzed silicate to polymer micelle. Based on previous literature [111], when the pH value is in the range from 1 to 2, the precipitation of mesoporous silicates is extremely slow, probably corresponding to the isoelectric point of orthosilicic acid.

Table 3.1: Molar ratio of starting materials to fabricate nanoporous silica thin films with different template polymers and their physical properties calculated by ellipsometry and $N_2$ adsorption/desorption isotherms for nanoporous silica thin films.

| Surfactant Polymer | Molar ratio of reactants TEOS:Polymer:$H_2O$:EtOH:HCl | Structure | Thickness (nm) | Reflective Index | Porosity (%) | BET surface area ($m^2/g$) | Pore volume (cc/g) | Average pore size (nm) |
|---|---|---|---|---|---|---|---|---|
| CTAB | 1:1.02x10-2:11:18:0.15 | 3D cubic | 750.36 ± 9.4 | 1.195 ± 0.005 | 51.9 ± 0.7 | 619.2 | 0.530 | 2.109 |
| F127 | 1:0.751x$10^{-2}$:11:18.2:0.16 | 3D cubic | 820.2 ± 1.3 | 1.220 ± 0.001 | 47.9 ± 0.1 | 191.5 | 0.427 | 3.921 |
| F127 | 1:1.13x$10^{-2}$:11:18.2:0.16 | 3D honeycomb hexagonal | 884.7 ± 0.7 | 1.201 ± 0.002 | 50.3 ± 0.1 | 640.6 | 0.558 | 3.692 |
| F127 | 1:1.51x$10^{-2}$:11:18.2:0.16 | 2D hexagonal | 920.4 ± 1.9 | 1.217 ± 0.003 | 48.5± 0.1 | 1131.0 | 0.742 | 3.700 |
| P123 | 1:9.4x$10^{-3}$:6:14.8:0.85 | 2D hexagonal | 905.5 ± 0.2 | 1.235 ± 0.001 | 48.8 ± 0.2 | 483.1 | 0.382 | 3.693 |
| L64 | 1:2.14x$10^{-2}$:6:11.5:0.16 | Worm-like | 890.5 ± 1.6 | 1.189 ± 0.002 | 56.0 ± 0.2 | 562.6 | 0.465 | 3.205 |
| L121 | 1:1.09x$10^{-2}$:6:14.8:0.16 | Worm-like | 857.2 ± 0.8 | 1.193 ± 0.001 | 55.2 ± 0.4 | 587.8 | 0.811 | 5.817 |
| L121+50%PPG | 1:1.09x$10^{-2}$:6:14.8:0.16 | Non-order | 871.5 ± 1.0 | 1.163 ± 0.002 | 60.9 ± 0.0 | 499.3 | 0.817 | 6.266 |
| L121+100%PPG | 1:1.09x$10^{-2}$:6:14.8:0.16 | Non-order | 940.3 ± 3.5 | 1.148 ± 0.003 | 65.5 ± 0.2 | 664.7 | 0.850 | 6.790 |

Porosity, normally generated from the hydrophobic part of triblock copolymers, was adjusted by changing the molar ratio of the polymers to silicate precursor in the mixture, regardless of the concentration of polymer template in the solution. Spin coating, superior to other deposition techniques for achieving uniform thickness and

porosity, was used to form the mesoporous silica thin films on a silicon substrate. The substrates were then cleaved to produce chips for quantitative proteomics analysis. Previous literature has demonstrated that mesoporous silica products can exhibit substantial non-uniformity as a result of inadequately controlled synthesis due to the weak interaction between molecules during the self-assembly process. [111] Other experimental parameters, such as aging time of the precursor solution, coating speed during solution deposition, and calcination temperature were studied to understand their impact on the final features of the mesoporous structure. To reduce experimental complexity, only the amphiphilic structure of the block co-polymers and their concentration in the precursor solution were adjusted, with all other process parameters held constant, to investigate their effect on pore geometry and morphology.

To characterize the pore architecture and physico-chemical properties of mesoporous silica thin films, various techniques were employed, including ellipsometry, 1-dimentional X-ray diffraction (1D-XRD), $N_2$ adsorption/desorption, transmission electron microscopy (TEM), X-ray photoelectron spectroscopy (XPS) and surface contact angle goniometry. Figure 3.4 depicts the overall purity and the atomic silicon-to-oxygen ratio of the mesoporous silica thin films prepared with L121 as the structure-directing template as determined by XPS using the Si2p, O1s and C1s regions of the spectra. The very weak signal for the C1s region can be attributed to minimal contamination (i.e. hydrocarbons) on the film surface. Both the Si2p and O1s regions consisted of a sharp and symmetric single peak at binding energies around 101.4 eV and 530.7 eV respectively, which strongly point to a silica framework with high

condensation. By calculating the areas under the peaks for Si2p and O1s, an atomic silicon-to-oxygen ratio of 1:2.004 was obtained to further confirm the high purity of mesoporous silica thin films. Similar XPS results were acquired for mesoporous silica thin films synthesized using the alternative polymer templates.

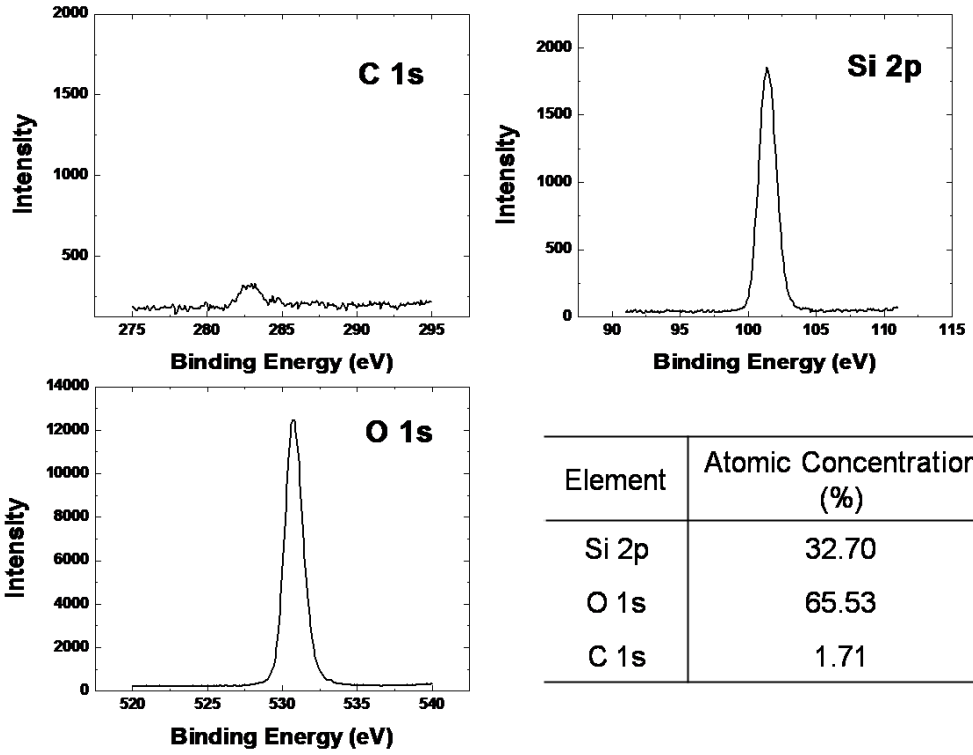


| Element | Atomic Concentration (%) |
|---|---|
| Si 2p | 32.70 |
| O 1s | 65.53 |
| C 1s | 1.71 |

Figure 3.4: The purity of Mesoporous Silica thin films. XPS core level spectra used to analyze the relative amounts of C, Si, and O on the surface of a mesoporous silica thin film prepared from Pluronic L121. The tabulated atomic concentration of each element is shown in the lower right.

### 3.3.1 Ionic Surfactant *vs.* Nonionic Surfactants

To obtain the various pore sizes required to harvest the specific proteome from serum based on size-exclusion, the polymer templates in this section were chosen from both ionic surfactant (cetyltrimethylammonium bromide: CTAB) and non-ionic triblock copolymers ($PEO_{106}$-$PPO_{70}$-$PEO_{106}$ : Pluronic F127, $PEO_5$-$PPO_{70}$-$PEO_5$: Pluronic L121). Using low molecular weight surfactant directing agent, such as CTAB, the resulting nanoporous silica thin film will possess a smaller average pore size than the films prepared with F127 and L121, which have much higher molecular weight and provide a controlled pathway for the preparation of large-pore silicate nanostructure. Herein, nanoporous silica thin films were first examined by X-ray diffraction (XRD to display the periodicity and the organization of pore's nanostructure prepared with CTAB, F127, L121+PPG (with molar ratio of 1:0.5), as shown in Figure 3.5. The XRD pattern in Figure 3.5.a showed nanoporous silica thin film prepared by CTAB on a silicon (1 0 0) substrate. The appearance of the peak for (200) reflection at 2.20° of 2θ with $d_{200}$=3.16 nm indicated that the periodic 3D cubic structure of silica nano-composite formed along the surface of substrate after calcination at 425°C. In figure 3.5.b, the XRD pattern of coating prepared with F127 exhibited an ordered nanoporous texture based on the highly intense (100) reflection peak at 2θ=0.99° ($d_{100}$=9.01nm). The lower intensity peaked at (110) with $d_{110}$=6.30nm and (200) with $d_{200}$=4.75nm indicated the formation of a 3D honeycomb-like nanostructure. In Figure 3.5.c the XRD patterns for those fabricated by L121 displayed a curve in the small angle range with the appearance of a peak, consequentlyillustrating the formation of disordered nanopores. Transmission electron microscopy (TEM) analysis was performed on the plane view, which was inserted below

with the XRD diagram of nanoporous silica thin film prepared by each polymer template. The TEM image confirms the conclusion regarding the identification of the ordering and nanostructure of the thin film which was postulated with the XRD patterns.

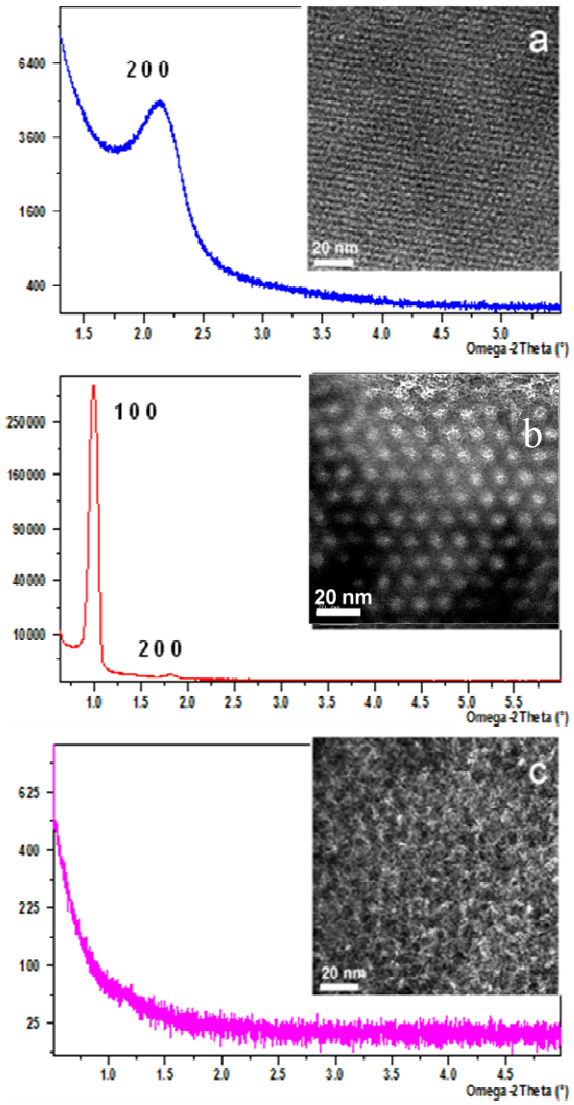


Figure 3.5: 1D XRD patterns and TEM image of plane-view (inserted) for mesoporous silica thin films prepared using **a.** CTAB, **b.** F127 and **c.** L121+50%PPG templates.

$N_2$ adsorption-desorption measurements were conducted to determine the entrance pore size distribution and surface area of mesoporous silica thin films prepared by three different polymers. In Figure 3.6, the BJH pore size distributions for chips prepared by CTAB (Fig.3.6.a), F127 (Fig.3.6.b), and L121+PPG (Fig. 3.6.c) were provided with their adsorption-desorption isotherms inserted. Due to the small pore size (2.01 nm) on the nanoporous silica thin film synthesized by CTAB, its sorption isotherm was Type II displaying a H1 hysteresis loop. All adsorption/desorption isotherms carried by chips prepared by non-ionic surfactants were Type IV with a well-defined $H_2$ hysteresis loop. In these figures, the inflection points appeared at $0.30 \leq P/P_0 \leq 0.80$ , which indicated the formation of ink-bottle shape nanopores. All their BJH pore size distributions exhibited sharp peaks, which suggested that both periodic and non-ordered nanophase were created on the chips with uniform pore size.

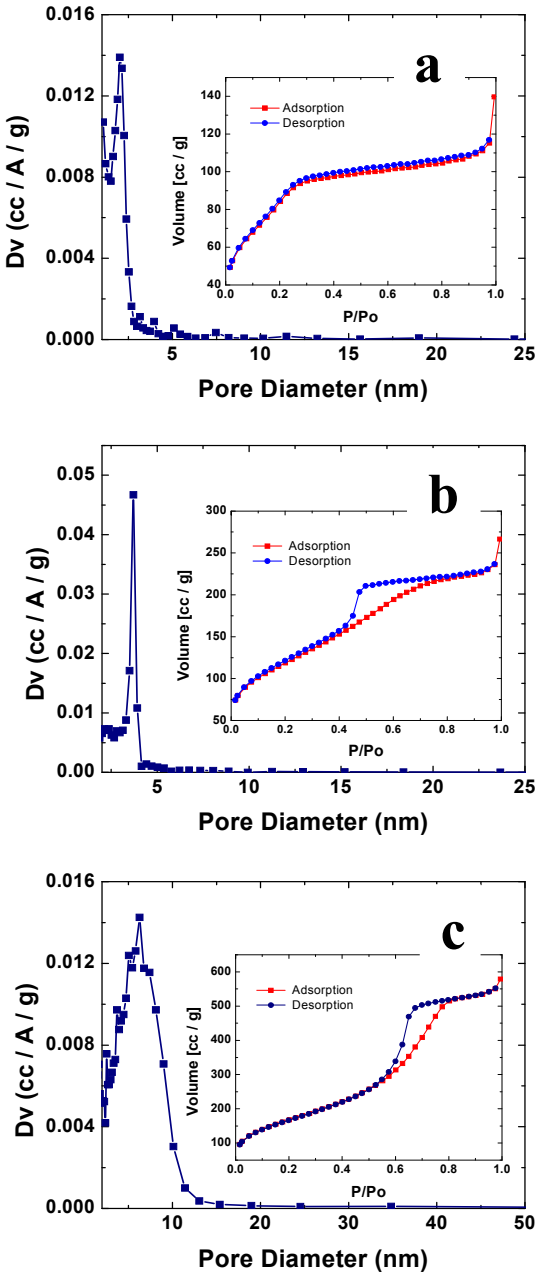


Figure 3.6: Pore size distribution from BJH adsorption for mesoporous silica thin films prepared using a. CTAB, b. F127 and c. L121+50%PPG. The corresponding adsorption/desorption isotherms are inserted.

### 3.3.2 Control on Pore Structure and Distributional Architecture

One main advantage of block copolymers with high molecular weight, in comparison to those of low molecular weight, is their ability to form a variety of structures by tuning experimental conditions during mesoporous silica thin film synthesis. The structural transformation of the mesoporous arrangement was carried out by tuning the concentration of the template polymer. Increasing the concentration of the template polymer resulted in a reduced interfacial curvature between the phases of the water, the copolymer, and the silicate, consequently initiating the interrelated progression from a spherical to a cylindrical structure. Pluronic F127, with its high molecular weight, possesses this high degree of structural periodicity. In this study, the concentrations of all starting materials, except F127, were kept constant. Figure 3.7 demonstrates the changes in the nanostructure of the mesoporous silica by characterization through XRD pattern,. When the F127 concentration in the precursor solution was kept at $4.0\times10^{-3}$ M, the final mesoporous silica thin film acquired a 3D cubic structure with reflection peaks at (100) and (110) and a low intensity peak at (220) as indicated by the XRD pattern (Fig.3.7.a) and further verified through TEM imaging (inset of Fig. 3.7.b). Increasing the F127 concentration to $6.0\times10^{-3}$ M yields a 3D honeycomb like nanostructure hexagonally arranged on the substrate, as confirmed by XRD, with peaks at (200) and (400) (Fig. 3.7.c), and TEM (Fig.3.7.d). A further increase of the F127 concentration to $8.0\times10^{-3}$ M resulted in a 2D hexagonal nanostructure parallel to the substrate surface. The sharp peaks at (100) and (300) in the XRD pattern (Fig. 3.7.e) and TEM imaging (Fig.3.7.f) confirm this conclusion. As we discussed in the last chapter, the structural transformation

of mesoporous silica can be tuned by changing the interfacial curvature between the phases of polymer-silicate-hydrophilic solvent.

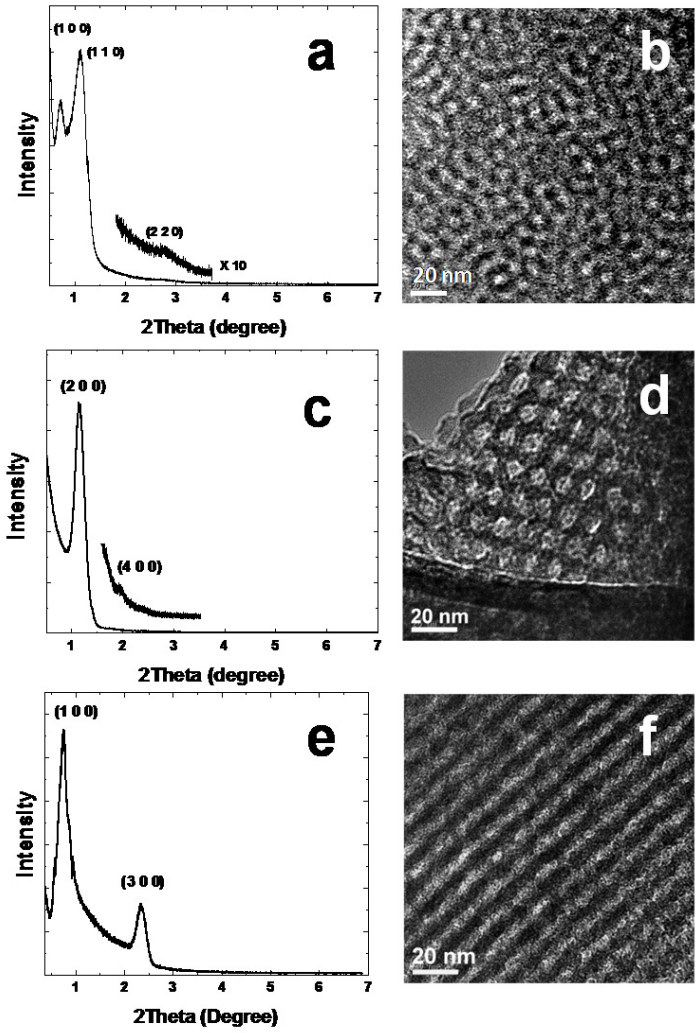


Figure 3.7: The physical characterizations of mesoporous silica thin films. XRD patterns (a, c, e), TEM (inset b, d, f) for the structural transformation of mesoporous thin films prepared using Pluronic F127 at different concentrations in the precursor solution: $4.0X10^{-3}$ M (a, b), $6.0X10^{-3}$ M (c, d) and $8.0X10^{-2}$ M (e, f).

$N_2$ adsorption/desorption curves were generated using a Quantachrome Autosorb-3b BET Surface Analyzer and the pore size distribution was calculated using the Barrett-Joyner-Halenda (BJH) method. In Figure 3.8.a, the adsorption/desorption isotherms describe a Type IV isotherm with a H2 hysteresis loop (sloping adsorption branch and nearly vertical desorption branch), indicating a nanoporous structure with interconnecting channels. Inflection points appearing at $0.40 \leq P/P_0 \leq 0.75$ indicated the formation of ink-bottle shape nanopores. Increasing the F127 concentration to $6.0\times10^{-3}$ M yields a 3D honeycomb like nanostructure hexagonally arranged on the substrate, as confirmed by the previous figure. The adsorption/desorption isotherms, depicted with the pore size distribution in the inset of Figure 3.8.b, vary slightly from the similar adsorption-desorption Type VI isotherms described for the lower concentration F127 mesoporous silica thin films due to the increased internal pore connectivity. A further increase of the F127 concentration to $8.0\times10^{-3}$ M resulted in a 2D hexagonal nanostructure parallel to the substrate surface. The adsorption/desorption isotherms (Fig. 3.8.c inset) displays a narrow hysteresis loop indicating significantly less inter-pore connectivity than either of the previous two mesoporous silica thin film morphologies. The similar pore size distributions of the 3 different nanostructures, with average pore sizes around 3.7 nm, illustrate that the change of pore size was minimally dependent on the molar ratios of the starting materials.

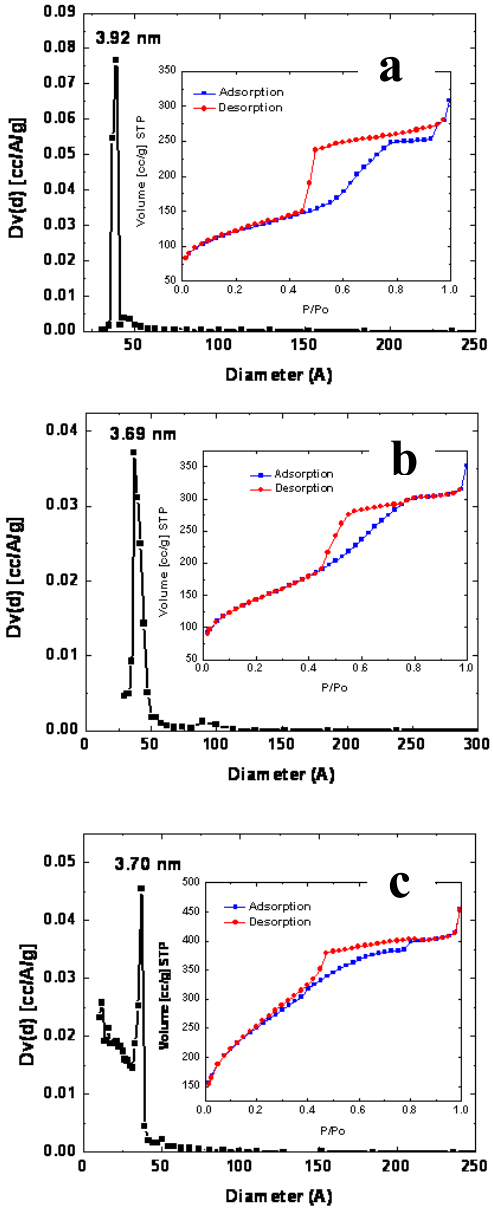


Figure 3.8: $N_2$ adsorption/desorption analysis (pore size distribution, isotherms in the insets), of the structural transformation of mesoporous thin films prepared using Pluronic F127 at different concentrations in the precursor solution: $4.0X10^{-3}$ M (a), $6.0X10^{-3}$ M (b) and $8.0X10^{-2}$ M (c).

### 3.3.3 Application of Different Types of Nonionic Surfactants

#### 3.3.3.1 Effect on Pore Structures of Mesoporous Silica

Another factor that influences the interfacial curvature between the polymer and the other solution components (TEOS, water, etc.), and thus determines the nanostructure and the pore size, is the hydrophilic/hydrophobic volume ratio of the copolymer. A series of tri-block copolymers with different hydrophobic (PPO) to hydrophilic (PEO) volume ratios were selected to synthesize the mesoporous silica thin films with different pore sizes and morphologies and subsequently investigated for their LMWP harvesting efficacy. Block copolymer compositions with longer PPO block lengths lead to increased pore size. Longer PEO block lengths for a given PPO block length (L121 versus P123 versus F127) lead to the formation of more highly ordered periodic nanostructures. [4] L-type (liquid phase) block copolymers (such as L64 and L121) with lower PEO block lengths offer increased porosity due to their greater deforming performance but more chaotic nanostructure. Figure 3.9 displays XRD patterns for mesoporous silica thin films prepared from P123, F127, L64 and L121+PPG (with molar ratio of 1:0.5) detailing their internal nanoscale organization. In the spectra for the mesoporous silica thin film prepared with P123 (molar ratio P123/TEOS = $5.9\times10^{-3}$) (Figure 3.9.a), the appearance of an intense and narrow peak for the (200) reflection at 1.66° of 2θ and $d_{200}$=5.31 nm combined with a lower intensity (310) peak at 2θ=2.99° indicate the formation of a hexagonally arranged periodic silica nano-composite thin film after calcination at 425°C. The absence of the (110) reflection indicates that the (100) plane of the 2D hexagonal unit cell was parallel to the surface of the silicon substrate. The mesoporous silica thin

film prepared with F127 (Figure 3.9.b) (molar ratio F127/TEOS = $1.13\times10^{-2}$) also exhibits an ordered nanoporous morphology indicated by the highly intense (100) reflection peak at 2θ=0.99° ($d_{100}$=8.89nm). The lower intensity peaked at (110) with $d_{110}$=6.27nm and (200) with $d_{200}$=4.80nm points to the formation of a 3D honeycomb-like hexagonal nanostructure. The XRD patterns for those fabricated by L-type block copolymers are shown in Figure 3.9.c (for L64) and 3.9.d (for L121 with PPG). Their low intensity and broad peaks in the small angle region were caused by the formation of unordered worm-like nanopores.

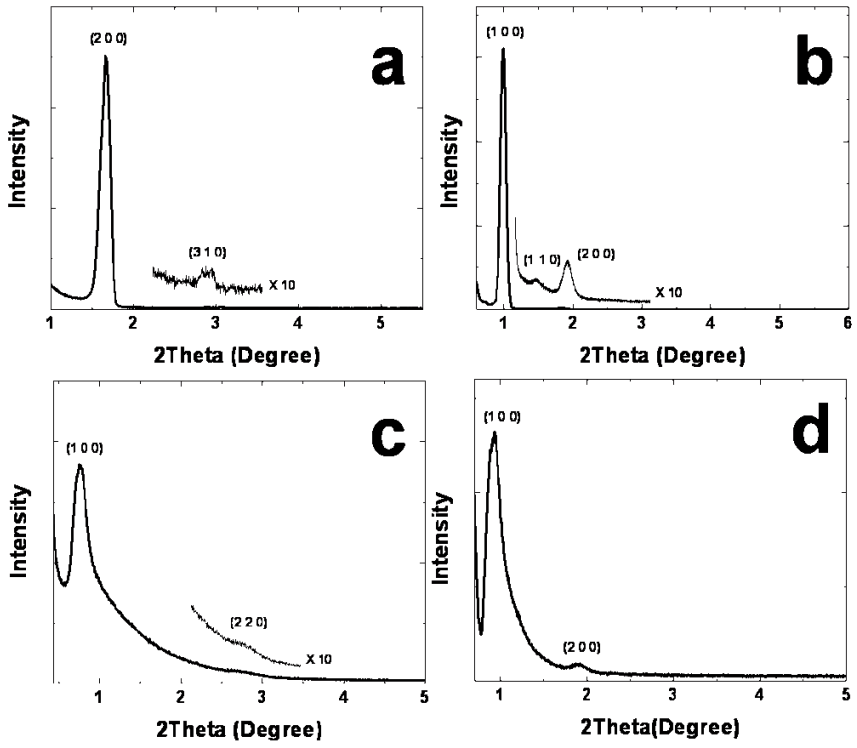


Figure 3.9: XRD patterns of nanoporous silica thin films prepared using (a) P123, (b) F127, (c) L64 and (d) L121+PPG (1:0.5) as structure-directing template polymers.

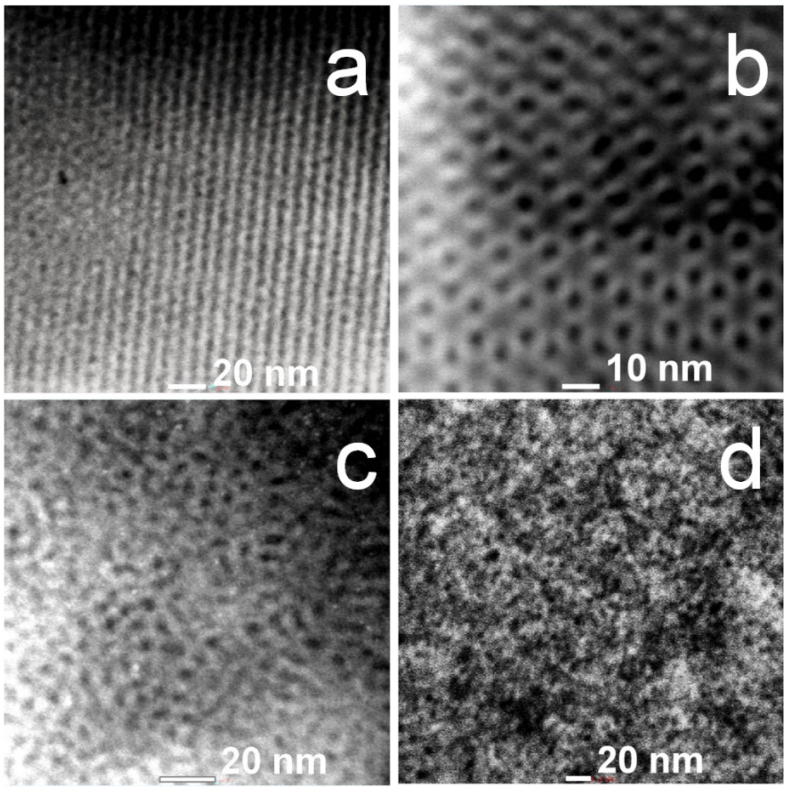


Figure 3.10: STEM images for plant view of nanoporous silica chips made by different surfactants with certain molar ratio of TEOS/surfactant. a. P123 at P123/TEOS = $9.4\times10^{-3}$, b. F127 at F127/TEOS = $9.4\times10^{-3}$, c. L64 at L64/TEOS=$4.14\times10^{-2}$, d. L121 at L121/TEOS = $1.09\times10^{-2}$.

Scanning transmission electron microscopy (STEM) analysis was performed on the plane view of mesoporous silica thin films. Figure 3.10 displays plane-view images of mesoporous silica thin films prepared with different copolymers under various experimental conditions. As shown in Figure 3.10.a, 2D-hexagonal nanostructure was formed with porous silica thin film prepared with P123 as template with the molar ratio of P123/TEOS = $5.9\times10^{-3}$ at a pH value of 1.38 in precursor solution. Figure 3.10.b

displays a 3D cubic nanostructure formed by F127 as template with a molar ratio of TEOS/F127 is $9.4\times10^{-3}$. As discussed above, a copolymer with a higher ratio of hydrophilic/hydrophobic chains that prefers to form an ordered nanoporous structure (such as P123 and F127), while L-type block copolymer (Pluronic L64 or L121) cannot provide periodic nanotexture with silicate. Figure 3.10.c and d are the STEM images of the top view of mesoporous silica thin film prepared with L64 and L121. With the short hydrophobic chain (PPO), the nanopore with L64 provides the smaller pore size than the one with L121.

### 3.3.3.2 Effect on Pore Size Distribution of Mesoporous Silica

$N_2$ adsorption-desorption isotherms were measured to assess pore size distribution and total surface area of the mesoporous silica thin films. The BJH pore size distributions for chips prepared by P123 (Fig.3.11.a), F127 (Fig.3.11.b), L64 (Fig.3.11.c) and L121 (Fig.3.11.d) showed low pore size dispersion as denoted by the sharp distribution peaks and the adsorption/desorption isotherms (insets). Figure 3.11.a, b and c show Type IV adsorption/desorption isotherms with well-defined $H_2$ hysteresis loops. The inflection points appearing at $0.40 \leq P/P_0 \leq 0.75$ indicate the formation of ink-bottle shape nanopores. The mesoporous silica thin films prepared using P123 and F127 possessed similar mean pore size (~3.7 nm) due to their identical PPO block volume, but the mesoporous silica prepared with P123 were characterized by a poor connectivity as indicated by the narrow hysteresis loop. Shown in Figure 3.11.d for chips prepared with L121, the pore diameter distribution peaks shift towards the right from 5.82nm to 6.79nm

and became broader with increasing amounts of the swelling agent. Their adsorption/desorption isotherms were also Type IV but with a H1 hysteresis loop which was attributed to the cylindrically shaped pores. Adding the certain amount of PPG did not result in any change in the loop shape, indicating that inner pore connectivity is not destroyed by the swelling agent used for the chips prepared with L121. Although the mesoporous silica thin films prepared with L64 possesses similar adsorption/desorption isotherms with L121, its shorter hydrophobic chain (PPO) led to nanopores with smaller pore size (~3.2 nm), as shown in Fig.3.11.c.

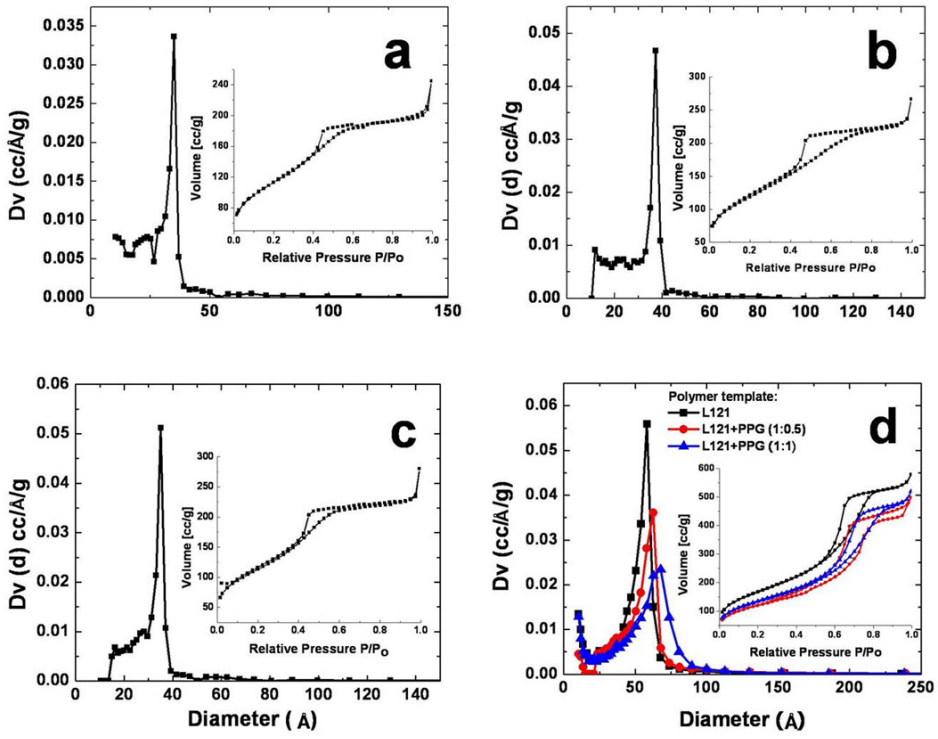


Figure 3.11: Pore size distribution of nanoporous silica thin films prepared by different polymer as templates: a. P123; b. F127; c. L64; d. L121 and L121 with the molar ratio of 0.5 and 1.0 swelling agent (PPG).

### 3.3.3.3 Surface Hydropholicity of Mesoporous Silica Thin Films

The hydrophilicity of chip surface was another factor to consider in selecting LMWP from serum. The contact angles of mesoporous silica thin film surfaces were tested by captive bubble contact angle goniometry to characterize the hydrophilicity of the chips' surface. All mesoporous silica chips prepared with the four different tri-block copolymers were hydrophilic (contact angle < 30 °).

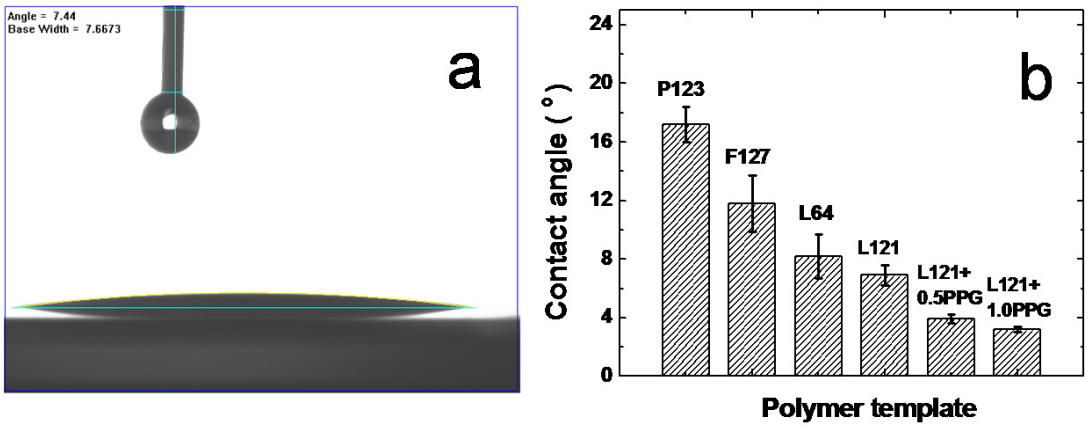


Figure 3.12: Contact angle goniometry for mesoporous silica thin films. a. A representative image of contact angle measurements for the mesoporous silica chips prepared using L121; b. A chart of contact angles for all mesoporous silica thin film chips developed.

Figure 3.12.a shows the image of a water droplet on the surface of a chip prepared with L121. This is a representative image illustrating the high hydrophilicity of the mesoporous silica thin film surface. The chart in Figure 3.12.b details the contact angles of all mesoporous silica thin film chips that have been developed. The mesoporous silica

thin films prepared from L121 exhibited the highest hydrophilicity due to the formation of their capillary condensation, increasing with the addition of the swelling agent. The mesoporous silica thin film surface prepared by P123 presented the lowest hydrophilicity among all the chips examined in this study resulting in the highest contact angle.

## 3.4 Conclusions

Synthetic surfactant directed self-assembly allows for formation of different mesoporous silica thin film periodic nanostructures, which are formed using high molecular weight triblock copolymers such as Pluronic F127 with similar pore size distributions. The structural transformation can be obtained by tuning the polymer concentration in the precursor solution. With the change of interfacial curvature between the phases of polymer and solvents, nanostructure of final porous products can vary from periodic 2D-hexagonal, 3D cubic, to 3D honeycomb hexagonal. Precisely controlled variations in pore size can be achieved through the use of copolymers with differing hydrophobic block lengths to form pore sizes from 2nm to 10 nm. This range of pore sizes led to the recovery of a different repertoire of peptides and proteins from the same serum sample via size and shape exclusion. In the next chapter, we will discuss how the individual or integral use of different mesoporous silica thin films with carefully tailored characteristics provides a novel platform for the rapid and efficient analysis of the LMWP in human serum.

# CHAPTER 4

# SERUM FRACTIONATION ON MESOPOROUS SILICA SUBSTRATES

## 4.1 Introduction

A promising strategy for early disease diagnosis is the detection of molecular biomarkers from readily available body fluids, such as blood. [147, 152, 153] Considerable attention has been devoted to the development of proteomic methods for the quantitative and simultaneous detection and identification of molecular biomarkers, including various proteins and peptides, using Mass Spectrometry (MS). [35-37] prior to MS analysis, several sample treatment strategies have been developed including conventional 2-dimensional gel electrophoresis, pre-fractionation processes, depletion of most abundant proteins, and beads equalization. In spite of these advances, less effort has been made to overcome the problems of sample denaturation and degradation during long sample handling procedures, maintenance of protein stability during sample processing, and stabilization of samples during long-term storage. Furthermore, as we discussed in the previous chapters, the detection of low abundance and low molecular weight (LMW) species remains a critical challenge due to experimental variability, limited reproducibility, long sample handling procedures, protein stability during sample processing, and generation of misleading artifacts as a consequence of unreliable experimental procedures. Innovative technologies addressing these issues are mandatory for discovery of new biomarkers. The development of nanomaterials, with controllable

features offering advantageous new physico-chemical properties, has widely improved the use of nanotechnology in biomedical applications.

In this chapter, we discuss the size-exclusion strategy for the exclusion of the high molecular weight proteins and for the specific isolation and enrichment of LMW species. This approach is based on combinatorial mesoporous silica substrate able to fractionate and selectively harvest peptides and proteins present in complex human biological fluids and protect them from enzymatic degradation. The mesoporous silica chips operate with rapidity, high reproducibility, no sample pre-processing, and substantial independence from sample acquisition and storage temperature.

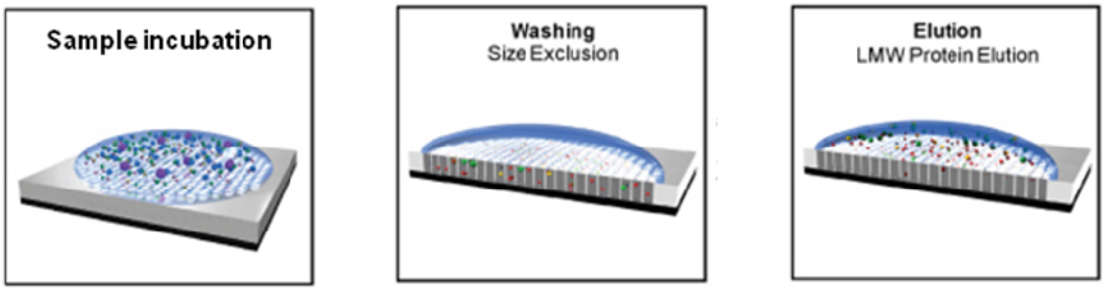


Figure 4.1: Principle of MSC fractionation and LMW enrichment. After sample spotting on the surface, LMW proteins and peptides are trapped into the pores while the larger species remained outside the pores and are removed during the washing steps. The enriched fractions are then eluted and analyzed by MALDI.

Detailed protocol for serum fractionation using our MPS thin films will be described in the experimental section. Briefly, the principle of this fast, on-chip fractionation strategy is shown in Figure 4.1: 1- The sample is spotted on the chip surface

and LMW molecules are trapped in the pores during the incubation step; 2- The larger protein species remain outside the pores and are removed during the washing steps; 3- The enriched small molecules are then eluted from the pores and further analyzed by MS. Matrix Assistant Laser Desorption/Ionization Time-of-Flight Mass Spectrometry (MALDI-TOF MS), a golden standard technology of today that is playing an essential role in proteomic study, will be briefly introduced before demonstrating the procedure of serum fractionation. To optimize the fractionation efficacy, several experimental parameters have been comprehensively investigated, such as temperature, sample amount, washing times, incubation duration, area of contact surface and selection of elution solvent. Due to the relative instability of blood samples, several publications have reported the importance of pre-analytical sample management to avoid the accumulation of artifacts and significant alterations in the proteomic profiles. [21] Therefore, fractionation reproducibility and reliability are mandatory for any further development of reliable proteomic and peptidomic screening techniques for clinical applications. [154, 155] To assess the consistency of our on-chip fractionation strategy, we screened multiple replicates with the same human serum sample using all of the mesoporous silica thin films we prepared. Finally, sample stability, the protection from degradation with mesoporous silica substrates, will be also illustrated in this chapter.

## 4.2 MALDI-TOF MS in Proteomics

### 4.2.1 Basic Principle

Mass spectrometry (MS), an analytical technique used to determine the elemental composition of a molecule or peptide, has been used as a diagnostic tool or disease biomarker discovery platform in clinical laboratories for many decades. [18, 21, 31, 156-161] The steps involved in MS are as follows: 1. ionizing chemical compounds to generate charged molecules or molecule fragments, 2. directing the ions into an electric and/or magnetic field, 3. measuring the *m/z* of the particles based on the details of motion of the ions as they transit through electromagnetic fields. In 1980s, the development of the two ionization MS methods, electrospray ionization (ESI) and matrix-assisted laser desorption/ionization (MALDI), revolutionized protein chemistry and fundamentally changed protein analysis. Coupled with gas chromatography, MS has been successfully used to identify and quantify relatively small molecules (with molecular mass <1,000 Da). Although ESI gained immediate popularity because of its easy operation which combined popular chromatographic and electrophoretic separation techniques, MALDI integrated with a time-of-flight (TOF) mass analyzer is more suited to sensitive identification of a large range of peptides and proteins in complex samples.

### 4.2.2 MALDI-TOF MS in Analysis of Peptides, Proteins and proteomics

MALDI-TOF MS provides a rapid approach to identify the heterogeneity of peptides and proteins by determining their unique molecular mass. [162-165] When laser pulses are used to achieve desorption/ionization of proteins, molecular ions are formed,

most of whom are ionized to a single positive charge. But the occurrence of multiple ionic forms complicates the overall pattern and depends on variables such as sample composition, sample preparation, and type of matrix used.

The restraints of MALDI-TOF MS depend on many factors that may change detection sensitivity by orders of magnitude, such as the ionization efficiency of different peptides, so any general statements about detection limits must be considered as rough approximations. For small peptides, the detection limits of MALDI-TOF MS can extend to 1 mol under optimal conditions. Usually, larger peptides and proteins are detected with lower sensitivity and require concentrations > 1 μmol/L for analysis. This is particularly true for complex mixtures of proteins such as human serum, where 22 large proteins constitute ~99% of protein content and protein concentration possesses an extremely high dynamic range. Therefore, most plasma proteins detected by MALDI-TOF MS have concentrations >1 μmol/L without the extensive sample fractionation.

In order to identify a specific peptide or protein by MALDI-TOF MS, the major challenge for many analyses of physiological fluids is to optimize the sample preparation which allows for the depletion of salts and enrichment of the protein or peptide of interest. Conventional methods for sample fractionation include chromatography, solid-phase extractions, dilution, and fractionation directly on specialized target surfaces in SELDI-TOF MS or separation with magnetic particles. [166-174] However, these approaches often exhibit some drawbacks such as low efficiency, low-throughput and they are often not suited to harvest the low molecular weight proteome, which

ultimately limits their potential to assist MALDI-TOF MS to be a key technology in clinical diagnostics.

### 4.2.3 Mass Spectrometry as a Biomarker Discovery and Diagnostic Tool

In 2006 the application of mass spectrometry as a diagnostic tool was first investigated by Petricoin and colleagues. [9] The MS profile in their study represented a paradigm shift in MS spectra between proteomic patterns in serum samples between patients with or without cancer identified by bioinformatics. It was realized that the potential to discriminate between different stages of disease should be further explored. As we discussed in origin of biomarkers, protein or protein fragments produced by a cell's mutation or produced in a tumors' microenvironment may eventually enter the general circulation. As a result, the change in concentration of these proteins/fragments could be analyzed by mass spectrometry and used for diagnostic purposes, in combination with biostatistics analysis. Studying the use of SELDI-TOF MS technology in the early diagnostics of ovarian cancer and prostate cancer has shown that the distinguishing peaks between cancer and non-cancer patients are very different between the various groups. However the disadvantages of this technique, including poor reproducibility and limited range of protein recovery, should be further considered.

### 4.2.4 MALDI-TOF MS with Proteomic Nanochips

In our study, the proteomic nanochips we developed were designed to overcome the drawbacks of conventional approaches used to detect serum biomarkers. This novel

nanotechnology-based method is showing the potential to extend the range of recovering proteomic biomarkers from human serum sample, particularly for those with low molecular weight, and improve the reproducibility of MS profiles for rigorous clinical request. The use of MALDI-TOF MS in this study plays a key role to providing the sensitive detection of LMWP. The serum fractionation on the proteomic nanochips has been discussed in the previous chapter. The details of operation on the extracted sample with MALDI-TOF MS are described as following.

## 4.3 Experimental

*Serum Fractionation* For each experiment, 10 μl of serum sample was pipetted onto the porous surface of the wafer square. The samples were incubated for 30 minutes at 25 degrees (room temperature) in a wet chamber (100% humidity) to prevent sample evaporation. The samples were washed 5 times with 15 μl of sterile, deionized water. Peptides and proteins were eluted from the pores using a 1:1 (v/v) mixture of acetonitrile and 0.1 % trifluoroacetic acid (TFA) (Sigma).

*Mass Spectrometry* A matrix solution of 5 mg/ml α-cyano-4-hydroxycinnamic acid (CHCA, Sigma) in a 1:1 mixture of acetonitrile and 0.1% TFA(v/v) or a saturated solution of trans-3,5-dimethoxy-4-hydroxycinnamic acid (SA, Sigma) in 2:1 mixture of acetonitrile and water (v/v) containing 0.1 % TFA was used for LMW and HMW analysis respectively. Each of the samples was mixed with the appropriate matrix in a ratio of 1:3, and spotted in duplicate onto the MALDI plate.

Mass spectra were acquired on a Voyager-DE$^{TM}$-STR MALDI-TOF (Applied Biosystems, Framingham, MA) mass spectrometer in liner positive-ion mode, using a 337nm nitrogen laser. Samples were evaluated at two m/z ranges. For LMW peptides and proteins, m/z of 800-10,000 Da, using α-CHCA as matrix. Settings were optimized at an acceleration voltage 20 KV, grid voltage 19KV, guide wire voltage 1KV, delay time 180 ns, and low-mass gate 800. 300 laser shots crossed spot were averaged for each mass spectrum. For HMW proteins, parallel analysis using SA (Sinapinic Acid) as matrix and detection range of 3,000-100,000 Da was performed. The instrument was optimized at acceleration voltage 25 KV, grid voltage of 23.25 KV, guide wire voltage 6.25KV, delay time of 500 ns and low mass gate 3,000.

The spectra were calibrated externally using the ProteoMass standards of peptides and proteins (Sigma) in each mass range.

*Statistical Analysis* The raw spectra were processed with the Voyager Data Explorer software version 4.0 (Applied Biosystems) and the data was exported to SpecAlign software for pretreatment. [175, 176] All spectra were aligned using the PAFFT correlation method and intensities were normalized to total ion current (TIC). The peak detection was performed with a height ratio of 2 with 0.3% of the mass window, and the baseline was corrected and the negative values were removed prior to analysis.

## 4.4 Results and Discussion

### 4.4.1 Serum Fractionation on Mesoporous Silica Thin Films

Figure 4.2.a and b show the MS spectra of a serum sample with peptides in the range of 900 to 10,000 Da and proteins in the range of (3,000 ~ 70,000 Da); these serum samples have not undergone fractionation by the MPS thin films. These spectra illustrate the signal suppression in the LMW region due to the presence of well ionized, highly abundant, high molecular weight (HMW) proteins (Albumin, ApoA1). Figure 4.2.c and d depict the MALDI-TOF spectra of the serum sample after fractionation by the MPS thin films synthesized using L121 and swelling agent PPG at a molar ratio of 1:0.5. Enrichment of the LWM components is clearly evident as the majority of the large molecules in the serum sample haven been removed. As a control, the same serum sample was applied onto a nonporous pure silica surface to evaluate the specificity of MPS thin films for LMWP recovery. As can be seen in Figure 4.2e and f, there was not significant harvesting of peptides or proteins from the nonporous silica surface observed in the range of interest for both the peptide and protein mass. Thus it can be concluded that it was the mesoporous architecture and not the silica surface affinity that plays the key role in the enrichment of LMWP.

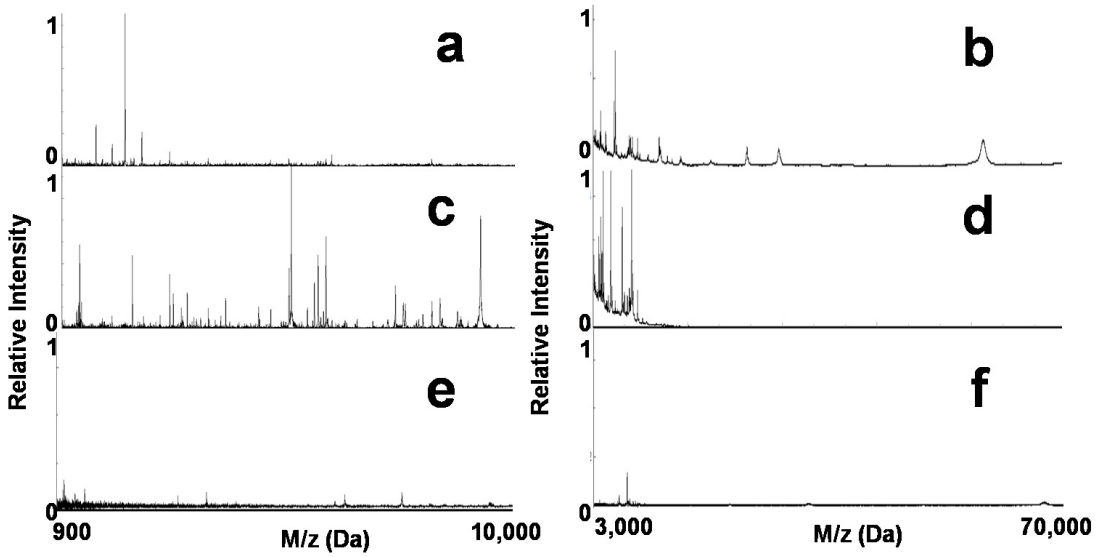


Figure 4.2: Efficacy of serum fractionation using the mesoporous silica thin film chips. MALDI MS profiles in both the low mass range (900 to 10,000 Da) and the high mass range (3,000 to 70,000 Da) before (a, b) and after (c, d) fractionation using the mesoporous silica thin films. The molecular recovery is significantly reduced when using blank non-porous silica surfaces for fractionation (e, f).

The substantial enrichment of LMW species is illustrated in Figure 4.3.a by comparing the MALDI intensities of common peptides and proteins before and after the on-chip fractionation. The efficient removal of the most abundant HMW proteins (Albumin, Apolipoprotein AI and Hemoglobin) is shown in Figure 4.3.b by comparing their signal intensities in crude serum and after fractionation.

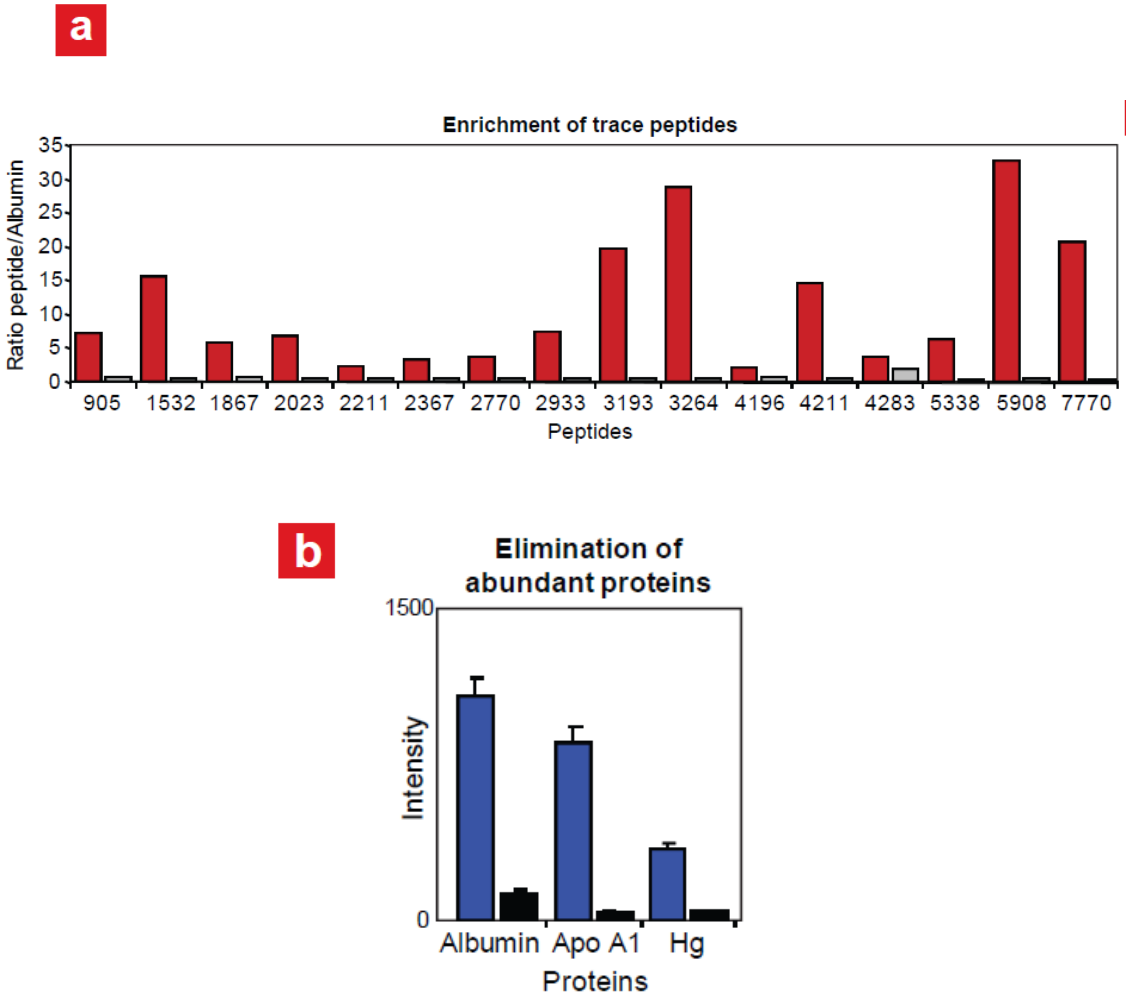


Figure 4.3: a, the comparison of the peptide/Albumin ratio illustrates the enrichment of LMW peptides detected in both serum (in red) and elution (in black). b, Comparison of the intensities of Albumin, Apolipoprotein A1, and Hemoglobin detected by MS in crude serum (in blue) and in the elution (in black).

### 4.4.2 Reproducibility of Serum Fractionation on Mesoporous Silica Thin Films

We screened 6 replicates with 6 aliquots of the same human serum sample using MPS thin films prepared by L121+PPG with a molar ratio of 1:0.5. Figure 4.4.a and b display the MALDI profiles in the mass range 900 to 10000 Da (peptide range) and 3,000 to 70,000 Da (protein range) of 6 independently processed replicates of fractionated serum. They exhibit a highly reproducible peak identity and intensity. The general variability of the peak signals is illustrated on the histogram displaying the repartition of the coefficients of variation (CV) measured for each detected peak (Fig.4.4.c). The average CV was estimated at 13.1%, which demonstrated a high reproducibility for the detected peaks over a wide mass range of 800 to 20,000Da. The regression curve and equation comparing the peak intensities recovered from the replicates are illustrated in Figure 4.4.d and exhibit a coefficient of regression $R^2 = 0.988$. These results confirmed that the on-chip serum fractionation did not induce any significant variability in the sample and demonstrated the reliability of our MPS chips in the pre-treatment of complex biological samples. The minor statistical variations are due to the internal variability of the MALDI instrument.

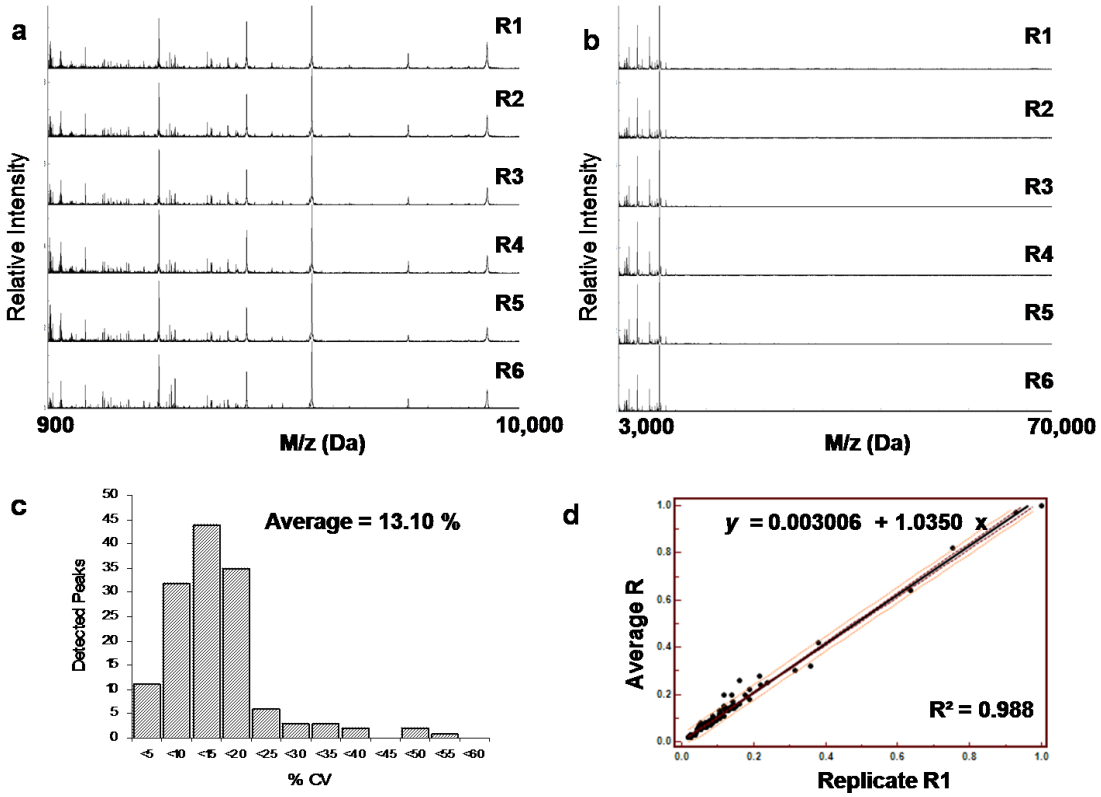


Figure 4.4: Statistic study of reproducibility of on-chip fractionation on MS profiles of a. low mass range and b. high mass range, c. Average CV from histogram and d. regression curve.

### 4.4.3 Evaluation of Protein Recovery

In order to determine the sensitivity of protein recovery from the nanoporous chips, absorbance values were converted into protein amounts using the formula calculated through a standardization curve in Figure 4.5. For every experiment performed, results were internally standardized using known amounts of Albumin (0.5µg/ml to 30µg/ml) based on the instructions of the microBCA kit.

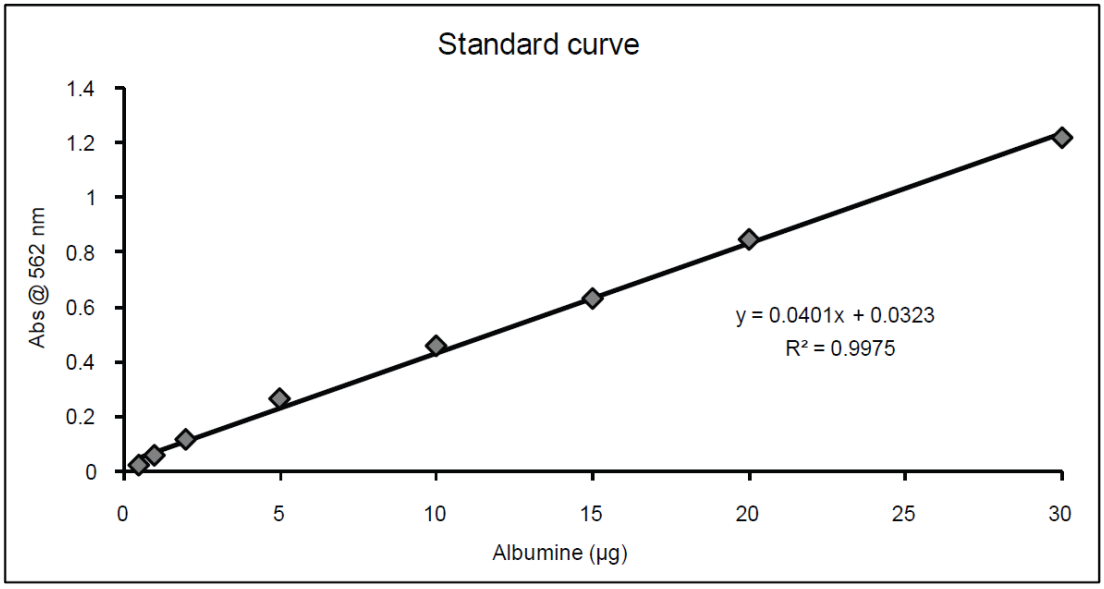


Figure 4.5: Standardization curve. A representative standardization curve made according with the instructions provided by the microBCA protein assay kit. The graph shows the regression curve that fits the experimental results, its formula and its coefficient of determination ($R^2$). The equation was used to convert the experimental data obtained through Spectrophotometer readings of sample absorbance at 562nm to the corresponding protein amount in µg.

## 4.5 Optimization of Serum Fractionation on Mesoporous Silica Chips

### 4.5.1 Effect of Contact Surface Area on Protein Fractionation

To optimize the fractionation efficiency, three different masking strategies were developed and assembled on the mesoporous silica chips, defininga circular spotting area (diameter 10, 6.5, 3.25, 2 mm, as shown in Figure 4.5). For each mask type, we studied

the protein binding properties and assayed serum confinement and stability in the spotting area.

The chips were patterned with a hydrophobic photoresist, SU-8 using photolithography. The SU-8 worked as a hydrophobic ring to confine the sample within the non-covered area. To define the SU-8 pattern, SU-8 was spin-coated on the nanoporous silica chip at 500 rpm for 20 seconds. Then the chip was baked on a hotplate (65°C 5 min, followed by 165°C 10 min). A pattern array of well defined shape and size was transferred to the silica film by contact photolithography. The resist was developed in SU-8 developer for 20 min, and the patterned wafer was post-baked at 95°C for 12 minutes. Fabrication of patterned PDMS film was started by mixing elastomeric base and curing gel at a weight ratio of 10:1 followed by bubble removal in vacuum. 10g of PDMS was slowly poured into the mold, and allowed to settle. The mold was transferred to an hotplate (145 C, 20 min). The PDMS film was gently peeled off the mold and delivered. Silicone rubber masks were manufactured using 1.6mm thick silicone rubber sheets (transparent, 40 DURO hardness, with adhesive layer from 3M) obtained from McMaster-Carr. The sheets were cleaned and cut to 100mmx100mm squares.

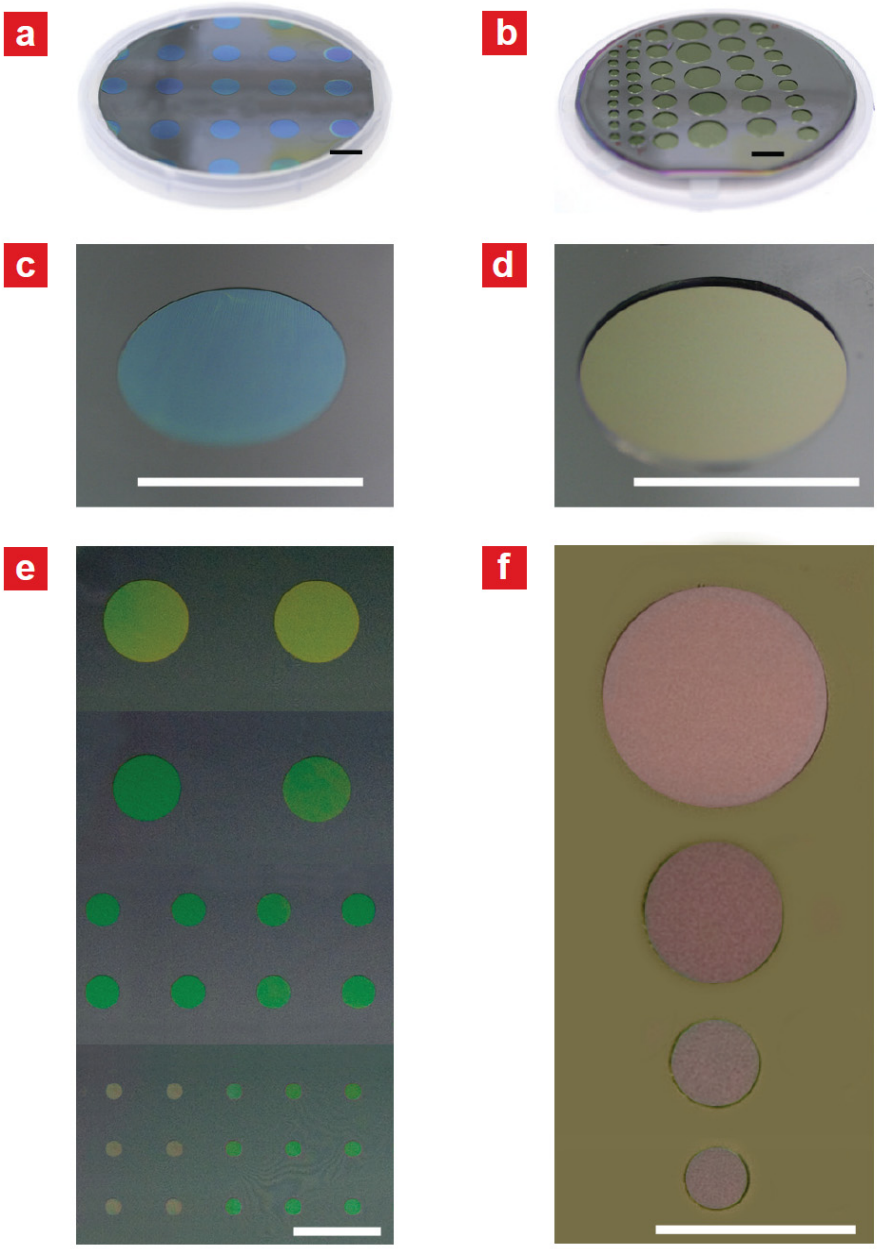
a
b
c
d
e
f

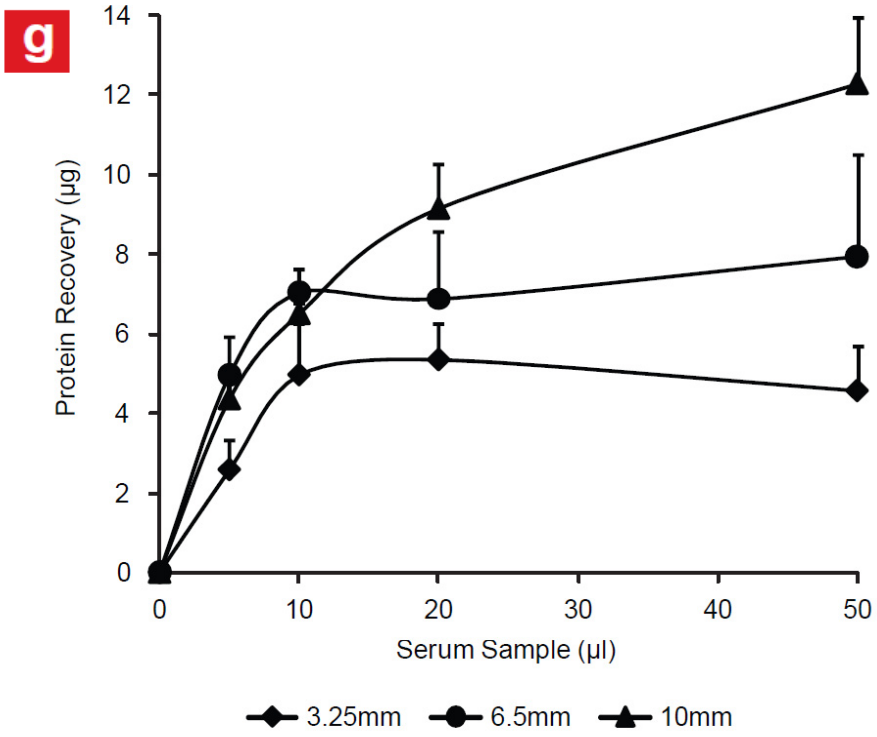


Figure 4.6: Photographs of mesoporous silica chips patterned either with a 50µm thick SU-8 hydrophobic photoresist (a, c, e) or with a 500µm thick molded PDMS film (b, d, f). In C and D, note the relative thickness of the different material masks (SU-8 and PDMS respectively). The top views of different SU-8 and PDMS patterned chips (E and F respectively) with decreasing fractionation areas show the uniformity of the surfaces employed for the sample fractionation. g. Protein recovery from 12 independent experiments performed with increasing amount of serum samples (5, 10, 20 and 50 µl) on different nanoporous surface areas (diameters equal to 3.25, 6.5 and 10mm; same chip type) using the same settings (temperature, time, washings).

### 4.5.2 Effect of Sample Amount on Protein Fractionation

To minimize the amount of serum needed, we studied the effect of sample volume on protein recovery on the different spotting areas. Depending on the profile of Figure 4.7 we demonstrated that 10µl was the optimal sample size.

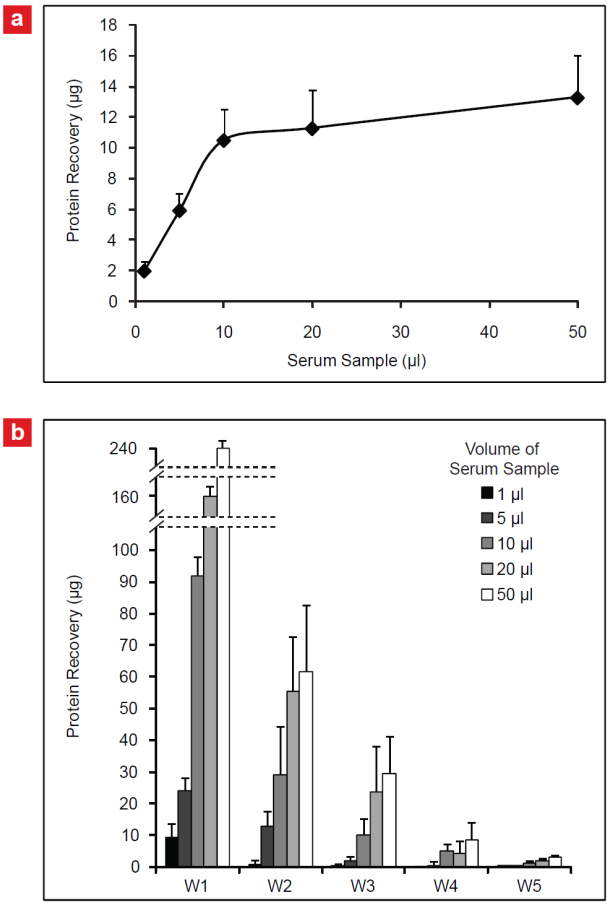


Figure 4.7: Effect of sample volume on protein fractionation. a, Evaluation of the protein recovery from a series of fractionation experiments performed using different amount of serum on the same chip type. The amount of protein recovered is very low when only 1 and 5 µl of serum are used. Protein recovery reaches a plateau when 10 µl of serum are used. The incubation of 20 and 50 µl of

serum did not result in a higher protein recovery. b, The amount of protein in the washing samples increased with the increase of the serum used for fractionation.

### 4.5.3 Effect of Washing Steps on Protein Fractionation

The washing procedure was optimized to ensure complete removal of the HMW proteins absorbed on the surface of the MSCs. After each washing step, we performed MALDI analysis and measured the protein content. We determined that after 5 washes large proteins were almost absent, and that their peak intensity was negligible compared to the peak intensity of the LMW proteins and peptides (Fig. 4.8.a intermediate panels). The amount of protein removed during the washings decreased with each step and by the fourth wash, the amount of HMW proteins on the mesoporous silica chips surface was negligible compared to the amount of protein eluted from the chip. Figure 4.8.b exhibits that after 5 washes large proteins were almost absent. Moreover, the MALDI analysis of the samples eluted from the wafer did not show the presence of any Albumin or HMW protein confirming that the pores of the silica wafers could retain only LMW proteins and peptides. As displayed in Fig 4.8.c, the amount of protein recovered from the chip in the elution step was significantly higher than the amount of protein measured in the last 2 washing steps. A possible explanation for this result is that by the fourth and fifth washes the amount of protein on the surface was almost null. Additional washing would remove the LMW proteins trapped into the nanopores of the mesoporous silica chips. On the basis of these considerations, we concluded that the minimal number of washing steps

required was 5 and performed all the experiments described in the paper accordingly.

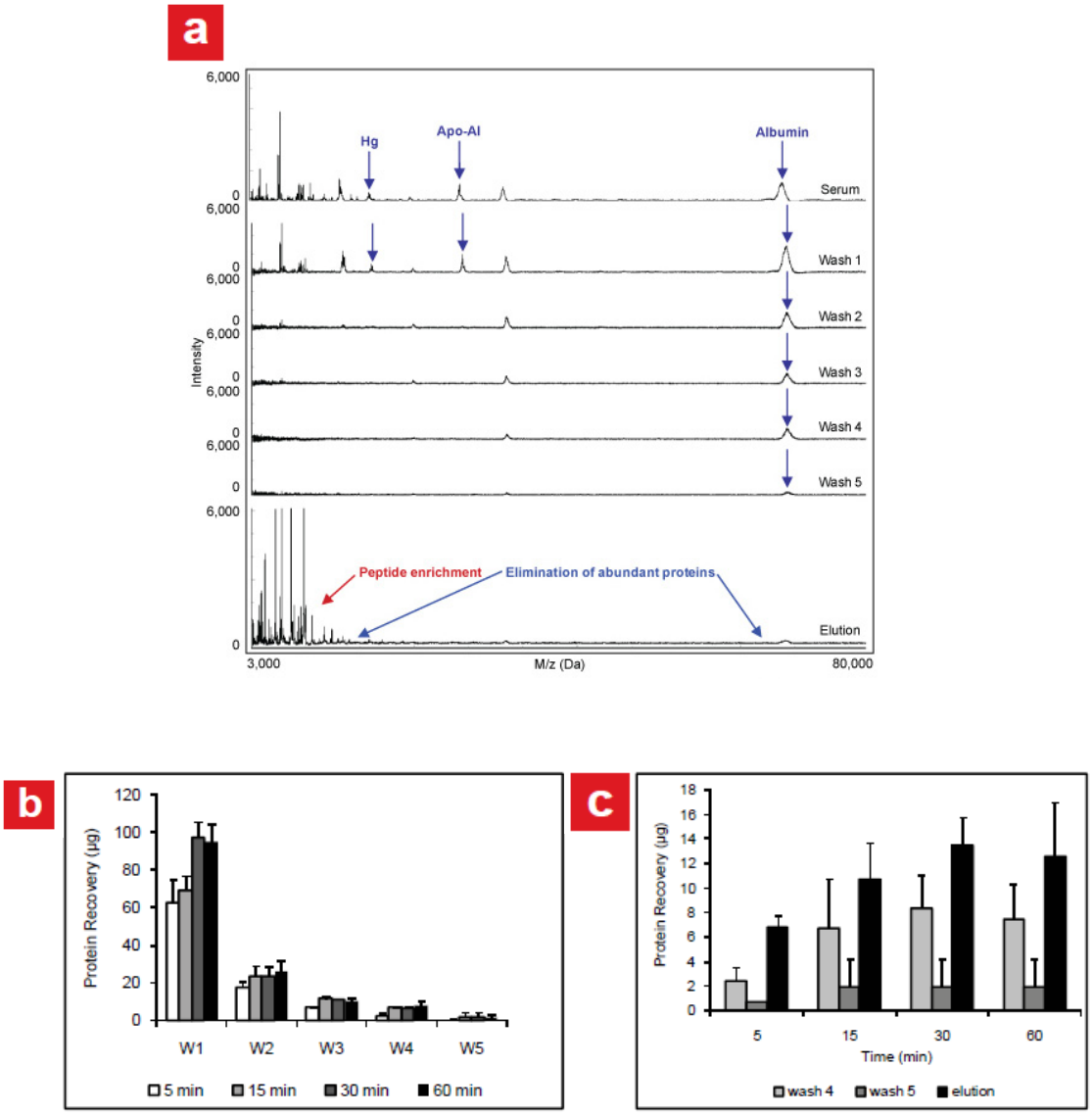


Figure 4.8: a. The MALDI profiles of the different steps of the methodology demonstrate the depletion of most abundant HMW proteins in the washings and enrichment of LMW species in the elution. b, Histogram comparing the

amount of protein removed during the washing steps. In the first wash, the amount of protein positively correlated with incubation time. Mean values and standard deviations of 3 independent experiments are shown. c, Comparison of protein recovery in the last 2 washing steps and in the final elution. In all conditions tested, the amount of eluted protein is significantly higher than the amount of protein removed from the surface during the last 2 washings.

### 4.5.4 Effect of Temperature on Protein Fractionation

To understand the effect of temperature on protein fractionation and identify the best working condition, experiments were performed at 4° C, 25° C and 37° C (Fig. 4.9). Protein recovery at 25° C and 37° C was not significantly different (Fig. 4.9.a), but 25° C was chosen as the optimal working temperature because of the associated higher reproducibility (Fig. 4.9.c and d). For all the chips tested, recovery was very low at 4° C. The low temperature might have affected process of diffusion into the nanopores [177] as well as the molecular interactions between the proteins and the silica surface [178].

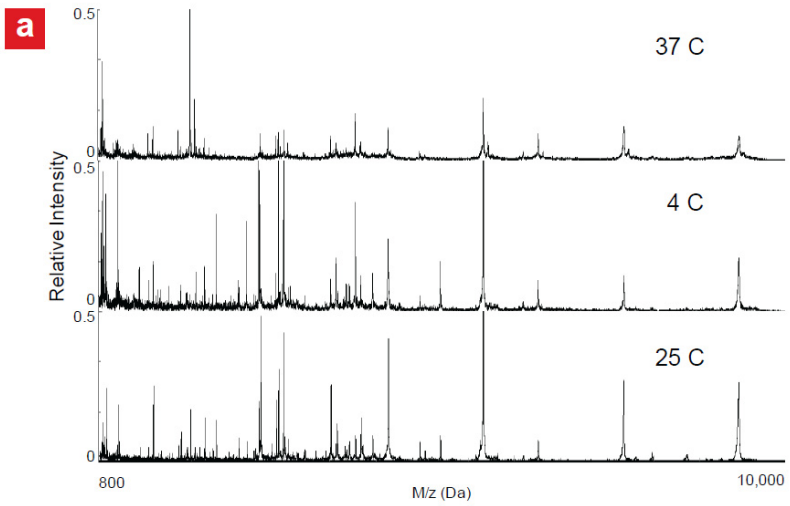

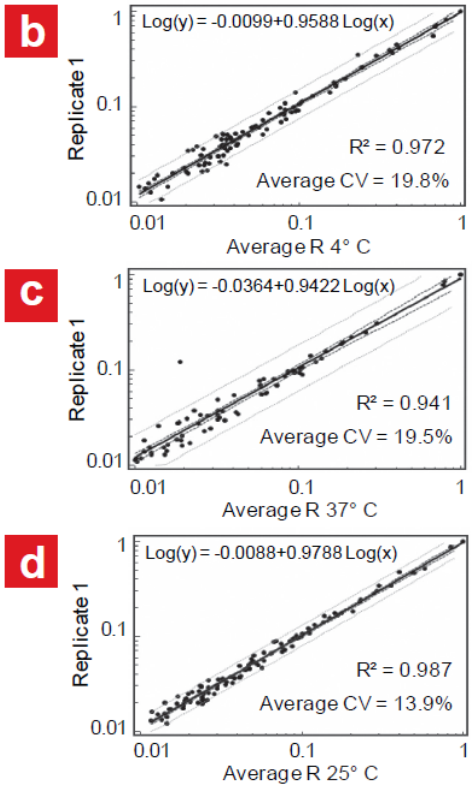


Figure 4.9: a, MALDI profiles of fractionated serum on X10 chip illustrate the increase of LMW peptides and proteins detection when the serum is processed at 25°C compared to 4°C and 37°C. b, c, d, Linear regression analysis of the average intensities of detected MS peak for each temperature. The comparison was plotted on a log–log scale to obtain a scatter-plot.

### 4.5.5 Effect of Incubation Duration on Protein Fractionation

By running the experiment at 25° C with fixed volumes of serum, we studied the influence of incubation time on protein recovery. 5, 15, 30 and 60 minutes of incubation time were carried out to investigate their effect to protein recovery. We concluded that

after 30 minutes of incubation, protein recovery reached a plateau, which is displayed in Figure 4.10. Further incubation time may increase protein degradation while not increasing protein recovery from the mesoporous silica chips. Figure 4.11.a exhibits MALDI profiles for protein recovery with four different incubation times. Statistical results (Fig 4.11.b) confirm 30 mins is the optimal duration to harvest the LMW peptides and proteins.

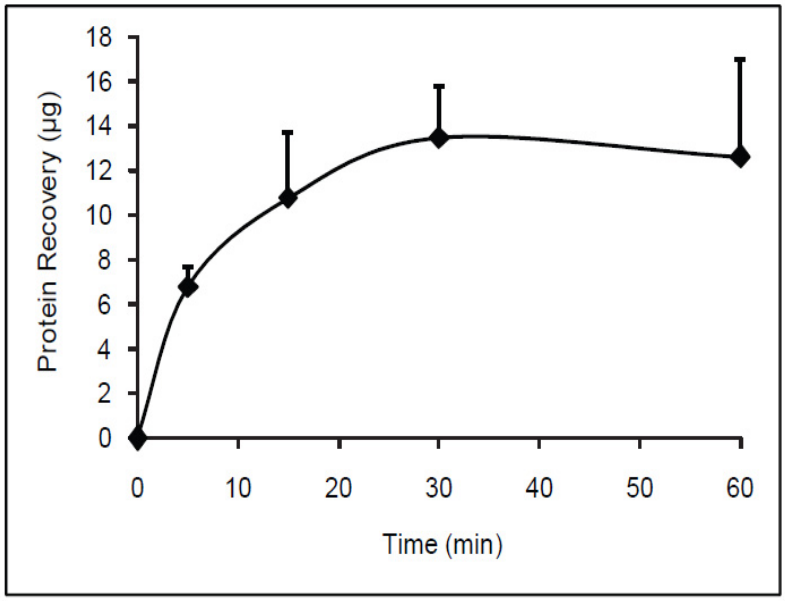


Figure 4.10: Effect of incubation time on protein fractionation. Total protein recovery after fractionation performed at different incubation times.

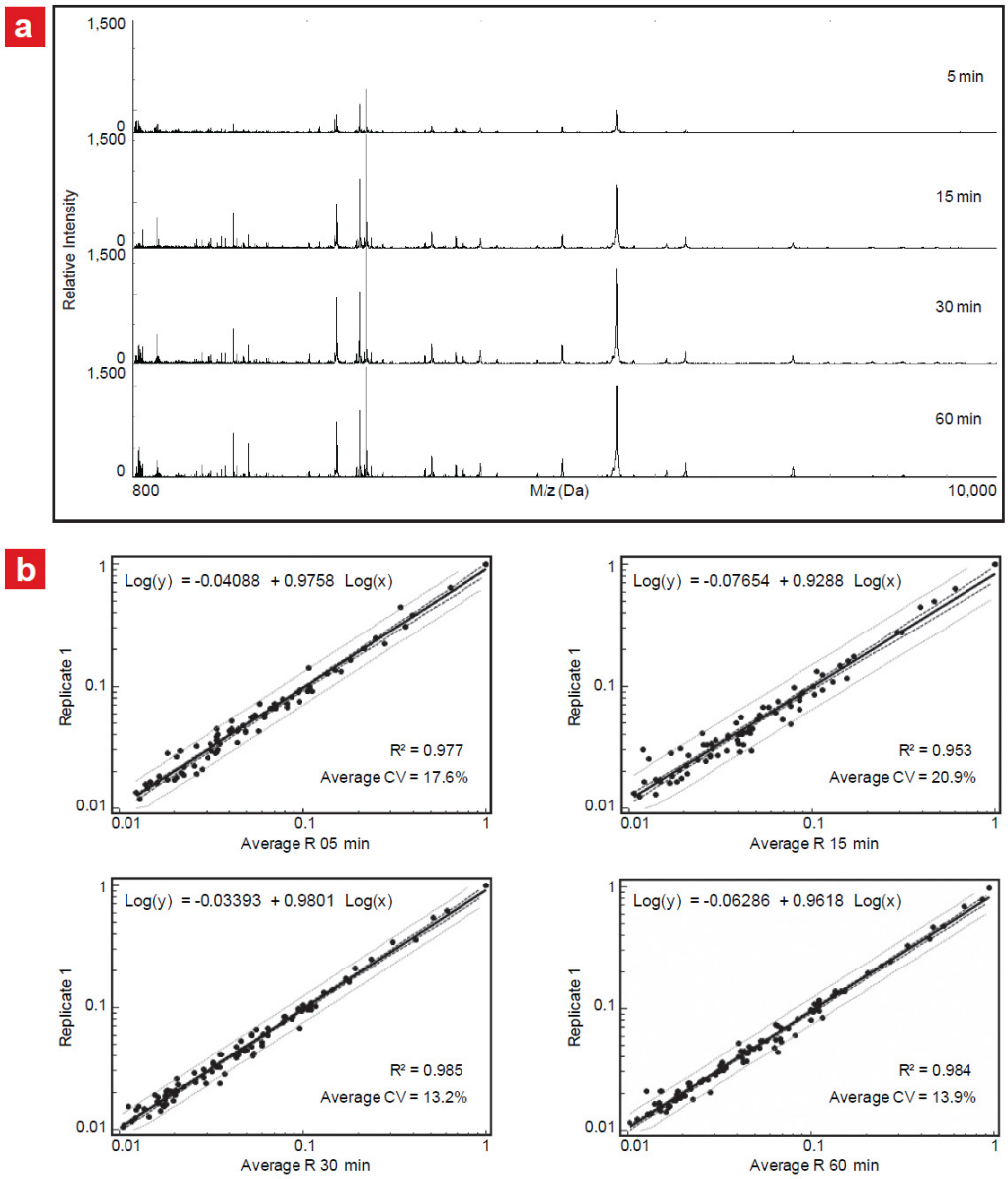


Figure 4.11: MALDI spectra obtained after different incubation times. a, MALDI profiles of fractionated serum on the mesoporous silica chip at different incubation time (5 min, 15 min, 30 min, and 60 min). The peak intensity is markedly lower for the 5 min incubation. The profiles for 15 min, 30 min, and 60 min show similar profiles. b, Linear regression analysis of the triplicate average

intensities of detected MS peak compared to replicate 1 for each incubation time. The comparison was plotted on a log–log scale to create a scatter-plot.

## 4.6 Sample Stability, Protection from Degradation

The use of MS profiling to correlate a disease with the specific changes in the circulating proteins is a promising tool to improve diagnosis, to allow the design of personalized therapies and to follow their efficacy in real time and with low invasiveness. Stability and reliability are crucial features for any clinical applications. To address the issue of protein stability we incubated the mesoporous silica chips with human serum, dried the chips after the washing steps, and stored them for 3 weeks. The same procedure was used to evaluate the stability of peptide and protein standards. Compared with a freshly fractionated sample, the results demonstrated similar peptide patterns as illustrated in Fig. 4.12.a and b. Based on mechanisms similar to those postulated by Luchini et al. [179] for hydrogel particles, we hypothesize that the LMW species trapped inside the nanopores were preserved from degradation through the exclusion of proteases from the nanopores, or by steric inhibition of their proteolytic activity in the confined space of the nanopores. The establishment of a simple sample acquisition and storage protocol and the ability to impede further degradation of the proteins and peptides once they are captured are crucial properties for translation of this new technology into the laboratory clinical practice [180, 181]. With previous methodologies, differences in blood sample acquisition, time elapsed before contact of the serum onto the capture surfaces,

environmental temperature and storage temperatures all resulted in the degradation-induced appearance of peaks that confounded the analyses and rendered meaningless the use of the profiles to derive any diagnostic or otherwise medically significant information. The fundamental advantage of the present approach, which makes it clinically viable, is that untreated blood can be drawn and directly placed onto the mesoporous silica chip, resulting in a pattern of stored information that is reproducible and stable in time, regardless of a broad range of temperature and environmental variables.

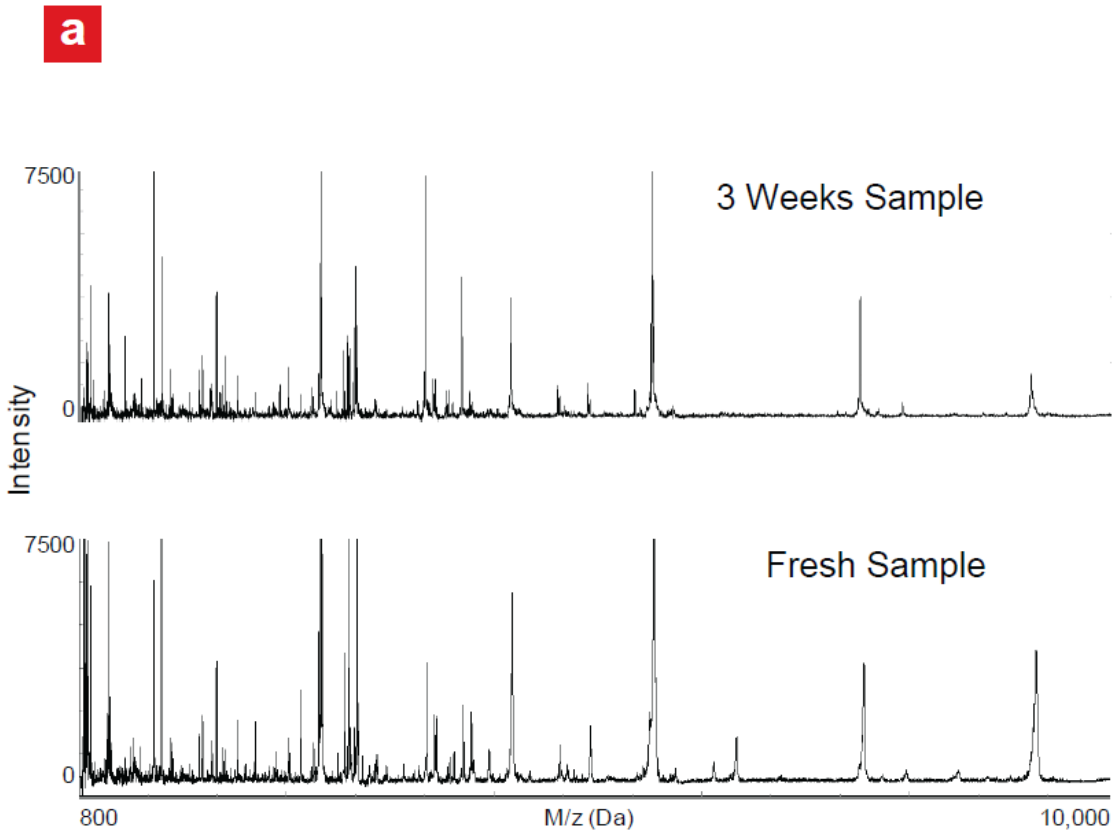

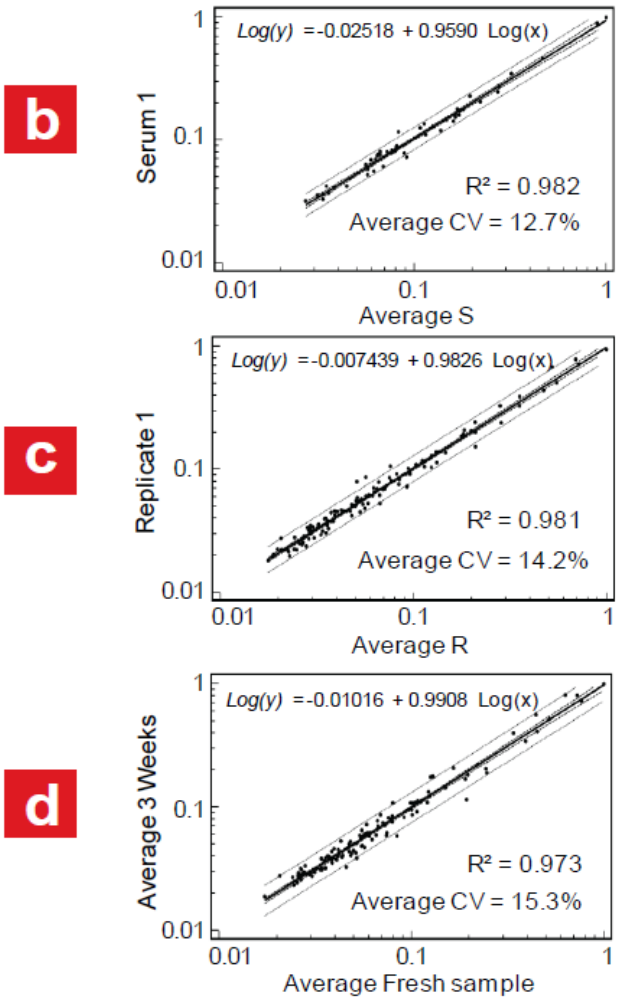


Figure 4.12: a. Representative MALDI profiles of LMW peptides and proteins eluted immediately after serum fractionation or after 3 week on-chip storage at room temperature. b, c, d, Linear regression analysis of average intensities of detected MS peak in each replicate compared to replicate 1 for crude, fractionated serum and fractionated serum after 3 week storage at room temperature respectively (the coefficient of variation (CV) and the coefficient of determination ($R^2$) are indicated in the insets).

## 4.7 Conclusion

The fractionation device composed of mesoporous silica thin films displays features that are desirable for exploratory screening and biomarker discovery. The constituent mesoporous silica chips may be custom-tailored for the sequestration and enrichment of extremely low abundance protein and peptides in desired ranges of the mass/charge spectrum. They are effective and yield highly reproducible extracts from extremely complex biological samples. They can process samples as small as 10 μl in a time as short as 30 minutes. They are inexpensive to manufacture, and their production can be easily scaled up to attain the simultaneous processing of a large number of samples. They are multiplexed, label-free diagnostic tools with the potential for additional modification with biological recognition moieties, for enhanced specificity. The mesoporous silica chips may be used to store, protect, and stabilize protein and peptide extracted from biological fluids to enable the collection and transport of clinical samples with simplified and cost-effective procedures. In the next few chapters, we will continue to expand the methods by whichour mesoporous silica chip based device may serve as diagnostic tool to complement histopathology, imaging and other conventional clinical techniques. The mesoporous silica chip-mediated identification of entire disease-specific protein networks may help in the selection of personalized therapeutic combinations, in the real-time assessment of therapeutic efficacy and toxicity, and in the rational modulation of therapy based on changes in the protein network associated with the prognosis and the drug resistance of the disease.

# CHAPTER 5

# SELECTIVE RECOVERY OF LMWP ON MESOPOROUS SILICA CHIPS WITH VARIOUS NANOTEXTURES

## 5.1 Introduction

In Chapter 3, we demonstrated that mesoporous silica films produced by evaporation-induced-self-assembly (EISA) during spin-coating showed tunable pore size, pore connectivity and structure. Using a range of processing conditions, we performed an extensive and rigorous characterization of the mesoporous silica thin films fabricated. In this chapter, we will control the nanotexturing (pore size and pore structure) with synthetic chemistry in order to selectively enrich fractions of interest of the serum proteome in the low molecular weight range. It is widely accepted that when the mesopore diameter is large enough to facilitate the comfortable entrapment of biomolecules, analytes will penetrate deep into mesoporous networks rather than become adsorbed onto the external surface. [182] We speculated that mesopores would have the right dimensions for tunable peptide entrapment. With the assistance of matrix-assisted laser desorption/ionization time-of-flight mass spectrometry (MALDI TOF MS) and statistical analysis, we demonstrated the correlation between the nanophase characteristics of the mesoporous silica thin film and the specificity and efficacy of low mass proteome harvesting. The tunable physico-chemical properties of mesoporous silica surfaces made this novel material a powerful tool in selectively separating and

concentrating the different low molecular weight subproteomes from complex biological fluids.

Generally speaking, the study on the relationship between pore nanotexturing and LMWP harvested is the key to enhancing our ability to recognize disease-biomarkers with this nanotechnology. As we mentioned in previous chapters, the large range and sheer complexity of make the characterization of human serum a challenging task. [183] Although the low mass peptidome has been fractionated and enriched from human serum with our novel nanotechnology, the necessary categorization and specific recovery of this resource are still an essential prerequisite for high-throughput and large-scale clinical studies.

Before testing with human blood, we mixed commercialized peptides and proteins with a broad range of molecular weights, sizes and structures to mimic the biological complex. All peptides and proteins were verified by MS for its identity and purity. Then the fractionation of the mixture was carried out on the mesoporous silica chips with different pore size distributions. MS profiles of the molecular weight standards in the peptide and protein range were analyzed respectively to avoid the interference of large proteins to identify peptides. The results presented in this paper reveal the potential of nanoporous chip based technology to provide a powerful alternative to conventional methods for LMWP harvesting from complex biological fluids.

In the analysis of the fractionation and purification of LMW species from human serum, the mesoporous silica chips used in this study were split into two categories based upon the properties of the material: 1. pore size, 2. pore structure. According to their

harvesting characteristics, selective enrichment and specific recovery patterns, each of the MSCs identified unique proteomic signatures.

## 5.2 Materials and Experimental

### 5.2.1 Materials

The materials used to fabricate the mesoporous silica thin films are the same as described in previous chapters. 26 standard peptides and proteins (proteoMass peptide and protein MALDI-MS calibration Kit, MSCAL1-1KT) were purchased from Sigma-Aldrich Co..

### 5.2.2 Experimental Sections

The molecular weight standards were combined, dispensed in equal amount, dried by vacuum centrifugation, and stored at -20$^{o}$C. 10 µl of the standard solution was spotted onto the nanoporous surface of the mesoporous silica chip. The samples were incubated for 30 minutes in a wet chamber (100% humidity) to prevent sample evaporation. The Chip surface was washed 5 times with 15µL of sterile, deionized water. Proteins were eluted from the pores by using 10µl of a 1:1 mixture of acetonitrile and 0.1 % trifluoroacetic acid (TFA) (v/v).

### 5.2.3 Mass Spectrometry

A matrix solution of 5 mg/ml α-cyano-4-hydroxycinnamic acid (αCHCA, Sigma) in a 1:1 mixture of acetonitrile and 0.1% TFA(v/v) and a saturated matrix solution of trans-3,5-dimethoxy-4-hydroxycinnamic acid (SA, Sigma) in 2:1 mixture of acetonitrile and 0.1 % TFA was used for LMW and HMW peptides and proteins

respectively. Each sample was mixed with the appropriate matrix solution in a 1:3 ratio, and spotted in duplicate onto the MALDI plate. Mass spectra were acquired on a Voyager-DE$^{TM}$-STR MALDI-TOF (Applied Biosystems, Framingham, MA) mass spectrometer in liner positive-ion mode, using a 337nm nitrogen laser. Samples were evaluated at two m/z ranges. For the m/z range of 800-10,000 Da, settings were optimized at acceleration voltage 20 KV, grid voltage 19KV, guide wire voltage 1KV, delay time 180 ns, and low-mass gate 800. For the m/z range of of 3,000-100,000 Da, the instrument was optimized at acceleration voltage 25 KV, grid voltage of 23.25 KV, guide wire voltage 6.25KV, delay time of 500 ns and low mass gate 3,000. Each spectrum was the average of 300 laser shots. The spectra were calibrated externally using the ProteoMass standards of peptides and proteins (Sigma) in each mass range.

**5.2.4 Data Processing and Statistics**

The raw spectra were processed with the Voyager Data Explorer software version 4.0 (Applied Biosystems) and the data were exported to SpecAlign software for pretreatment. [175, 176] All spectra were aligned using the PAFFT correlation method and normalized to total ion current intensity. The Peak detection was performed with a height ratio of 2 with 0.3% of the mass window. The baseline was corrected and the negative values were removed prior to analysis.

We used t-test (Student) to select differentially harvested peptides and proteins among the different nanoporous proteomic chips. Hierarchical clustering was performed using Cluster software and visualized with Treeview software [184].

## 5.3 Standard Peptides and Proteins Mixture

### 5.3.1 Effect of Pore Size on Fractionation

Table 5.1: Summary of physico-chemical properties of the selected peptide and protein standards and variability of peak intensities for each LMW marker. The standards were combined, dispensed in equal amount, dried by vacuum centrifugation, and stored at -20$^{o}$C. The stability of the set of standard was investigated by MS and no degradation was found. The coefficient of variations of the intensities of peaks after 2, 3, 5, and 8 days storage at -20$^{o}$C compared to freshly prepared sample were calculated (CV2, CV3, CV5, and CV8 respectively).

| | Mass | Ip | CV Day2 | CV Day3 | CV Day5 | CV Day8 |
|---|---|---|---|---|---|---|
| des-Arg1-Bradykinin | 905.05 | 10.18 | 15.76 | 6.55 | 1.55 | 1.97 |
| Angiotensin II | 1046.54 | 6.74 | 19.22 | 11.65 | 2.73 | 6.56 |
| Bradykinin | 1060.23 | 12 | 7.83 | 3.22 | 0.51 | 2.29 |
| Angiotensin I | 1297.51 | 6.92 | 18.69 | 12.48 | 7.29 | 6.31 |
| Substance P-amide | 1348.66 | 11 | 3.9 | 0.22 | 0.11 | 2.15 |
| Glu1-Fibrinopeptide B | 1571.61 | 4 | 2.28 | 5.51 | 7.32 | 0.83 |
| Neurotensin | 1673.96 | 9.7 | 0.05 | 0.07 | 0.11 | 0.09 |
| a-Endorphin | 1746.95 | 6 | 1.14 | 10.39 | 11.32 | 3.75 |
| ACTH(1-17) | 2094.46 | 10.45 | 3.52 | 0.63 | 2.92 | 0.51 |
| ACTH(18-39) | 2466.72 | 4.25 | 4.57 | 2.92 | 0.79 | 4.77 |
| Insulin oxidized B chain | 3496.96 | 6.9 | 26.36 | 22.03 | 17.54 | 24.2 |
| ACTH(7-38) | 3660.19 | 9.4 | 9.03 | 7.88 | 0.35 | 10.12 |
| Insulin | 5734.51 | 5.3 | 3.88 | 0.41 | 9.47 | 2.79 |
| EGF | 6217.01 | 4.78 | 4.77 | 5.03 | 10.62 | 2.24 |
| Insulin-like GF II | 7475.46 | 6.46 | 0.8 | 3.39 | 5.66 | 4.12 |
| Ubiquitin | 8565 | 6.56 | 13.75 | 3.72 | 0.4 | 5.27 |
| B2-Microglobulin | 11730 | 5.6 | 2.03 | 1.35 | 0.12 | 2.11 |
| Cytochrome c | 12361.96 | 9.59 | 1.49 | 1.13 | 5.99 | 10.04 |
| a-Lactalbumin | 14179 | 4.8 | 1.92 | 3.32 | 5.96 | 0.84 |
| Apomyoglobin | 16952.27 | 7.36 | 1.77 | 0.52 | 2.38 | 3.58 |
| B-lactoglobulin B | 18282.21 | 5.3 | 0.07 | 11.71 | 3.39 | 3.63 |
| Retinol Binding | 20575.99 | 5.15 | 2.63 | 5.66 | 3.68 | 3.3 |
| Carbonic anhydrase 1 | 28739 | 6.4 | 0.39 | 0.44 | 0.03 | 2.21 |
| Aldolase | 39,212.28 | 8.4 | 0.1 | 1.62 | 2.5 | 1.59 |
| Enolase | 46,672.00 | 6.17 | 7.63 | 3.98 | 8.55 | 6.78 |
| Albumin | 66431 | 5.6 | 14.12 | 8.12 | 6.42 | 3.16 |
| | | **Average CV** | **6.45** | **5.15** | **4.53** | **4.43** |

We selected 26 peptides and proteins (Table 5.1) with a broad range of molecular weights (900-66,500 Da), isoelectric points (pI 4.0-10.2), and structures and used them to standardize the chips, the sample preparation, the MS analysis and the data processing. Each peptide and protein was verified by MS for its identity and purity (see Figure 5.1).

In order to assess size exclusion during the fractionation, we selected mesoporous silica chips with pore sizes ranging from 2.7 nm to 8.9 nm. Figure 5.2.a and b illustrate the MS profiles of the molecular weight standards in the peptide and protein range respectively. When the peptide standard mix (16 markers from 900 to 8500 Da) and the protein standard mix (16 markers from 3400 to 66500 Da) were resolved by MALDI, their spectra showed a high detection signal and clear identification of all the molecular species. The spectra in Figure 5.2.a include the MS profiles for 16 peptides mixture (top), the peptide fraction in 26 peptides and proteins mixture (middle) and the recovered peptides from fractionation on mesoporous silica chips (bottom). It clearly implies that when combined in a unique solution, the detection signal in the peptide range dramatically decreased while the larger proteins remained well detected (Fig. 5.2.a and b). The signal suppression in the LMW was due to the presence of large amount of well ionized HMW molecules such as Albumin and mimicked the limits of MS analysis of serum and plasma. After fractionation on the mesoporous silica chips, larger proteins were removed and the detection of the LMW species significantly increased. Figure 5.2.c shows a magnified view of the spectra illustrating the size-dependent removal of larger proteins and the experimental molecular cut-off observed for each chip. Figure 5.2.d

presents a two-way hierarchical clustering showing the positive correlation between pore size, molecular weight of the trapped species and enrichment of the LMW standards. Mesoporous silica chips with larger pores preferentially harvested bigger peptides (from 3600 to 8500 Da), while smaller peptides (from 900 to 3500 Da) were recovered more efficiently by the chips with smaller pores.

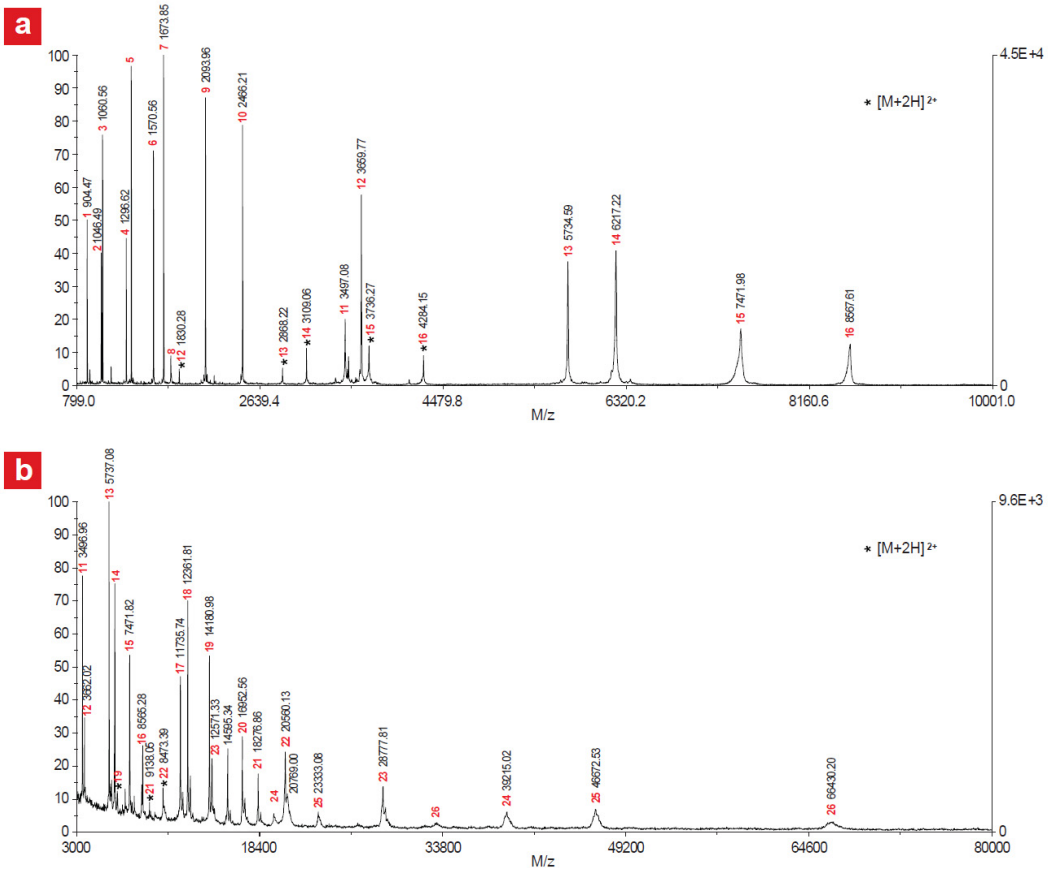


Figure 5.1: Stability of peptide and protein standards. Representative MALDI profile of the LMW (a) and HMW (b) standards respectively. The stability of the set of peptide (16 weight markers from 900 to 8,500 Da) and protein (16 weight markers from 3,500 to 66,500 Da) in stock solution was

investigated by MALDI-TOF MS after 1, 2, 3, 5, and 8 days storage at -20°C.

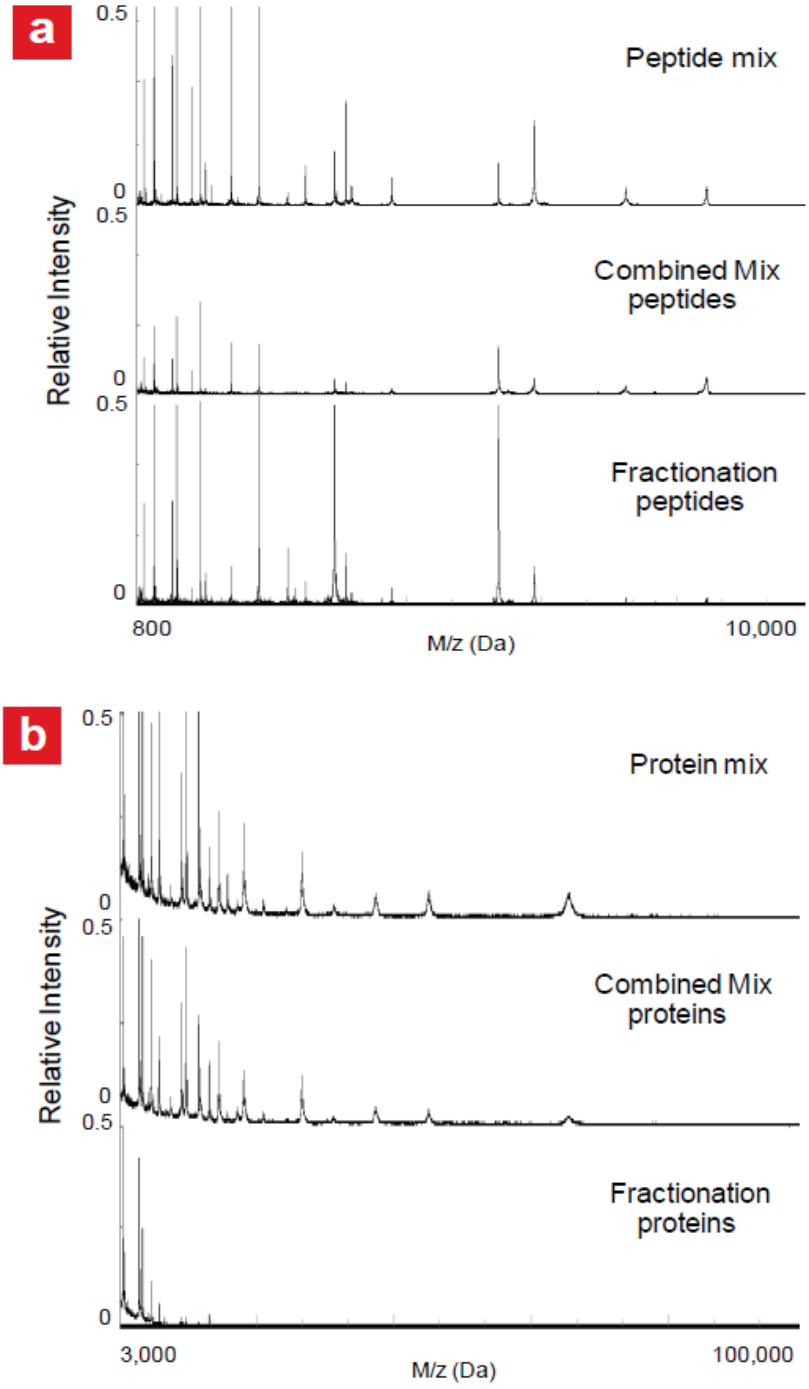

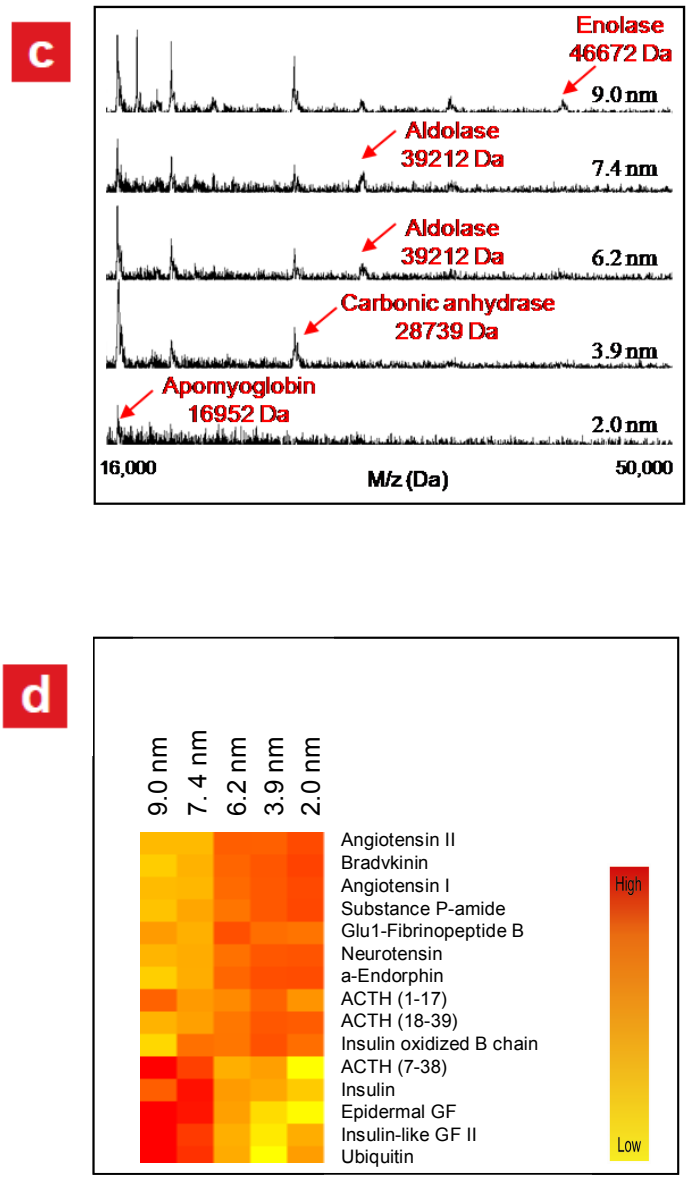


Figure 5.2: Evaluation of the molecular cut-off of the MSCs using a library of peptide and protein markers. a, b, Detection of the molecular weight standards by MALDI-TOF in the peptide (800 to 10000 Da) and in the protein range (3000 to 100000 Da). For the separated mixes of peptides (16 markers from 900 to 8500 Da) and proteins (16 markers from 3400 to 66500 Da), the profiles

present a high level of detection for each species. In the combined mix, the signal suppression of LMW standards is due to the high concentration of HMW proteins. In the MALDI profiles of the combined standard mix after fractionation on the MSC with 7.36 nm pore size, the detection of LMW markers is significantly increased compared to the unprocessed sample. c, Magnified view of the MALDI spectra demonstrating the characteristic molecular cut-off of each MSCs correlates to the pore size. d, Two-way hierarchical clustering of the peptide mix features among the different chips. The intensity of the red or yellow color indicates the relative peptide concentration. Larger pores enhanced the harvesting of bigger peptides (from 3600 to 8500 Da), while the small peptides (from 900 to 3500 Da) were preferentially recovered from the chips with smaller pores.

### 5.3.2 Effect of Pore Structure on Fractionation

As we demonstrated in Chapter 3, it was possible to fabricate MPS thin films with different pore morphology. Herein the effect of the structural variation of the mesoporous F127 nanochips (3D cubic, honeycomb hexagonal and 2D hexagonal) on the specific enrichment of LMW species was investigated. As shown in Figure 5.3, mesoporous silica thin films with similar pore size distributions, around 3.7 to 3.9 nm, and the three different nanostructures (Figures 5.3.a for 3D cubic, Figures 5.3.b for 3D honeycomb-like hexagonal and Figures 5.3.c for 2D hexagonal) exhibit the same molecular cut-off for peptide and protein recovery from serum fractionation. For both 3D nanoporous morphologies, the increased pore connectivity and the reduced steric hindrance imposed on the diffusion of peptides and proteins resulted in higher recovery efficacy. The dramatic difference in the MS profiles for peptides recovery in the range of 800 ~

10,000Da between 3D nanostructures and 2D hexagonal framework was shown in Figure 5.4.a, b and c. The average coefficient of variation (CV) determined from the histograms, for 3D cubic structure (Fig.5.4.d) or 3D honeycomb hexagonal structure (Fig.5.4.e) is considerably lower than that of the 2D hexagonal architecture (Fig.5.4.f), which shows a broader CV distribution. These results indicate that the serum fractionation on the MPS thin film with a 3D nanotexture possesses a comparatively lower variability because of the 3D structures' greater pore connectivity.

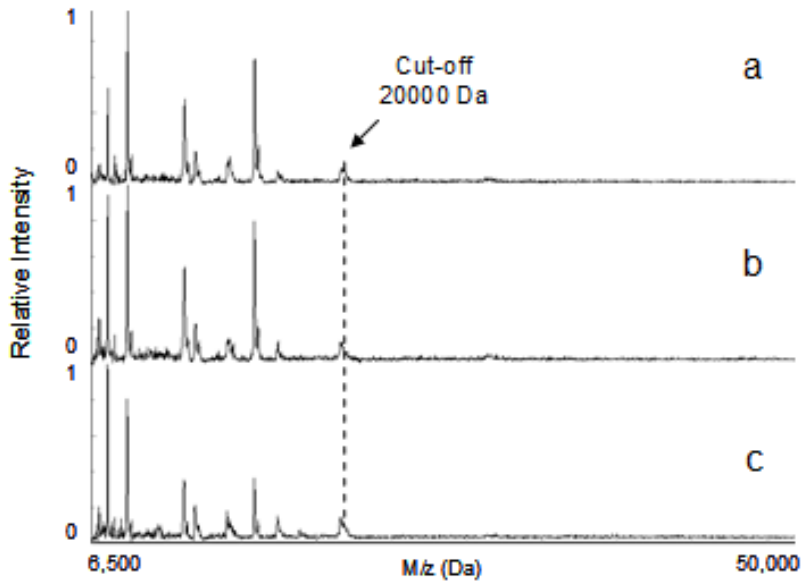


Figure 5.3: Molecular cut-off for F127 chips. The Molecular cut-off of recovered proteins shown for the MPS thin films prepared by Pluronic F127 with different nanoscale morphologies: 3D cubic (a), 3D honeycomb hexagonal (b) and 2D hexagonal (c).

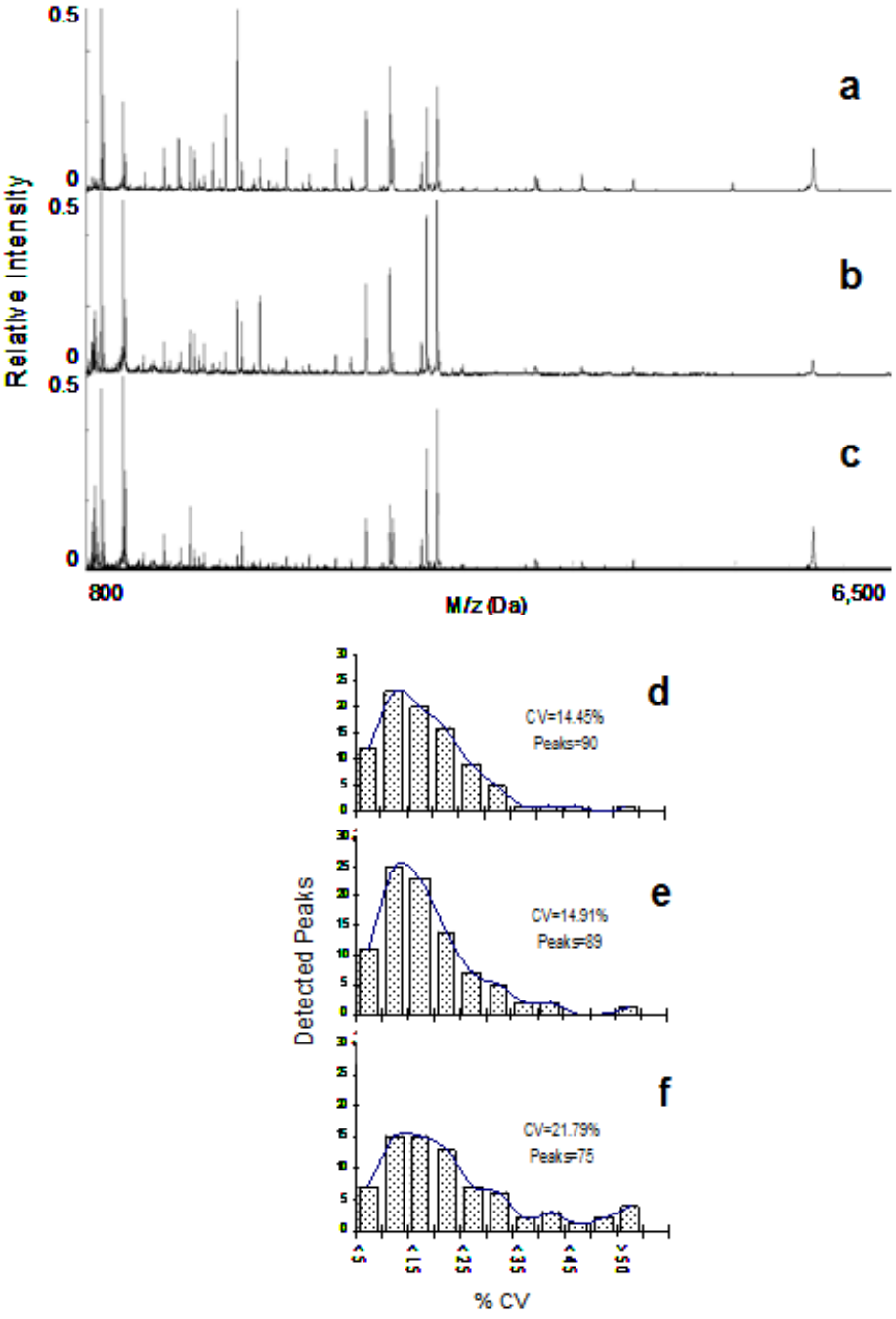


Figure 5.4: Effect of pore structural transformation on LMWP recovery from F127 chips. The MALDI profiles for the 3D cubic (a), 3D honeycomb hexagonal (b) and

2D hexagonal (c) nanoscale morphologies, respectively. The coefficients of variation (CV) distributions of MS peak intensities for each of the MALDI profiles are also shown (d, e, f). The average CV and the number of detected peaks are indicated in each histogram.

For some specific peptides or proteins, the 2D hexagonal and 3D nanostructures display differential peptide enrichment. As shown in figure 5.5, there is a significant increase of the capture of ACTH and Insulin peptides on the hexagonal surface while Substance P and a-Endorphin peptides are specifically recovered from the mesoporous silica chip with 3D cubic structure.

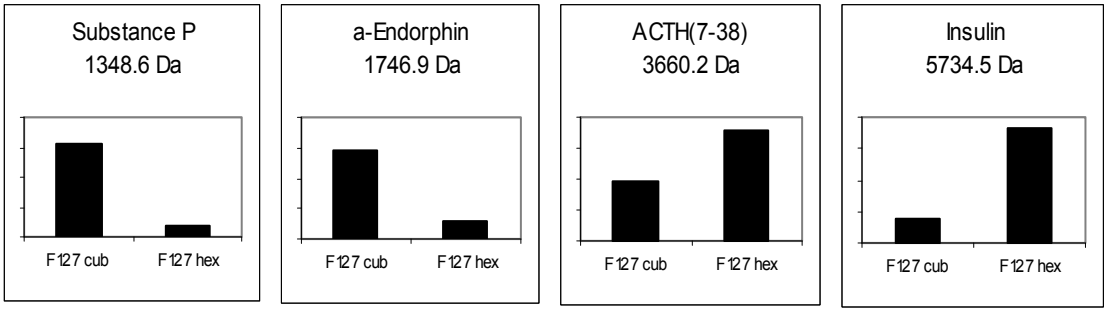


Figure 5.5: Intensity Bar graph of specific peptides recovery on 3D-Cubic and 3D-Hexagonal F127 mesoporous silica chips. The different structural modifications present a selective enrichment.

## 5.4 Selective Recovery of LMW Peptides and Proteins from Human Serum

The different LMW peptide and protein enrichment spectra are illustrated in Figure 5.6.a for the mesoporous silica chips prepared with L64, F127, L121+50%PPG and L121+100%PPG. Though it possessed a similar pore size to the MPS thin film prepared from F127, the relatively higher hydrophobicity, smaller pore volume, and poor pore connectivity of the mesoporous silica thin film fabricated with polymer P123 presented limited harvesting capability, as shown in Figure 5.6.b. With the largest average pore size and the highest surface hydrophilicity, the mesoporous silica chip produced using L121+PPG captured peptides and proteins in a wider molecular mass range. The chips with small pore size were prepared with F127 and L64 and preferentially enriched the peptides in the lower mass range. To assess this size-dependant ability of the mesoporous silica chips to capture LMWP, a hierarchical clustering analysis of peptides extracted from four different mesoporous silica chips with various pore sizes was performed (Fig.5.6.c). The clustering algorithm clearly separates the samples into two major clusters representing specific proteomic patterns for smallest pore and largest pore chips. The high intensity of smaller LMWP was obtained with the chips prepared with L64 and F127 due to their preferred pore sizes, 3.20nm and 3.71nm respectively. However, the periodic pore structure and uniform small pore size provided by F127 chips demonstrate a more homogeneous enrichment pattern. The mesoporous silica chips prepared by L121, with the pore sizes enlarged using the swelling agent (molar ratios of 50% to 100% PPG to template polymer,) offer increased selective capture of peptides and proteins with higher molecular weight. The larger pore size

presented by the L121 with 100% PPG resulted in more efficient recovery as illustrated by the higher intensity of the enrichment pattern observed on the hierarchical clustering.

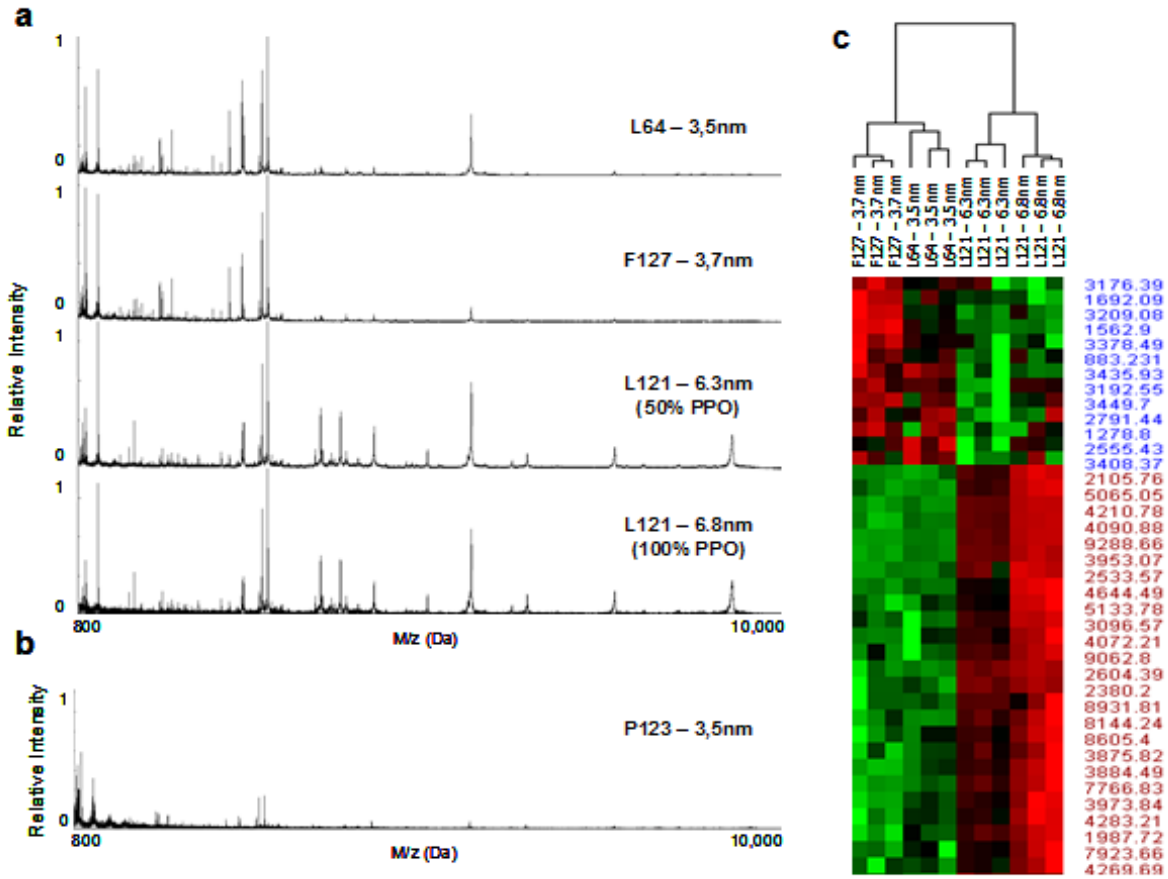


Figure 5.6: Effect of pore size on LMWP recovery. a. Mass spectra of the proteins and peptides collected from samples fractionated using chips prepared with L64, F127, L121+50%PPG and L121+100%PPG (top to bottom), b. MS profiles of the samples fractionated using chips prepared with P123, c. The supervised hierarchical clustering analysis of peak intensities for samples fractionated using chips prepared with F127, L64, L121+50%PPG and L121+100%PPG. Red indicates peak intensities higher than the median value, green is for peak intensities lower than the median value, and black

represents peak intensities equal to the median value. Each row represents an individual mass peak (MALDI MS peak) and each column represents a mesoporous thin film chip produced using a specific triblock copolymer.

## 5.5 Conclusion

In conclusion, the fractionation device presented here displays features that are desirable for exploratory screening and biomarker discovery. The constituent mesoporous silica chips may be custom-tailored for desired pore sizes and surface properties as needed for the sequestration and enrichment of extremely low abundance protein and peptides in desired ranges of the mass/charge spectrum. They are effective and yield highly reproducible extracts from extremely complex biological samples. After being optimized, they can process samples as small as 10 µl in a time as short as 30 minutes, as described in Chapter 4. They are inexpensive to manufacture, and their production can be easily scaled up to attain the simultaneous processing of a large number of samples. They are multiplexed, label-free diagnostic tools with the potential for additional modification with biological recognition moieties for enhanced specificity.

# CHAPTER 6

# TREATMENT ON THE SURFACE OF MESOPOROUS SILICA CHIPS AND ITS EFFECT ON SELECTIVE RECOVERY OF LMWP

## 6.1 Introduction

The selective isolation and enrichment of low molecular weight peptides and proteins from human serum are of considerable interest. As we discussed in previous chapters, due to the extremely high dynamic range of protein concentration and the interference of large proteins (i.e. albumin), specific recovery of LMW proteome is a considerable challenge. In Chapter 5, we demonstrated the efficacy of mesoporous silica chip in harvesting LMW peptides and proteins from biological complex (i.e. human serum). In this study, surface affinity for water is tuned by applying high power oxygen plasma (to induce hydrophilicity) or coating gas-phase hexamethyldisilazane (HMDS, to induce hydrophobicity). In addition, several common organic functional groups were conjugated on the surface of mesoporous silica thin film to enhance the selectivity of recovering low mass peptides.

Organic-inorganic hybrid materials prepared by the sol-gel approach have attracted a great deal of attention in materials science. Sol–gel, a highly adaptable process, allows for homogeneous mixing of inorganic and organic components at a nanoscale, leading to the so-called hybrid organic–inorganic nanocomposites. [78, 185-188] Through the covalent coupling of organic or organo-metallic moieties, chemical

functionalization of the inorganic framework of porous materials has been recognized as a promising approach to tailor pore surface properties such as charge, polarity, optical activity, and electronic activity. [135, 189, 190] The synthesis of hybrid mesoporous silica materials could open up new avenues for organometallic chemistry, catalysis, and organic-inorganic host-guest chemistry. There are two main approaches for organo-functionalization of ordered mesoporous silica-based solids: post-synthetic methods [137, 191-193] and one-pot synthesis [194-198] that are shown in Figure 6.1.

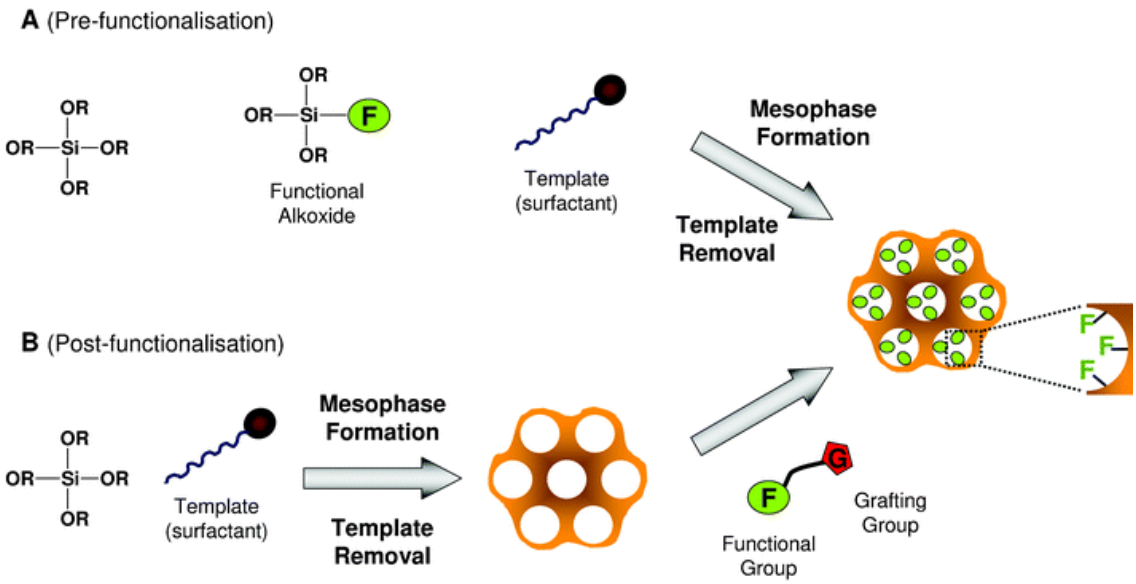


Figure 6.1: Pre-functionalization (A) and post-functionalization (B) routes towards hybrid materials organized in the mesoscopic scale. The meso-organized precursors are synthesized by reacting an inorganic precursor in the presence of a supramolecular template (surfactant). By route A, organic functions can also be embedded within the walls. Adapted from reference [199].

Post-grafting is a straight-forward method to add organic groups, such as $R_xSi(OR')_{3-x}$ or $R_xSiCl_{4-x}$, onto the surface of the pores. This approach has been widely employed to conjugate various organic groups onto the surface of the pores, including organometallic species, amino and thiol group, and epoxide group. However, post-grafting often leads to a quite low loading content and an inhomogeneous distribution of the functional groups. [190] Therefore, more research groups focus their attention on one-spot synthesis. This technology involves co-condensation of tetraalkoxysilanes and organotrialkoxysilanes in the presence of surfactants during synthesis, resulting in higher organic content and a more homogeneous organic distribution in the material. Functional groups, such as vinyl, phenyl, aminopropyl, cyanoethyl and diphenylphosphanylpropyl, have been incorporated into the inorganic network by this method. However, co-condensation in one-spot synthesis also caused several difficulties in addition to the control of the main parameters related to the EISA process. For instance, homogeneous solubility of the organic functionalities with silicate precursor in the medium limits the selection of surface modification. When the silylated probe is poorly soluble or insoluble in the alcoholic solvent, segregation or aggregation may take place. In the other hand, because of the consideration about the calcination step, surfactant templates have to be chose in a small range, where the polymers should own the distinguished melting point with that of organotrialkoxysilanes. Another influencing factor is the choice of co-solvents. One-spot synthesis requires the co-solvent not only to dissolve the desired organo-functional molecules but also to be miscible with the silicate precursor. In the case of mesoporous silica thin film preparation, the co-solvent must be

evaporable and must possess good wettability towards chip substrates. Lastly, the participation of organosilane into nanostructured films may lead to the significant damage in the silica network.

We improved the method of conjugating various organosilane compounds on the mesoporous silica chips. Herein, based on post-grafting approach, plasma ashing was used for the first time for the treatment of the mesoporous silica surface prior to chemical modification. The results show the improvement of functional group loading and the compatibility of this method for all synthetic templates and organosilanes. Opposite surface charges, due to the different functional groups used, resulted in distinctive selectivity of the low molecular weight proteins from the serum sample.

## 6.2 Materials and Experimental

### 6.2.1 Materials

The materials used to fabricate the mesoporous silica thin films are the same as those described in previous chapters. All organosilanes were purchased from Sigma-Aldrich Co., including Aminopropyltrimethoxysilane (APTES), Mercaptopropyltrimethoxysilane (MPTES), Cyanoalkyltriethoxysilane and 3-Chloropropyltriethoxysilane. Their chemical formula is displayed in Figure 6.2.

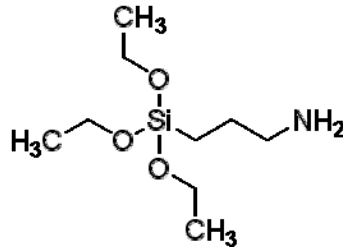


(3-Aminopropyl)trimethoxysilane

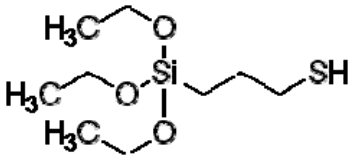


Mercaptopropyltrimethoxysilane

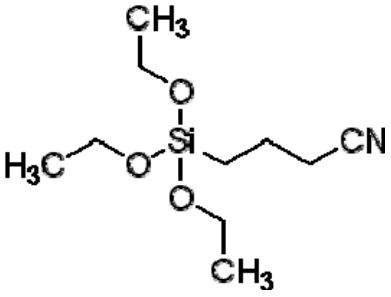


Cyanoalkyltriethoxysilane

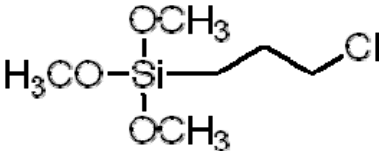


(3-Chloropropyl)triethoxysilane

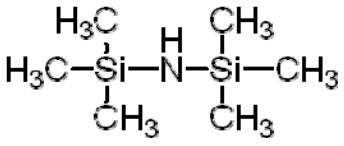


Hexamethyldisiazane

Figure 6.2: Chemical formula of organosilanes

### 6.2.2 Experimental Sections

#### 6.2.2.1 Control on Surface Hydrophilicity

Oxygen plasma treatment was performed in a Plasma Asher (March Plasma System) to ensure hydrophilicity. The treatment was carried out in a Plasma Asher (March Plasma System) with an O2 flow rate at 80 sccm and a power of 300 W for 10 minutes. Coating of Hexamethyldisilazane (HMDS) was performed in a HMDS vapor prime oven (YES) at 150$^{o}$C for 5 min, in order to make the surface hydrophobic. Contact angles of MSC surface were measured by a goniometer with captive bubble contact angle measurement to evaluate the hydrophilicity of the films.

#### 6.2.2.2 Conjugation of Organic Functional Groups on Chip Surface

The Mesoporous silica chips were treated by plasma ashing before silanization. Then silanate chips in a 3% organosilane in a Methanol:DI water (19:1) solution for 72 hours at room temperature in $N_2$ glovebox. Rinse sequentially with Methanol and DI water. Finally chips were cured at 110°C for 15 min in a fan-operated oven.

### 6.2.3 Characterization

Several characterization techniques are used in the section of surface modification, including ellipsometry, XRD, contact angle, TEM and N2 adsorption/desorption. The description about these techniques has been listed in Chapter 3. XPS was extensively used in this study to investigate the loading density of organosilane on the mesoporous silica chips.

### 6.2.4 Sample Fractionation

Same description as Chapter 5.

### 6.2.5 Mass Spectrometry

Same description as Chapter 5.

### 6.2.6 Data Processing and Statistics

Same description as Chapter 5.

## 6.3 Results and Discussion

### 6.3.1 Surface Treatment

#### 6.3.1.1 Oxygen Plasma

Plasma ashing is a well-known technique for removing the photoresist in semiconductor manufacturing. Using a plasma source, a monatomic reactive species is generated. Oxygen is the most common reactive species. Photoresist combines with the reactive oxygen to form ash and can be removed under a vacuum condition.

Although it experiences recombination during the channeling, monatomic oxygen is electrically neutral. The positively or negatively charged free radicals attract one another at a higher rate. Effectively, this means that when all of the free radicals have recombined, there is still a portion of the active species available for process. The objective to use oxygen plasma in our study to modify the defect on mesoporous silica thin film caused during their formation under high temperature. Calcination temperatures higher than 350 °C are often employed for this purpose. This process causes loss of

surface hydroxyl groups due to extensive dehydration. It is supposed that the reason for damage to the intermediate silica film in this case is that Si--R group (R refers to lower alkyl group or hydrogen atom) is decomposed (R group is separated) by the ashing process and a Si--OH bond is produced. The surface with Si-OH bond has been proved to be more hydrophilic than that with Si-H.

Table 6.1 listed the ellipsometry results before and after oxygen plasma treatment for mesoporous silica thin films respectively prepared by three surfactant templates: CTAB, F127, and L121 with 50% of PPG. Either thickness or porosity for the chips with/without oxygen plasma doesn't exhibit the significant difference, which illustrates that the surface treatment does not affect the configuration of silica thin film and pore dimension. However, the change of surface contact angle (Fig.6.3) indicates that the hydrophilicity of mesoporous silica thin film has been improved after being treated with oxygen plasma. Figure 6.3.a, c and e show the surface contact angles for the chips prepared with CTAB, F127 and L121+50%PPG. The water drop in the image has displayed their hydrophilic property (CTAB chip: 18.13°, F127 chip: 12.48°, L121+PPG chip: 7.83°). After the treatment of oxygen plasma, their surfaces become much more hydrophilic (CTAB chip: 6.73°, F127 chip: 7.50°, L121+PPG Chip: 3.76°). Clearly, the plasma-treatment process leads to effective retention of the silanol group on the pore surface.

Table 6.1: Ellipsometry results for mesoporous silica chips prepared by CTAB, F127 and L121+50%PPG, with different surface treatment, oxygen plasma or HMDS coating.

| Samples | Average Thickness (nm) | Average Porosity (%) |
|---|---|---|
| CTAB | 530.23 | 44.348 |
| CTAB w/ oxygen plasma | 534.83 | 46.823 |
| CTAB w/ HMDS coating | 542.59 | 32.262 |
| F127 | 548.86 | 43.347 |
| F127 w/ oxygen plasma | 548.26 | 43.854 |
| F127 w/ HMDS coating | 547.83 | 32.500 |
| L121 +50%PPG | 575.69 | 62.085 |
| L121 +50% PPG w/ oxygen plasma | 574.11 | 62.476 |
| L121+50% PPG w/ HMDS coating | 582.68 | 56.404 |

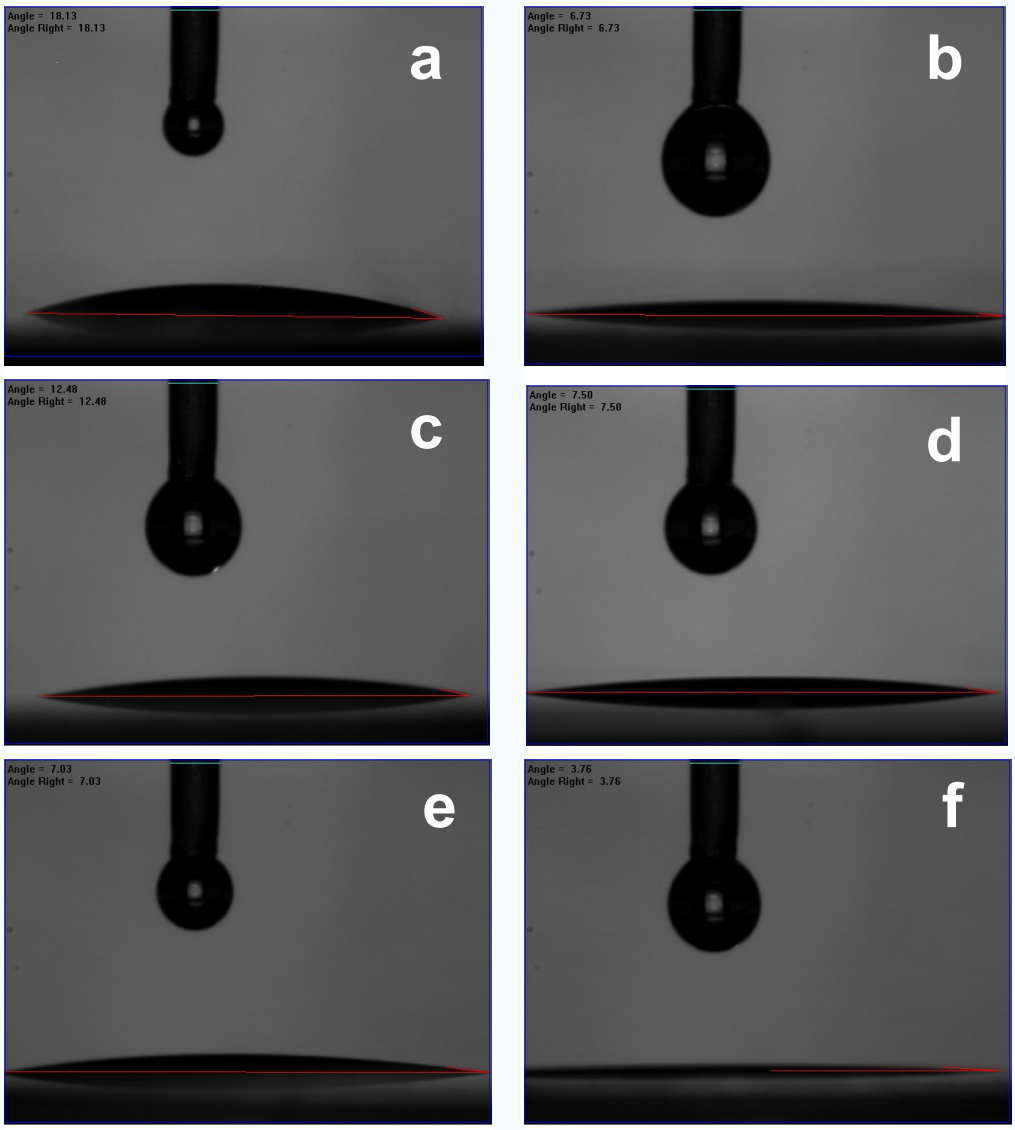


Figure 6.3: Contact angle images for the mesoporous silica chips prepared with a. CTAB b. CTAB with oxygen plasma, c. F127, d. F127 with oxygen plasma, e. L121+50%PPG and f. L121+50%PPG with oxygen plasma.

### 6.3.1.2 HMDS Coating

In contrast, we improve the hydrophobicity of mesoporous silica films by treating them with HMDS (hexamethyldisilazane) vapor at 160 °C. The resulting pore surface is occupied by hydrophilic silanol groups, and can be further modified through HMDS silyation to become hydrophobic. [200, 201] With a reaction:

$$2{\equiv}Si{-}OH + (Me)_3Si{-}NH{-}Si(Me)_3 \rightarrow 2{\equiv}Si{-}O{-}Si(Me)_3 + NH_3$$

HMDS coating is also a popular technique in semiconductor industry. A commonly known problem in photolithography on siliconoxide ($SiO_2$ or glass) and silicon (Si) surfaces is poor adhesion of the photoresist. Therefore, an adhesion promoter is applied. Compared to other adhesion promoter HMDS not only reacts with water but also with silanol groups at the $SiO_2$ or Si surface, respectively. For maximum adhesion of photoresist, the wafer surface must be completely free of moisture. The quality of the photoresist adhesion sets the stage for all that follows. Vapor Priming allows the application of HMDS in a monolayer. Contamination issues are reduced by exposing the wafers to HMDS vapor rather than liquid. The reduction of liquid required for a vapor deposition lower the cost compared to the liquid application of spin priming.

With the coating of a HMDS layer, the thickness of mesoporous silica layer is increased but the porosity is reduced, as listed in Table 1. Meanwhile, their surfaces become more hydrophobic as displayed in Figure 6.4.

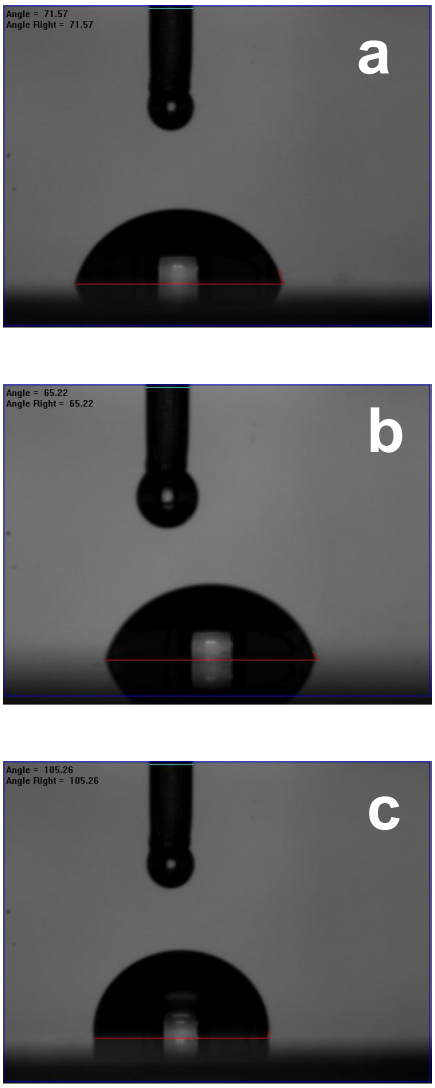


Figure 6.4: Contact angle images for the mesoporous silica chips prepared with a. CTAB with HMDS coating, b. F127 with HMDS coating, c. L121+50%PPG with HMDS coating.

#### 6.3.1.3 Selective Recovery on the Chip Surface with Various Hydrophilicities

In order to improve the fractionation and purification of LMW species from human serum, we generated a large set of nanoporous silica chips with controlled

hydrophobicity. To further illustrate the specific recovery pattern of our nanoporous surfaces, we performed supervised hierarchical clustering (Figure 6.5). An independent Student t-test was used for comparison between groups (n = 2 groups) for each detected MS peak. A P value of 0.02 or lower was considered significant to select differentially harvested peptides and proteins among the different nanoporous proteomic chips (Hydrophobic vs. Hydrophilic). These results show the selective enrichment pattern obtained after serum fractionation on proteomic nanochips with different surface hydrophilicity.

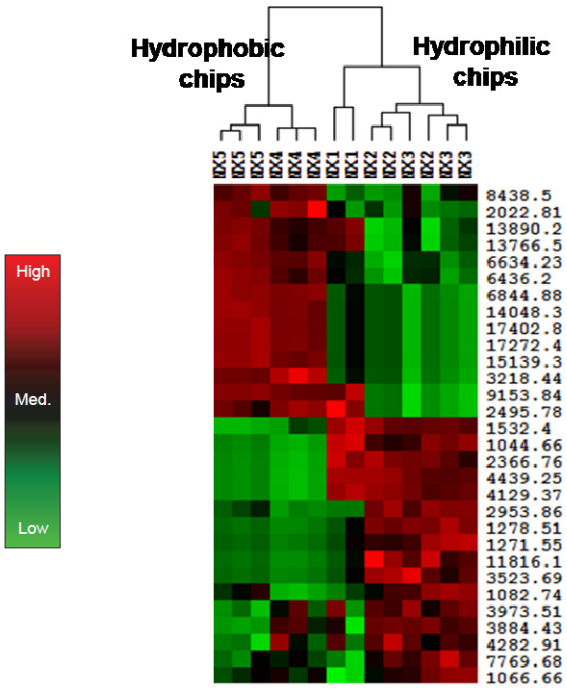


Figure 6.5: Effect of surface hydrophilicity on serum peptide harvesting. Supervised hierarchical clustering and specific recovery pattern for each set of nanochips as indicated in the figure. The relative intensity is gradually

indicated with red squares (high intensity), black squares (median) and green squares (low intensity or absence of a peak).

Figure 6.6 are MS profiles for the chips made by the same polymer template, but with different surface treatment. It illustrates that the hydrophobic surface prefers to enrich peptides present in the very low molecular weight region, while hydrophilic surface can provide a greater range. On the hydrophilic surface, both electrostatic attraction and size-exclusion work in recovering proteins, but on the hydrophobic surface, only pore size works for filtering small molecules.

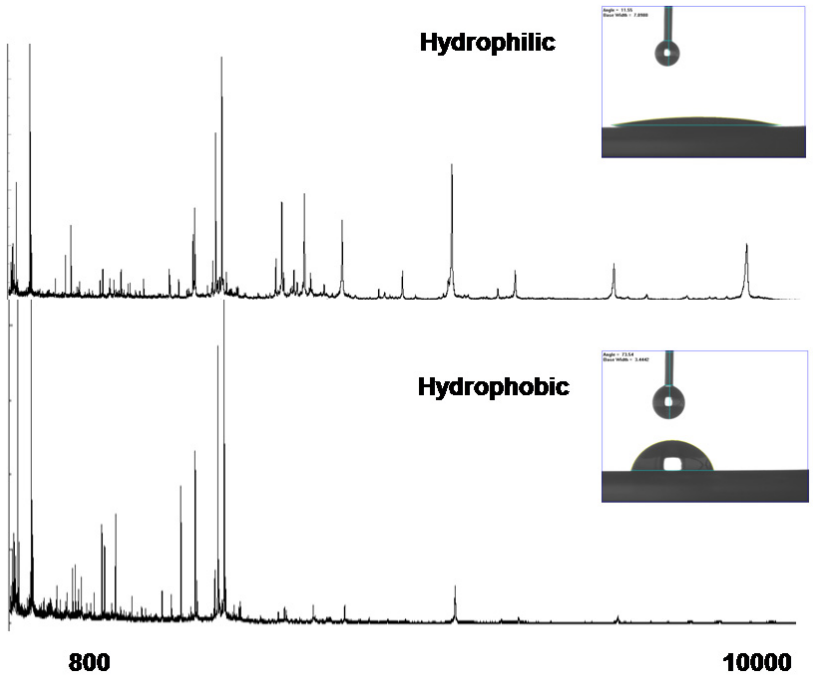


Figure 6.6: Mass spectra for low mass range of peptides recovered on the mesoporous silica chips with different hydrophilicity (top: hydrophilic surface, bottom: hydrophobic surface).

### 6.3.2 Organic Functionalization

Mesoporous silica possesses many silanol (Si-OH) groups on the surface that can act as convenient anchoring points for organic functionalization. Because of this fact, a post-synthesis process can be employed to anchor specific organic groups onto the surface of silica. [202-206] However, as we discussed above, the high temperature during calcinations process may cause a portion of surface silanol groups to be extensively dehydrated, resulting in a substrate incompatible with potentially conjugating organosilane groups. One-spot synthesis is also limited to use in our study due to the

restrictions of this method in the selection of polymer templates. To resolve the problem, the oxygen plasma is first used to treat the surface of mesoporous silica chip before the post-grafting. Not only can Oxygen plasma increase the surface hydrophilicity, but it can also fix the defect point (Si-H) on the surface with a high density of Si-OH groups.

To analyze the loading efficacy of organosilianes, the XPS method has been used to study the composite of thin film. Figure 6.7.a shows a comparison of XPS intensity of C content on the APTES modified chips before and after chemical modification. The significant increase of C 1s peak for the chips after modification, resulting from the alkyl chain on APTES, validates the efficacy of post-grafting on the chip surface treated with oxygen plasma.

Figure 6.7.b exhibits the comparison for N 1s peak on the 3 mesoporous silica chips APTES-modified under different method (black curve: N 1s on the chips after one-spot modification, red curve: N 1s on the chips after post-grafting without any pre-treatment, blue curve: N 1s on the chips after post-grafting method with pre-treatment by oxygen plasma. ) The difference for N 1s peak around the binding energy of 397 eV clearly implies the efficacy of oxygen plasma in grafting the functional groups on the pore surface. The chip that received pre-treatment of oxygen plasma is capable of conjugating four times the amino content than a chip without any surface treatment. Although the intensity for N 1s peaks are similar, the chip carried by post-grafting with oxygen plasma pre-treatment consisted of a sharper and more symmetric single peak at binding energies around 397 eV, which strongly points to a loading of APTES with high condensation on the pore surface. By calculating the areas under the peaks for Si2p, O1s,

Cis and N1s, an atomic carbon-to-nitrogen ratio of 1:5.994 was obtained in table 6.2 to further confirm the high purity of mesoporous silica thin films with APTES modification.

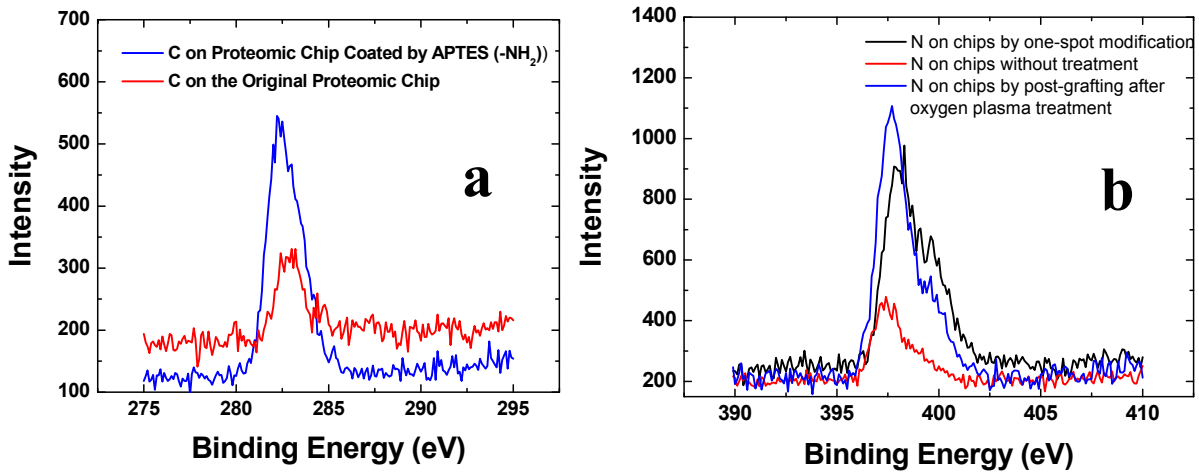


Figure 6.7: XPS spectra of mesoporous silica chips with APTES modification. a. Comparison of C content in XPS on the mesoporous silica chips before and after APTES modification. b. Comparison of N content in XPS on the mesoporous silica chips modified with one-spot synthesis (black curve), modified with post-grafting without pre-treatment (red curve) and modified with post-grafting with oxygen plasma treatment (blue curve).

Table 6.2: The tabulated atomic concentrations of each element on the mesoporous silica chips with APTES modification.

| Element | Atomic Concentration (%) |
|---|---|
| Si 2p | 26.69 |
| O 1s | 54.58 |
| C 1s | 16.05 |
| N 1s | 2.68 |

The XPS spectra in Figure 6.7 show the conjugation of MPTES on the mesoporous silica chips by post-grafting. Fig.6.7.a shows the signal at 162 eV corresponding to the existence of thiol group on the pore surface. In Fig.6.7.b, the spectra showing C 1s signals on the chips before and after grafting MPTES disclose the condense loading of the organosilane on the pore surface. The ratio of atomic concentration of Si 2p, O1s, C 1s and S 2p is listed in Table 6.3. An atomic carbon-to-sulfur ratio of 1:6.24 was obtained

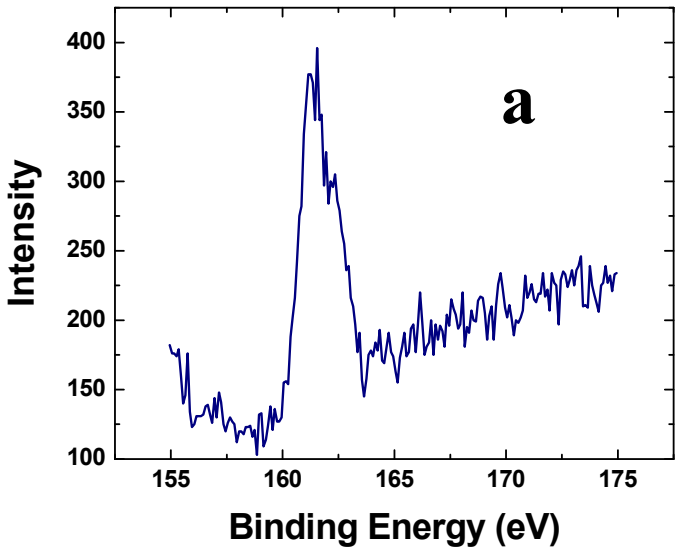

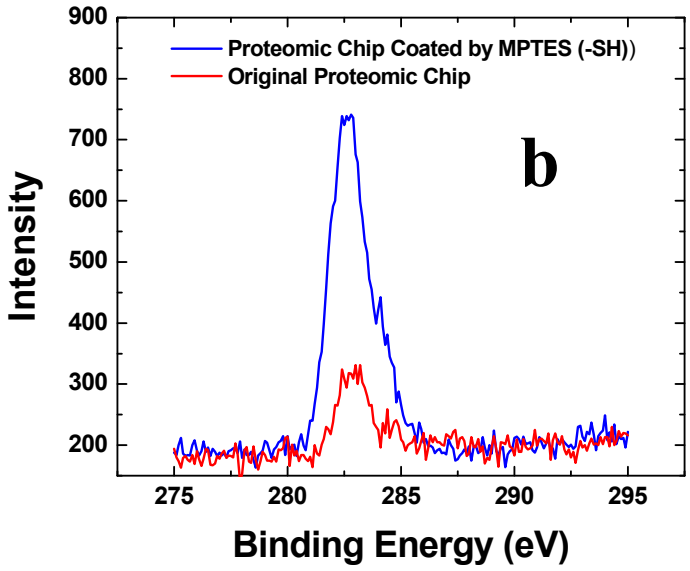


Figure 6.7: XPS spectra of mesoporous silica chips with MPTES modification. a. S content in XPS on the mesoporous silica chips with MPTES modification. b. Comparison of C content in XPS on the mesoporous silica chips before and after MPTES modification.

Table 6.3: The tabulated atomic concentrations of each element on the mesoporous silica chips with MPTES modification.

| Element | Atomic Concentration (%) |
|---|---|
| Si 2p | 29.67 |
| O 1s | 50.12 |
| C 1s | 17.43 |
| S 2p | 2.79 |

With the improved post-grafting pathway, we are able to conjugate many functional groups on the mesoporous silica chips, such as nitride and epoxy. After oxidizing the nitride group in hydrogen peroxide, the nitride group can be easily converted to carboxyl acid and become more active in attaching the biomolecules. Epoxy groups have proven to be a good candidate for linking DNA, Aptmer or other biological species on the substrate. A double peak of C 1s respectively at 283 eV and 285 eV is observed in Figure 6.8.a, which is corresponding to the carboxyl acid group and alkyl group. In Figure 6.8.b, the double peak for C 1s at 283 eV for –C-O-C- and at 285 eV for $–CH_{2,}$ confirming the adhesion of the Epoxy group on the nanopore surface.

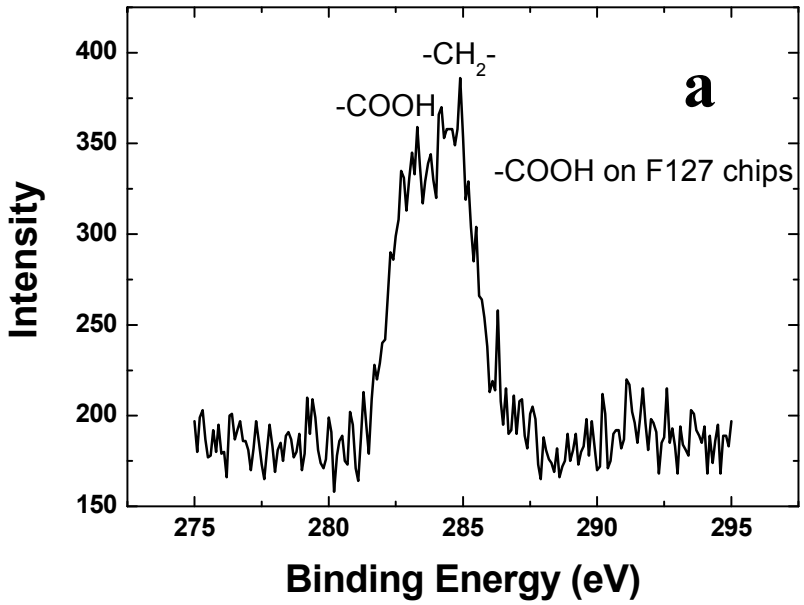

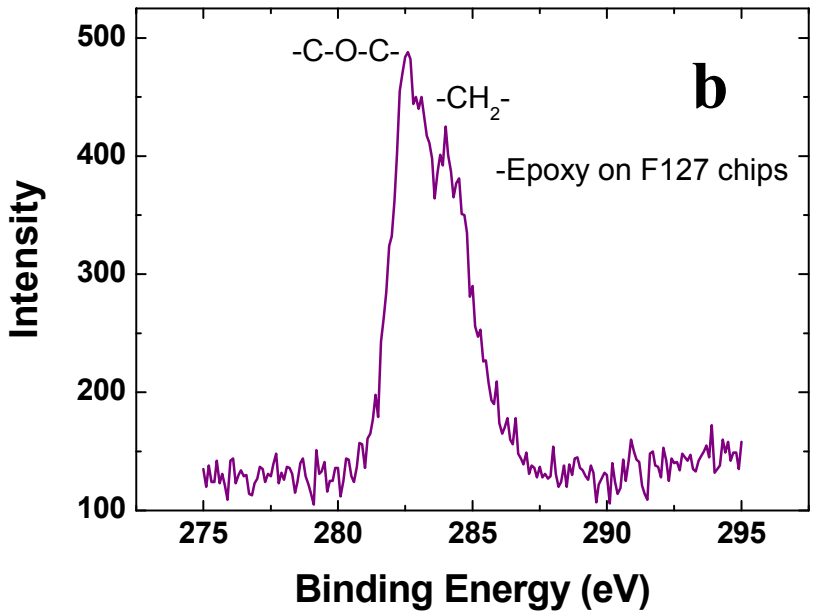


Figure 6.8: XPS spectra of mesoporous silica chips with the modification of a. Carboxyl acid, b. Epoxy group.

We also investigated the effect of chemical modification on the surface hydrophilicity of thin films. As displayed in Figure 6.9, contact angles were tested by goniometer with captive bubble contact angle measurement for all functionalized chips in our study. The results demonstrate that there is no significant change in the surface hydrophilicity with chemical modification.

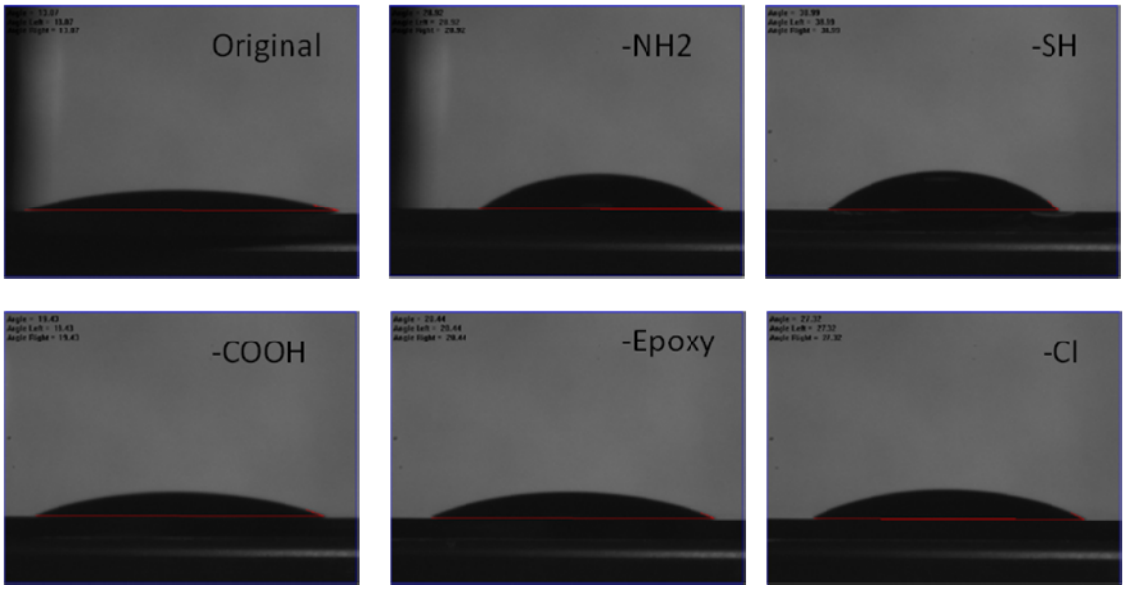


Figure 6.9: Images for showing surface contact angles of mesoporous silica chip and their functionalized derivatives with $–NH_2$, -SH, -COOH, -Epoxy and –Cl.

### 6.3.3 Sample Fractionation on Mesoporous Silica Chips with Chemical Modification

In previous chapters, we extensively investigated the effect of pore size and pore structure on the recovery of LMW peptides and proteins from biological complexes. Another important factor for improving the enrichment capacity of the mesoporous silica chips is to resolve the complexity of biological samples in different sub-proteomes according to their chemical properties. We have developed mesoporous silica chips conjugated with chemical functional groups to provide cationic and anionic surfaces respectively. MS analysis of the proteomic standard solutions fractionated on the mesoporous silica chips prepared by L121+50%PPG and conjugated with the chemical functional groups (-NH2 and –SH) is presented in Figure 6.10. According to their

Isoelectric Point (IP), the positively charged and negatively charged LMW standards are captured on the anionic and the cationic chips respectively. HMW proteins remain excluded from the chips independently of their charge (See Figure 6.11). For example, Albumin has a net negative charge and remains excluded from the cationic chip. These results and the identical molecular cut-off offer displayed by the chips demonstrate the dual properties of the functionalized mesoporous silica chips: 1- the size dependant depletion of HMW proteins by the porous surface; 2- the specific enrichment of differentially charged LMW peptides.

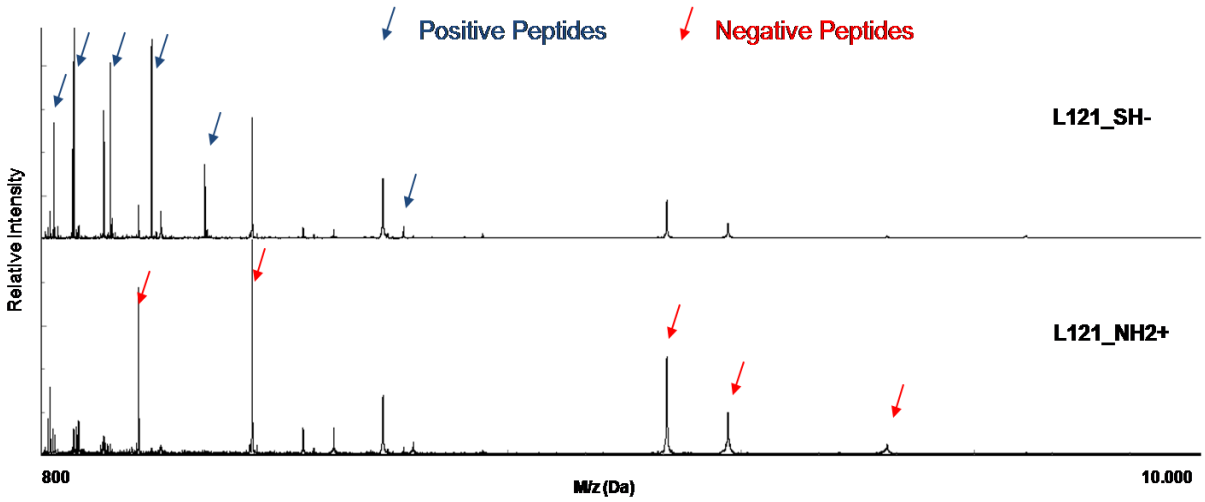


Figure 6.10: MS profiles of selectively captured peptides on the chemically modified chips. Positively and negatively charged MSC specifically enrich negative and positive peptides respectively.

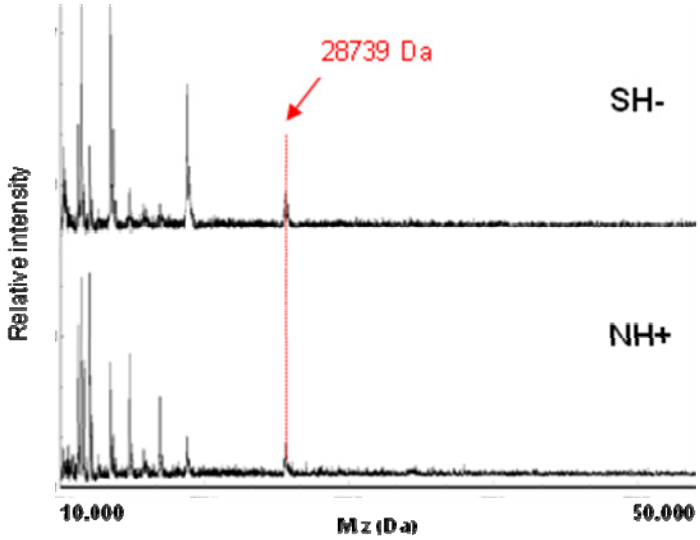


Figure 6.11: MS profiles of selectively captured or excluded proteins on the chemically modified chips.

# CHAPTER 7

# CONCLUSION AND SUGGESTED FUTURE WORKS

## 7.1 General Conclusions

Evidence is mounting that the low molecular-weight region of the circulatory proteome is a rich source of diagnostic biomarkers for the early detection of disease. Using surfactant-templated mesoporous silica thin films, we have developed a size-exclusion method for rapid and specific isolation and analysis of LMW peptides from complex biological samples. The fractionation devices are effective and yield highly reproducible extracts from extremely complex biological samples. By optimizing the experimental parameters, we are able to process samples as small as 10 μl in a time as short as 30 minutes with the mesoporous silica chips.

Besides the depletion of HMW protein, our mesoporous silica chips have allowed us to establish the correlation between the harvesting capacity and the physico-chemical properties of mesoporous silica surfaces. We fabricated a series of mesoporous silica thin films with a variety of nanotexutures and comprehensively explored their use in selective capturing and enriching LMW peptides and proteins from human serum. Different MPS thin film periodic nanostructures, formed using high molecular weight triblock copolymers such as Pluronic F127 with similar pore size distributions, can be obtained by tuning the polymer concentration in the precursor solution. The 3D cubic and honeycomb hexagonal nanostructures, which posses more desirable nanopore interconnectivity and more accessible nanopore morphology, exhibit superior performance in selectively

enriching LMW peptides compared to 2D hexagonal structure, even though they share similar pore size distributions and the same molecular cut-off for serum fractionation. Precisely controlled variations in pore size can be achieved through the use of copolymers with differing hydrophobic block lengths. The effect of pore size on the LMW peptide and protein recovery efficacy was investigated using MPS thin films prepared from four Pluronic surfactants (F127, P123, L64, L121, and L121 plus swelling agent) with different volume ratios of the hydrophilic and hydrophobic components to form pore sizes of 3nm, 4nm, 6nm, and 7nm respectively. This range of pore sizes led to the recovery of a different repertoire of peptides and proteins from the same serum sample via size and shape exclusion. The chemical functionalization of the porous silica surface further increases the specificity of peptides enrichment.

The wealth of finely tunable and controlled properties on mesoporous silica surfaces could be used for MS-based peptide and protein profiling of complex biological fluids, providing a powerful tool in the selective separation and concentration of the low molecular weight proteome. In addition, the mesoporous silica chips may be used to store, protect and stabilize protein and peptide extracted from biological fluids to enable the collection and transport of clinical samples with simplified and cost-effective procedures. We further envision that our mesoporous silica chip based device may serve as diagnostic tool to complement histopathology, imaging, and other conventional clinical techniques. The mesoporous silica chips mediated identification of entire disease-specific protein network may help in the selection of personalized therapeutic combinations, in the real-time assessment of therapeutic efficacy and toxicity, and in the

rational modulation of therapy based on changes in the protein network associated with the prognosis and the drug resistance of the disease.

## 7.2 Suggested Future Works

To obtain enhanced sensitivity and protocol standardization in the proposed study, the proteomic chips will be dramatically improved by 1) investigating the relationship between pore sizes and structures and the particular cancer-biomarkers harvested, and 2) integrating microfluidic circulating systems in order to achieve of increased pre-concentration, improved automation and compactness, reduced waste generation, and enhanced operational simplicity.

Proteomics research requires the development of new analytical tools and procedures that will allow high-throughput, sensitive analysis and data mining through bioinformatics. Microfluidics opens new avenues for developing application-specific microstructured channels and capillaries. Since no amplification process such as PCR can be performed in proteomics, the sensitivity and dynamic range of a microanalytical system are critical parameters. Microanalysis technologies, particularly microfluidics, offers promising key features to augment high-throughput and efficient proteomics research. One key feature is a decreased analysis time since going from a mm-range process to a μm-range allows for a gain in time of $10^6$. In addition, the ability to control the aspect ratio of microfluidic systems greatly improves the surface-to-volume ratio for proteomic analysis where most reactions take place on the sensor surface. Integrating microfluidics with our proteomic nanochips will greatly improve the sensitivity and

efficiency of harvesting LMWP from blood serum. Certain parameters of microfluidic systems need to be tested to enhance the surface contact of blood serum to the nanoporous silica thin film substrate.

The individual or integral use of different MPS thin films in microfluidic system with carefully tailored characteristics provides a novel platform for the rapid and efficient analysis of the LMWP in human serum and may be implemented for the diagnosis of disease onset in many clinical settings.

## 7.3 Remarks in Future Nanotechnology for Diagnostics

A major challenge in diagnosis for the 21st century is to be able to determine the exact relationship between disease biomarkers and clinical pathologies coupled with the ability to detect biomarkers non-invasively at an early stage of disease progression. In breast cancer, for instance, the goal of molecular imaging is to be able to accurately determine when a tumor mass has reached a population size of approximately 100-1000 cells, in contrast to the current techniques like mammography which require more than a million cells for accurate clinical diagnosis. The ability of nanotechnology components to interact with matter on the molecular scale provides not only the capability to ascertain the molecular constituents of the disease, but also the way in which these constituents affect the totality of biological function. The ability to incorporate an array of structural and chemical functionalities onto the same micro- and nanoscale architecture should also enable more accurate, sensitive, and precise screening of diseases which present themselves with more significant pathological heterogeneity. This same flexibility should

also enable a new generation of clinical constructs, referred to as theranostics, which combine both diagnostic and therapeutic elements. These theranostic constructs would facilitate rapid screening and therapeutic intervention while allowing for disease progression monitoring and therapeutic tailoring moving eventually towards a new era in personalized medicine. This article has reviewed a few of the many applications of nanotechnology being developed for application to disease diagnosis. The nanodevices described herein, including nanoporous chips, nanowire biosensors, single electron transistors, and micro- and nanocantilevers, are able to detect extremely low concentrations of target proteins as well as DNA and RNA sequences of interest, many of them label-free, in real-time, and at-point-of-care. Researchers are also making progress in using nanomaterials to spot disease biomarkers both *in vitro* and *in vivo*. The application of gold nanoparticles in biobarcode assays can help detect protein and DNA signatures for a number of diseases, including cancer, at concentration limits in the attomolar range. In addition, with the assistance of quantum dots and magnetic nanoparticles, tumor imaging contrast and resolution has been significantly improved. Many of these nanomaterials have the potential to be incorporated with more traditional imaging and diagnostic techniques or can be used in conjunction with the aforementioned nanodevices to further enhance their diagnostic, screening, and biomarker profiling sensitivity and flexibility. The development of nanodevices and nanomaterials for diagnostics spans a diverse collection of disciplines, combining biology, chemistry, physics, materials science, and manufacturing to name a few. In order to realize its enormous potential, cross-discipline cooperation is essential. This wide range of

expertise will be crucial in the design, fabrication, characterization, and implementation of future nanotechnological diagnostic platforms capable of the direct observation, manipulation, and analysis of the molecular signatures of disease, from a single molecule to an entire proteomic library.

Personalized medicine is the concept of incorporating novel biotechnologies into the diagnosis and treatment for a single individual, factoring in the genetic and environmental variables that may affect the choice of therapy. Nanotechnology is constantly refining personalized medicine through offering the ability to create devices capable of rapidly screening for biomarkers of diseases. The identification of these biomarkers for distinct diseases will lead to more individualized therapeutic approaches. Through the use of nanotechnolgy, it is now obvious that the immediate study of DNA and proteins dramatically increases the speed and accuracy of the conventional molecular diagnostic methods. This approach is stretching the limits of current molecular diagnostics, and will eventually lead to the combination of diagnostics with therapeutics for the ultimate advancement of personalized medicine. Nanomaterials can be used for bio-labeling, which is an important element in the study of biomarkers. Proteomic technologies assist in the detection of biomarkers, thus facilitating the analysis of low-abundant proteins. Molecular imaging is a valuable diagnostic modality, capable of combining with therapeutics and playing a key role in personalized medicine. The multiple functionalities that can be imparted to some nano-platforms make them advantageous over traditional approaches. Both nanomedicine and personal medicine

already exist in the clinical realm. However, the creation of new nanotechnologies will only expedite the connection between individualized diagnostics and treatments.

# References


1. Bouck, N., V. Stellmach, and H. SC., *How tumors become angiogenic. Adv. Cancer Res.*, 1996. **69**: p. 135-174.
2. DeBerardinis, R.J., et al., *The Biology of Cancer: Metabolic Reprogramming Fuels Cell Growth and Proliferation.* Cell Metabolism, 2008. **7**(1): p. 11-20.
3. Su, M., S. Li, and V.P. Dravid, *Microcantilever resonance-based DNA detection with nanoparticle probes.* Applied Physics Letters, 2003. **82**(20): p. 3562-3564.
4. Cheng, M.M.-C., et al., *Nanotechnologies for biomolecular detection and medical diagnostics.* Current Opinion in Chemical Biology, 2006. **10**(1): p. 11-19.
5. Jemal, A., et al., *Cancer Statistics. CA. Cancer J. Clin.*, 2008. **58**: p. 71-96.
6. Berg, W.A., et al., *Diagnostic Accuracy of Mammography, Clinical Examination, US, and MR Imaging in Preoperative Assessment of Breast Cancer.* Radiology, 2004. **233**(3): p. 830-849.
7. Howell, L.P. and L. Lin-Chang, *Cytomorphology of Common Malignant Tumors of the Breast.* Clinics in Laboratory Medicine, 2005. **25**(4): p. 733-760.
8. Anderson, N.L. and N.G. Anderson, *The Human Plasma Proteome: History, Character, and Diagnostic Prospects.* Mol Cell Proteomics, 2002. **1**(11): p. 845-867.
9. Petricoin Iii, E.F., et al., *Use of proteomic patterns in serum to identify ovarian cancer.* The Lancet, 2002. **359**(9306): p. 572-577.

10. Levenson, V.V., *Biomarkers for early detection of breast cancer: What, when, and where?* Biochimica et Biophysica Acta (BBA) - General Subjects, 2007. **1770**(6): p. 847-856.

11. Georganopoulou, D.G., et al., *Nanoparticle-Based Detection in Cerebral Spinal Fluid of a Soluble Pathogenic Biomarker for Alzheimer's Disease.* Proceedings of the National Academy of Sciences of the United States of America, 2005. **102**(7): p. 2273-2276.

12. Gao, X., et al., *In vivo cancer targeting and imaging with semiconductor quantum dots.* Nat Biotech, 2004. **22**(8): p. 969-976.

13. Wu, X., et al., *Immunofluorescent labeling of cancer marker Her2 and other cellular targets with semiconductor quantum dots.* Nat Biotech, 2003. **21**(1): p. 41-46.

14. Lee, J.-H., et al., *Artificially engineered magnetic nanoparticles for ultra-sensitive molecular imaging.* Nat Med, 2007. **13**(1): p. 95-99.

15. Na, H., et al., *Development of a T1 contrast agent for magnetic resonance imaging using MnO nanoparticles. Angew. Chem., Int. Ed.* , 2007. **46**: p. 5397-5401.

16. Hanahan, D. and R.A. Weinberg, *The Hallmarks of Cancer.* Cell, 2000. **100**(1): p. 57-70.

17. Liotta, L. and E. Petricoin, *Molecular profiling of human cancer.* Nat Rev Genet, 2000. **1**(1): p. 48-56.

18. Srinivas, P.R., B.S. Kramer, and S. Srivastava, *Trends in biomarker research for cancer detection.* The Lancet Oncology, 2001. **2**(11): p. 698-704.

19. Sidransky, D., *Emerging molecular markers of cancer.* Nat Rev Cancer, 2002. **2**(3): p. 210-219.

20. Alizadeh, A.A., et al., *Distinct types of diffuse large B-cell lymphoma identified by gene expression profiling.* Nature, 2000. **403**(6769): p. 503-511.

21. Petricoin, E.F., et al., *Clinical proteomics: translating benchside promise into bedside reality.* Nat Rev Drug Discov, 2002. **1**(9): p. 683-695.

22. Bild, A.H., et al., *Oncogenic pathway signatures in human cancers as a guide to targeted therapies.* Nature, 2006. **439**(7074): p. 353-357.

23. Peri, S., et al., *Development of Human Protein Reference Database as an Initial Platform for Approaching Systems Biology in Humans.* Genome Research, 2003. **13**(10): p. 2363-2371.

24. Rual, J.-F., et al., *Towards a proteome-scale map of the human protein-protein interaction network.* Nature, 2005. **437**(7062): p. 1173-1178.

25. Stelzl, U., et al., *A Human Protein-Protein Interaction Network: A Resource for Annotating the Proteome.* Cell, 2005. **122**(6): p. 957-968.

26. George Chambers, L.L., Phil Cash, Graeme I. Murray,, *Proteomics: a new approach to the study of disease.* The Journal of Pathology, 2000. **192**(3): p. 280-288.

27. JAMES, P., *Protein identification in the post-genome era: the rapid rise of proteomics.* Quarterly Reviews of Biophysics, 1997. **30**(04): p. 279-331.

28. Riera, C., et al., *Detection of Leishmania infantum cryptic infection in asymptomatic blood donors living in an endemic area (Eivissa, Balearic Islands, Spain) by different diagnostic methods.* Transactions of the Royal Society of Tropical Medicine and Hygiene, 2004. **98**(2): p. 102-110.

29. De Paepe, B., et al., *Immunohistochemical analysis of the oxidative phosphorylation complexes in skeletal muscle from patients with mitochondrial DNA encoded tRNA gene defects.* J Clin Pathol, 2009. **62**(2): p. 172-176.

30. Thomas O. Joos, et. al., *A microarray enzyme-linked immunosorbent assay for autoimmune diagnostics.* Electrophoresis, 2000. **21**(13): p. 2641-2650.

31. Wulfkuhle, J.D., L.A. Liotta, and E.F. Petricoin, *Proteomic applications for the early detection of cancer.* Nat Rev Cancer, 2003. **3**(4): p. 267-275.

32. Ebert, M.P.A., et al., *Identification of Gastric Cancer Patients by Serum Protein Profiling.* Journal of Proteome Research, 2004. **3**(6): p. 1261-1266.

33. Sasaki, K., et al., *Peptidomics-based Approach Reveals the Secretion of the 29-Residue COOH-Terminal Fragment of the Putative Tumor Suppressor Protein DMBT1 from Pancreatic Adenocarcinoma Cell Lines.* Cancer Res, 2002. **62**(17): p. 4894-4898.

34. Kennedy, S., *The role of proteomics in toxicology: identification of biomarkers of toxicity by protein expression analysis.* Biomarkers, 2002. **7**: p. 269-290.

35. Liotta, L.A., M. Ferrari, and E. Petricoin, *Clinical proteomics: Written in blood.* Nature, 2003. **425**(6961): p. 905-905.

36. Petricoin, E.F., et al., *The blood peptidome: a higher dimension of information content for cancer biomarker discovery.* Nat Rev Cancer, 2006. **6**(12): p. 961-967.

37. Villanueva, J., *Differential exoprotease activities confer tumor-specific serum peptidome patterns.* The Journal of Clinical Investigation, 2006. **116**(1): p. 271-284.

38. Tirumalai, R.S., et al., *Characterization of the Low Molecular Weight Human Serum Proteome.* Mol Cell Proteomics, 2003. **2**(10): p. 1096-1103.

39. Aebersold, R. and M. Mann, *Mass spectrometry-based proteomics.* Nature, 2003. **422**(6928): p. 198-207.

40. Hanash, S.M., S.J. Pitteri, and V.M. Faca, *Mining the plasma proteome for cancer biomarkers.* Nature, 2008. **452**(7187): p. 571-579.

41. Kulasingam, V. and E.P. Diamandis, *Strategies for discovering novel cancer biomarkers through utilization of emerging technologies.* Nat Clin Prac Oncol, 2008. **5**(10): p. 588-599.

42. Lu, Y., et al., *Continuous formation of supported cubic and hexagonal mesoporous films by sol-gel dip-coating.* Nature, 1997. **389**(6649): p. 364-368.

43. Dongyuan Zhao, et al., *Continuous Mesoporous Silica Films with Highly Ordered Large Pore Structures.* Advanced Materials, 1998. **10**(16): p. 1380-1385.

44. Rosa Terracciano, M.G., Flaviano Testa, Luigi Pasqua, Pierosandro Tagliaferri, Mark Ming-Cheng Cheng, A. Jasper Nijdam, Emanuel F. Petricoin, Lance A. Liotta, Giovanni Cuda, Mauro Ferrari, Salvatore Venuta,, *Selective binding and enrichment for low-molecular weight biomarker molecules in human plasma after*

*exposure to nanoporous silica particles.* PROTEOMICS, 2006. **6**(11): p. 3243-3250.

45. Geho, D., et al., *Fractionation of Serum Components Using Nanoporous Substrates.* Bioconjugate Chemistry, 2006. **17**(3): p. 654-661.

46. Gaspari, M., et al., *Nanoporous Surfaces as Harvesting Agents for Mass Spectrometric Analysis of Peptides in Human Plasma.* Journal of Proteome Research, 2006. **5**(5): p. 1261-1266.

47. Bergveld, P., *Development, Operation, and Application of the Ion-Sensitive Field-Effect Transistor as a Tool for Electrophysiology.* Biomedical Engineering, IEEE Transactions on, 1972. **BME-19**(5): p. 342-351.

48. Cui, Y., et al., *Nanowire Nanosensors for Highly Sensitive and Selective Detection of Biological and Chemical Species.* Science, 2001. **293**(5533): p. 1289-1292.

49. Patolsky, F., et al., *Nanowire-based nanoelectric devices in the life sciences. MRS Bull.*, 2007. **32**: p. 142-149.

50. Patolsky, F., G. Zheng, and C.M. Lieber, *Nanowire-Based Biosensors.* Analytical Chemistry, 2006. **78**(13): p. 4260-4269.

51. Patolsky, F., G. Zheng, and C.M. Lieber, *Fabrication of silicon nanowire devices for ultrasensitive, label-free, real-time detection of biological and chemical species.* Nat. Protocols, 2006. **1**(4): p. 1711-1724.

52. Lee, H.-S., et al., *Electrical detection of VEGFs for cancer diagnoses using anti-vascular endotherial growth factor aptamer-modified Si nanowire FETs.* Biosensors and Bioelectronics, 2009. **24**(6): p. 1801-1805.

53. Ferrari, M., *Cancer nanotechnology: opportunities and challenges.* Nat Rev Cancer, 2005. **5**(3): p. 161-171.

54. Hansen, K.M. and T. Thundat, *Microcantilever biosensors.* Methods, 2005. **37**(1): p. 57-64.

55. ZhangJ, et al., *Rapid and label-free nanomechanical detection of biomarker transcripts in human RNA.* Nat Nano, 2006. **1**(3): p. 214-220.

56. Lee, J.H., et al., *Immunoassay of prostate-specific antigen (PSA) using resonant frequency shift of piezoelectric nanomechanical microcantilever.* Biosensors and Bioelectronics, 2005. **20**(10): p. 2157-2162.

57. Corot, C., et al., *Recent advances in iron oxide nanocrystal technology for medical imaging.* Advanced Drug Delivery Reviews, 2006. **58**(14): p. 1471-1504.

58. Tueng Shen, R.W., Mikhail Papisov, Alexei Bogdanov Jr., Thomas J. Brady,, *Monocrystalline iron oxide nanocompounds (MION): Physicochemical properties.* Magnetic Resonance in Medicine, 1993. **29**(5): p. 599-604.

59. Conroy Sun, O.V., Jonathan Gunn, Chen Fang, Stacey Hansen, Donghoon Lee, Raymond Sze, Richard G. Ellenbogen, Jim Olson, Miqin Zhang,, *In Vivo MRI Detection of Gliomas by Chlorotoxin-Conjugated Superparamagnetic Nanoprobes.* Small, 2008. **4**(3): p. 372-379.

60. Michalet, X., et al., *Quantum Dots for Live Cells, in Vivo Imaging, and Diagnostics.* Science, 2005. **307**(5709): p. 538-544.

61. Medintz, I.L., et al., *Quantum dot bioconjugates for imaging, labelling and sensing.* Nat Mater, 2005. **4**(6): p. 435-446.

62. Kim, S., et al., *Near-infrared fluorescent type II quantum dots for sentinel lymph node mapping.* Nat Biotech, 2004. **22**(1): p. 93-97.

63. Azzazy, H.M.E., M.M.H. Mansour, and S.C. Kazmierczak, *From diagnostics to therapy: Prospects of quantum dots.* Clinical Biochemistry, 2007. **40**(13-14): p. 917-927.

64. Azzazy, H.M.E., M.M.H. Mansour, and S.C. Kazmierczak, *Nanodiagnostics: A New Frontier for Clinical Laboratory Medicine.* Clin Chem, 2006. **52**(7): p. 1238-1246.

65. Sukhanova, A. and I. Nabiev, *Fluorescent nanocrystal-encoded microbeads for multiplexed cancer imaging and diagnosis.* Critical Reviews in Oncology/Hematology, 2008. **68**(1): p. 39-59.

66. Jain, P.K., I.H. El-Sayed, and M.A. El-Sayed, *Au nanoparticles target cancer.* Nano Today, 2007. **2**(1): p. 18-29.

67. Willets, K.A. and R.P. Van Duyne, *Localized Surface Plasmon Resonance Spectroscopy and Sensing.* Annual Review of Physical Chemistry, 2007. **58**(1): p. 267-297.

68. Baptista, P., et al., *Gold nanoparticles for the development of clinical diagnosis methods.* Analytical and Bioanalytical Chemistry, 2008. **391**(3): p. 943-950.

69. West, J.L. and N.J. Halas, *ENGINEERED NANOMATERIALS FOR BIOPHOTONICS APPLICATIONS: Improving Sensing, Imaging, and Therapeutics.* Annual Review of Biomedical Engineering, 2003. **5**(1): p. 285-292.

70. Wilson, R., *The use of gold nanoparticles in diagnostics and detection.* Chemical Society Reviews, 2008. **37**(9): p. 2028-2045.

71. Nam, J.-M., C.S. Thaxton, and C.A. Mirkin, *Nanoparticle-Based Bio-Bar Codes for the Ultrasensitive Detection of Proteins.* Science, 2003. **301**(5641): p. 1884-1886.

72. Thaxton, C.S., et al., *A Bio-Bar-Code Assay Based upon Dithiothreitol-Induced Oligonucleotide Release.* Analytical Chemistry, 2005. **77**(24): p. 8174-8178.

73. Mirkin, C.A., et al., *A DNA-based method for rationally assembling nanoparticles into macroscopic materials.* Nature, 1996. **382**(6592): p. 607-609.

74. Elghanian, R., et al., *Selective Colorimetric Detection of Polynucleotides Based on the Distance-Dependent Optical Properties of Gold Nanoparticles.* Science, 1997. **277**(5329): p. 1078-1081.

75. Park, S.-J., T.A. Taton, and C.A. Mirkin, *Array-Based Electrical Detection of DNA with Nanoparticle Probes.* Science, 2002. **295**(5559): p. 1503-1506.

76. Kresge, C.T., et al., *Ordered mesoporous molecular sieves synthesized by a liquid-crystal template mechanism.* Nature, 1992. **359**(6397): p. 710-712.

77. Brinker, C.J. and G.W. Scherer, *Sol-gel science: The physics and chemistry of sol-gel processing.* . 1990.

78. Sanchez, C., et al., *Designed Hybrid Organic/Inorganic Nanocomposites from Functional Nanobuilding Blocks.* Chemistry of Materials, 2001. **13**(10): p. 3061-3083.

79. Livage, J., M. Henry, and C. Sanchez, *Sol-gel chemistry of transition metal oxides.* Progress in Solid State Chemistry, 1988. **18**(4): p. 259-341.

80. Wen, J. and G.L. Wilkes, *Organic/Inorganic Hybrid Network Materials by the Sol 鉴扦el Approach.* Chemistry of Materials, 1996. **8**(8): p. 1667-1681.

81. Zhao, D., et al., *Triblock Copolymer Syntheses of Mesoporous Silica with Periodic 50 to 300 Angstrom Pores.* Science, 1998. **279**(5350): p. 548-552.

82. Zhao, D., et al., *Nonionic Triblock and Star Diblock Copolymer and Oligomeric Surfactant Syntheses of Highly Ordered, Hydrothermally Stable, Mesoporous Silica Structures.* Journal of the American Chemical Society, 1998. **120**(24): p. 6024-6036.

83. Bates, F.S. and G.H. Fredrickson, *Block Copolymers---Designer Soft Materials.* Physics Today, 1999. **52**(2): p. 32-38.

84. Hamley, I.W., et al., *Aqueous mesophases of block copolymers of ethylene oxide and 1,2-butylene oxide.* Physical Chemistry Chemical Physics, 2001. **3**(15): p. 2972-2980.

85. Stephan Foster and Markus Antonietti, *Amphiphilic Block Copolymers in Structure-Controlled Nanomaterial Hybrids.* Advanced Materials, 1998. **10**(3): p. 195-217.

86. Flodstrom, K. and V. Alfredsson, *Influence of the block length of triblock copolymers on the formation of mesoporous silica.* Microporous and Mesoporous Materials, 2003. **59**(2-3): p. 167-176.

87. Schmidt-Winkel, P., et al., *Mesocellular Siliceous Foams with Uniformly Sized Cells and Windows.* Journal of the American Chemical Society, 1998. **121**(1): p. 254-255.

88. Tian, B., et al., *Syntheses of High-Quality Mesoporous Materials Directed by Blends of Nonionic Amphiphiles under Nonaqueous Conditions.* Journal of Solid State Chemistry, 2002. **167**(2): p. 324-329.

89. Beck, J.S., et al., *A new family of mesoporous molecular sieves prepared with liquid crystal templates.* Journal of the American Chemical Society, 2002. **114**(27): p. 10834-10843.

90. Attard, G.S., J.C. Glyde, and C.G. Goltner, *Liquid-crystalline phases as templates for the synthesis of mesoporous silica.* Nature, 1995. **378**(6555): p. 366-368.

91. Christine G. Goltner and Markus Antonietti, *Mesoporous materials by templating of liquid crystalline phases.* Advanced Materials, 1997. **9**(5): p. 431-436.

92. Firouzi, A., et al., *Cooperative organization of inorganic-surfactant and biomimetic assemblies.* Science, 1995. **267**(5201): p. 1138-1143.

93. Monnier, A., et al., *Cooperative Formation of Inorganic-Organic Interfaces in the Synthesis of Silicate Mesostructures.* Science, 1993. **261**(5126): p. 1299-1303.

94. Boissiere, C., et al., *A New Synthesis of Mesoporous MSU-X Silica Controlled by a Two-Step Pathway.* Chemistry of Materials, 2000. **12**(10): p. 2902-2913.

95. Boissiere, C., et al., *Design, Synthesis, and Properties of Inorganic and Hybrid Thin Films Having Periodically Organized Nanoporosity鈥?AU - Sanchez, Cl茅ment.* Chemistry of Materials, 2008. **20**(3): p. 682-737.

96. Anderson, M.T., et al., *Surfactant-Templated Silica Mesophases Formed in Water:Cosolvent Mixtures.* Chemistry of Materials, 1998. **10**(1): p. 311-321.

97. Ogawa, M., *Formation of Novel Oriented Transparent Films of Layered Silica-Surfactant Nanocomposites.* Journal of the American Chemical Society, 1994. **116**(17): p. 7941-7942.

98. Yang, H., N. Coombs, and G.A. Ozin, *Morphogenesis of shapes and surface patterns in mesoporous silica.* Nature, 1997. **386**(6626): p. 692-695.

99. C. Jeffrey Brinker, et al., *Evaporation-Induced Self-Assembly: Nanostructures Made Easy.* Advanced Materials, 1999. **11**(7): p. 579-585.

100. Grosso, D., et al., *Two-Dimensional Hexagonal Mesoporous Silica Thin Films Prepared from Block Copolymers: Detailed Characterization and Formation Mechanism.* Chemistry of Materials, 2001. **13**(5): p. 1848-1856.

101. Nishiyama, N., et al., *Vapor-Phase Synthesis of Mesoporous Silica Thin Films.* Chemistry of Materials, 2003. **15**(4): p. 1006-1011.

102. Sayari, A., et al., *Characterization of Large-Pore MCM-41 Molecular Sieves Obtained via Hydrothermal Restructuring.* Chemistry of Materials, 1997. **9**(11): p. 2499-2506.

103. Muth, O., C. Schellbach, and M. Froba, *Triblock copolymer assisted synthesis of periodic mesoporous organosilicas (PMOs) with large pores.* Chemical Communications, 2001(19): p. 2032-2033.

104. Cho, E.-B., K.-W. Kwon, and K. Char, *Mesoporous Organosilicas Prepared with PEO-Containing Triblock Copolymers with Different Hydrophobic Moieties.* Chemistry of Materials, 2001. **13**(11): p. 3837-3839.

105. Zhu, H., et al., *Periodic large mesoporous organosilicas from lyotropic liquid crystal polymer templates.* Chemical Communications, 2001(24): p. 2568-2569.

106. Matos, J.R., et al., *Periodic Mesoporous Organosilica with Large Cagelike Pores.* Chemistry of Materials, 2002. **14**(5): p. 1903-1905.

107. Abdelhamid Sayari, et al., *New Approaches to Pore Size Engineering of Mesoporous Silicates.* Advanced Materials, 1998. **10**(16): p. 1376-1379.

108. Blin, J.L. and B.L. Su, *Tailoring Pore Size of Ordered Mesoporous Silicas Using One or Two Organic Auxiliaries as Expanders.* Langmuir, 2002. **18**(13): p. 5303-5308.

109. Ryan, K.M., et al., *Control of Pore Morphology in Mesoporous Silicas Synthesized from Triblock Copolymer Templates.* Langmuir, 2002. **18**(12): p. 4996-5001.

110. Burleigh, M.C., et al., *Synthesis of Periodic Mesoporous Organosilicas with Block Copolymer Templates.* Chemistry of Materials, 2001. **13**(12): p. 4411-4412.

111. Wan, Y., Y. Shi, and D. Zhao, *Designed synthesis of mesoporous solids via nonionic-surfactant-templating approach.* Chemical Communications, 2007(9): p. 897-926.

112. Ryoo, R., et al., *Block-Copolymer-Templated Ordered Mesoporous Silica: Array of Uniform Mesopores or Mesopore/Micropore Network?* The Journal of Physical Chemistry B, 2000. **104**(48): p. 11465-11471.

113. Urade, V.N., et al., *Controlling Interfacial Curvature in Nanoporous Silica Films Formed by Evaporation-Induced Self-Assembly from Nonionic Surfactants. II. Effect of Processing Parameters on Film Structure.* Langmuir, 2007. **23**(8): p. 4268-4278.

114. Bollmann, L., V.N. Urade, and H.W. Hillhouse, *Controlling Interfacial Curvature in Nanoporous Silica Films Formed by Evaporation-Induced Self-Assembly from Nonionic Surfactants. I. Evolution of Nanoscale Structures in Coating Solutions.* Langmuir, 2007. **23**(8): p. 4257-4267.

115. Klotz, M., et al., *Synthesis conditions for hexagonal mesoporous silica layers.* Journal of Materials Chemistry, 2000. **10**(3): p. 663-669.

116. Alberius, P.C.A., et al., *General Predictive Syntheses of Cubic, Hexagonal, and Lamellar Silica and Titania Mesostructured Thin Filmss.* Chemistry of Materials, 2002. **14**(8): p. 3284-3294.

117. Grosso, D., et al., *An in Situ Study of Mesostructured CTAB鋯扮ilica Film Formation during Dip Coating Using Time-Resolved SAXS and Interferometry Measurements.* Chemistry of Materials, 2002. **14**(2): p. 931-939.

118. Cagnol, F., et al., *Humidity-controlled mesostructuration in CTAB-templated silica thin film processing. The existence of a modulable steady state.* Journal of Materials Chemistry, 2003. **13**(1): p. 61-66.

119. Eggiman, B.W., J.D. Kowalski, and H.W. Hillhouse, *Order and Orientation Control of Mesoporous Silica Films on Conducting Gold Substrates Formed by Dip-Coating and Self-Assembly: A Grazing Angle of Incidence Small-Angle X-ray Scattering and Field Emission Scanning Electron Microscopy Study鈥?AU - Tate, Michael P.* Langmuir, 2005. **21**(22): p. 10112-10118.

120. Gibaud, A., et al., *Evaporation-Controlled Self-Assembly of Silica Surfactant Mesophases.* The Journal of Physical Chemistry B, 2003. **107**(25): p. 6114-6118.

121. Smarsly, B., et al., *Quantitative SAXS Analysis of Oriented 2D Hexagonal Cylindrical Silica Mesostructures in Thin Films Obtained from Nonionic Surfactants.* Langmuir, 2005. **21**(9): p. 3858-3866.

122. Takahashi, H., et al., *Catalytic Activity in Organic Solvents and Stability of Immobilized Enzymes Depend on the Pore Size and Surface Characteristics of Mesoporous Silica.* Chemistry of Materials, 2000. **12**(11): p. 3301-3305.

123. Han, Y.-J., G.D. Stucky, and A. Butler, *Mesoporous Silicate Sequestration and Release of Proteins.* Journal of the American Chemical Society, 1999. **121**(42): p. 9897-9898.

124. Lai, C.-Y., et al., *A Mesoporous Silica Nanosphere-Based Carrier System with Chemically Removable CdS Nanoparticle Caps for Stimuli-Responsive Controlled*

*Release of Neurotransmitters and Drug Molecules.* Journal of the American Chemical Society, 2003. **125**(15): p. 4451-4459.

125. Slowing, I., B.G. Trewyn, and V.S.Y. Lin, *Effect of Surface Functionalization of MCM-41-Type Mesoporous Silica Nanoparticles on the Endocytosis by Human Cancer Cells.* Journal of the American Chemical Society, 2006. **128**(46): p. 14792-14793.

126. Supratim Giri, et al., *Stimuli-Responsive Controlled-Release Delivery System Based on Mesoporous Silica Nanorods Capped with Magnetic Nanoparticles13.* Angewandte Chemie International Edition, 2005. **44**(32): p. 5038-5044.

127. Qiao, S.Z., et al., *Synthesis and Bio-adsorptive Properties of Large-Pore Periodic Mesoporous Organosilica Rods.* Chemistry of Materials, 2005. **17**(24): p. 6172-6176.

128. Hartmann, M., *Ordered Mesoporous Materials for Bioadsorption and Biocatalysis.* Chemistry of Materials, 2005. **17**(18): p. 4577-4593.

129. Davis, M.E., *Ordered porous materials for emerging applications.* Nature, 2002. **417**(6891): p. 813-821.

130. Yiu, H.H.P., et al., *Size selective protein adsorption on thiol-functionalised SBA-15 mesoporous molecular sieve.* Physical Chemistry Chemical Physics, 2001. **3**(15): p. 2983-2985.

131. Chong, A.S.M. and X.S. Zhao, *Design of large-pore mesoporous materials for immobilization of penicillin G acylase biocatalyst.* Catalysis Today, 2004. **93-95**: p. 293-299.

132. Jie Fan, et al., *Cubic Mesoporous Silica with Large Controllable Entrance Sizes and Advanced Adsorption Properties13.* Angewandte Chemie International Edition, 2003. **42**(27): p. 3146-3150.

133. Yiu, H.H.P. and P.A. Wright, *Enzymes supported on ordered mesoporous solids: a special case of an inorganic-organic hybrid.* Journal of Materials Chemistry, 2005. **15**(35-36): p. 3690-3700.

134. Shui, W., et al., *Nanopore-Based Proteolytic Reactor for Sensitive and Comprehensive Proteomic Analyses.* Analytical Chemistry, 2006. **78**(14): p. 4811-4819.

135. Sayari, A. and S. Hamoudi, *Periodic Mesoporous Silica-Based Organic鋆扦norganic Nanocomposite Materials.* Chemistry of Materials, 2001. **13**(10): p. 3151-3168.

136. Avnir, D., et al., *Recent bio-applications of sol-gel materials.* Journal of Materials Chemistry, 2006. **16**(11): p. 1013-1030.

137. Maschmeyer, T., et al., *Heterogeneous catalysts obtained by grafting metallocene complexes onto mesoporous silica.* Nature, 1995. **378**(6553): p. 159-162.

138. Liu, J., et al., *Structural Relation Properties of Hydrothermally Stable Functionalized Mesoporous Organosilicas and Catalysis.* The Journal of Physical Chemistry B, 2005. **109**(25): p. 12250-12256.

139. Wan, Y., et al., *Ordered Mesoporous Pd/Silica鋆扒arbon as a Highly Active Heterogeneous Catalyst for Coupling Reaction of Chlorobenzene in Aqueous Media.* Journal of the American Chemical Society, 2009. **131**(12): p. 4541-4550.

140. McCullen, S.B., et al., *A New Family of Mesoporous Molecular Sieves*, in *Access in Nanoporous Materials*. 2002. p. 1-11.

141. Tanev, P.T. and T.J. Pinnavaia, *Mesoporous Silica Molecular Sieves Prepared by Ionic and Neutral Surfactant Templating: A Comparison of Physical Properties.* Chemistry of Materials, 1996. **8**(8): p. 2068-2079.

142. Rossinyol, E., et al., *Nanostructured metal oxides synthesized by hard template method for gas sensing applications.* Sensors and Actuators B: Chemical, 2005. **109**(1): p. 57-63.

143. Scott, B.J., G. Wirnsberger, and G.D. Stucky, *Mesoporous and Mesostructured Materials for Optical Applications.* Chemistry of Materials, 2001. **13**(10): p. 3140-3150.

144. Yamada, T., et al., *Experimental and Theoretical NOx Physisorption Analyses of Mesoporous Film (SBA-15 and SBA-16) Constructed Surface Photo Voltage (SPV) Sensor.* The Journal of Physical Chemistry B, 2004. **108**(35): p. 13341-13346.

145. Vallet-Regi, M., et al., *A New Property of MCM-41: Drug Delivery System.* Chemistry of Materials, 2000. **13**(2): p. 308-311.

146. Deere, J., et al., *Mechanistic and Structural Features of Protein Adsorption onto Mesoporous Silicates.* The Journal of Physical Chemistry B, 2002. **106**(29): p. 7340-7347.

147. Etzioni, R., et al., *The case for early detection.* Nat Rev Cancer, 2003. **3**(4): p. 243-252.

148. Glatter, O. and O. Kratky, *Small Angle X-ray Scattering.* 1982.

149. Gregg, S.J. and K.S.W. Sing, *Adsorption, surface area and porosity.* 1982.

150. Rouquerol, F. and J.S. Rouquerol, K. , *Adsorption by Powders and Porous Solids;* . 1999.

151. Barrett, E.P., L.G. Joyner, and P.P. Halenda, *The Determination of Pore Volume and Area Distributions in Porous Substances. I. Computations from Nitrogen Isotherms.* Journal of the American Chemical Society, 1951. **73**(1): p. 373-380.

152. Papadopoulos, M.C., et al., *A novel and accurate diagnostic test for human African trypanosomiasis.* The Lancet, 2004. **363**(9418): p. 1358-1363.

153. Hye, A., et al., *Proteome-based plasma biomarkers for Alzheimer's disease.* Brain, 2006. **129**(11): p. 3042-3050.

154. Findeisen, P., et al., *Preanalytical Impact of Sample Handling on Proteome Profiling Experiments with Matrix-Assisted Laser Desorption/Ionization Time-of-Flight Mass Spectrometry.* Clin Chem, 2005. **51**(12): p. 2409-2411.

155. Seam, N., et al., *Quality Control of Serum Albumin Depletion for Proteomic Analysis.* Clin Chem, 2007. **53**(11): p. 1915-1920.

156. Bonk, T., et al., *Matrix-assisted Laser Desorption/Ionization Time-of-Flight Mass Spectrometry-based Detection of Microsatellite Instabilities in Coding DNA Sequences: A Novel Approach to Identify DNA-Mismatch Repair-deficient Cancer Cells.* Clin Chem, 2003. **49**(4): p. 552-561.

157. Maggie Merchant, S.R.W., *Recent advancements in surface-enhanced laser desorption/ionization-time of flight-mass spectrometry.* Electrophoresis, 2000. **21**(6): p. 1164-1177.

158. Fung, E.T. and C. Enderwick, *ProteinChip clinical proteomics: computational challenges and solutions. BioTechniques*, 2002. **81**(Suppl. 34): p. 40-41.

159. Issaq, H.J., et al., *The SELDI-TOF MS Approach to Proteomics: Protein Profiling and Biomarker Identification.* Biochemical and Biophysical Research Communications, 2002. **292**(3): p. 587-592.

160. Issaq, H.J., et al., *Peer Reviewed: SELDI-TOF MS for Diagnostic Proteomics.* Analytical Chemistry, 2003. **75**(7): p. 148 A-155 A.

161. Pusch, W., et al., *Mass spectrometry-based clinical proteomics.* Pharmacogenomics, 2003. **4**(4): p. 463-476.

162. Michael Karas, et. al., *Ionization in matrix-assisted laser desorption/ionization: singly charged molecular ions are the lucky survivors.* Journal of Mass Spectrometry, 2000. **35**(1): p. 1-12.

163. Cristina Sottani, M.F., Claudio Minoia,, *Matrix Performance in Matrix-assisted Laser Desorption/Ionization for Molecular Weight Determination in Sialyl and Non-sialyl Oligosaccharide Proteins.* Rapid Communications in Mass Spectrometry, 1997. **11**(8): p. 907-913.

164. Omar Belgacem, A.B., Katharina Pock, Djuro Josic, Chris Sutton, Andreas Rizzi, Gter Allmaier,, *Molecular mass determination of plasma-derived glycoproteins by ultraviolet matrix-assisted laser desorption/ionization time-of-flight mass*

*spectrometry with internal calibration.* Journal of Mass Spectrometry, 2002. **37**(11): p. 1118-1130.

165. Sekiya, S., Y. Wada, and K. Tanaka, *Derivatization for Stabilizing Sialic Acids in MALDI-MS.* Analytical Chemistry, 2005. **77**(15): p. 4962-4968.

166. Gilar, M., E.S.P. Bouvier, and B.J. Compton, *Advances in sample preparation in electromigration, chromatographic and mass spectrometric separation methods.* Journal of Chromatography A, 2001. **909**(2): p. 111-135.

167. Kiernan, U.A., et al., *High-Throughput Analysis of Hemoglobin from Neonates Using Matrix-assisted Laser Desorption/Ionization Time-of-Flight Mass Spectrometry.* Clin Chem, 2002. **48**(6): p. 947-949.

168. Ya Jin, T.M., *Direct targeting of human plasma for matrix-assisted laser desorption/ionization and analysis of plasma proteins by time of flight-mass spectrometry.* Electrophoresis, 2005. **26**(14): p. 2823-2834.

169. Hortin, G.L., B. Meilinger, and S.K. Drake, *Size-Selective Extraction of Peptides from Urine for Mass Spectrometric Analysis.* Clin Chem, 2004. **50**(6): p. 1092-1095.

170. Ning Tang, P.T., Scot R. Weinberger,, *Current developments in SELDI affinity technology.* Mass Spectrometry Reviews, 2004. **23**(1): p. 34-44.

171. Petricoin, E.F. and L.A. Liotta, *SELDI-TOF-based serum proteomic pattern diagnostics for early detection of cancer.* Current Opinion in Biotechnology, 2004. **15**(1): p. 24-30.

172. Aivado, M., et al., *Optimization and evaluation of surface-enhanced laser desorption/ionization time-of-flight mass spectrometry (SELDI-TOF MS) with reversed-phase protein arrays for protein profiling.* Clinical Chemistry and Laboratory Medicine, 2005. **43**(2): p. 133-140.

173. Villanueva, J., et al., *Serum Peptide Profiling by Magnetic Particle-Assisted, Automated Sample Processing and MALDI-TOF Mass Spectrometry.* Analytical Chemistry, 2004. **76**(6): p. 1560-1570.

174. Baumann, S., et al., *Standardized Approach to Proteome Profiling of Human Serum Based on Magnetic Bead Separation and Matrix-Assisted Laser Desorption/Ionization Time-of-Flight Mass Spectrometry.* Clin Chem, 2005. **51**(6): p. 973-980.

175. Wong, J.W.H., G. Cagney, and H.M. Cartwright, *SpecAlign--processing and alignment of mass spectra datasets.* Bioinformatics, 2005. **21**(9): p. 2088-2090.

176. Wong, J.W.H., C. Durante, and H.M. Cartwright, *Application of Fast Fourier Transform Cross-Correlation for the Alignment of Large Chromatographic and Spectral Datasets.* Analytical Chemistry, 2005. **77**(17): p. 5655-5661.

177. Conlisk, A., et al., *Biomolecular Transport Through Hemofiltration Membranes.* Annals of Biomedical Engineering, 2009. **37**(4): p. 722-736.

178. Leili, J., M.R.R. Tabar, and S. Muhammad, *Molecular simulation of protein dynamics in nanopores. II. Diffusion.* The Journal of Chemical Physics, 2009. **130**(8): p. 085105.

179. Luchini, A., et al., *Smart Hydrogel Particles: Biomarker Harvesting: One-Step Affinity Purification, Size Exclusion, and Protection against Degradation.* Nano Letters, 2007. **8**(1): p. 350-361.

180. Banks, R.E., et al., *Influences of Blood Sample Processing on Low-Molecular-Weight Proteome Identified by Surface-Enhanced Laser Desorption/Ionization Mass Spectrometry.* Clin Chem, 2005. **51**(9): p. 1637-1649.

181. Ransohoff, D.F., *Lessons from Controversy: Ovarian Cancer Screening and Serum Proteomics.* J. Natl. Cancer Inst., 2005. **97**(4): p. 315-319.

182. Jie Fan, et al., *Mesoporous Silica Nanoreactors for Highly Efficient Proteolysis.* Chemistry - A European Journal, 2005. **11**(18): p. 5391-5396.

183. Anderson, N.L. and N.G. Anderson, *The human plasma proteome: History, character, and diagnostic prospects.* Mol Cell Proteomics, 2002: p. R200007-MCP200.

184. Eisen, M.B., et al., *Cluster analysis and display of genome-wide expression patterns.* Proceedings of the National Academy of Sciences of the United States of America, 1998. **95**(25): p. 14863-14868.

185. Schubert, U., N. Huesing, and A. Lorenz, *Hybrid Inorganic-Organic Materials by Sol-Gel Processing of Organofunctional Metal Alkoxides.* Chemistry of Materials, 2002. **7**(11): p. 2010-2027.

186. Loy, D.A. and K.J. Shea, *Bridged Polysilsesquioxanes. Highly Porous Hybrid Organic-Inorganic Materials.* Chemical Reviews, 2002. **95**(5): p. 1431-1442.

187. Corriu, R., *Les materiaux hybrides monophases organique-inorganique.* Comptes Rendus de l'Academie des Sciences - Series IIC - Chemistry, 1998. **1**(2): p. 83-89.

188. C. Sanchez, et al., *Optical Properties of Functional Hybrid Organic-Inorganic Nanocomposites.* Advanced Materials, 2003. **15**(23): p. 1969-1994.

189. Moller, K. and T. Bein, *Inclusion Chemistry in Periodic Mesoporous Hosts.* Chemistry of Materials, 1998. **10**(10): p. 2950-2963.

190. A. Stein, B. J. Melde, and R. C. Schroden, *Hybrid Inorganic-Organic Mesoporous Silicates Nanoscopic Reactors Coming of Age.* Advanced Materials, 2000. **12**(19): p. 1403-1419.

191. Brunel, D., et al., *MCM-41 type silicas as supports for immobilized catalysts*, in *Studies in Surface Science and Catalysis*. 1995, Elsevier. p. 173-180.

192. Brunel, D., *Functionalized micelle-templated silicas (MTS) and their use as catalysts for fine chemicals.* Microporous and Mesoporous Materials, 1999. **27**(2-3): p. 329-344.

193. Brunel, D., et al., *New trends in the design of supported catalysts on mesoporous silicas and their applications in fine chemicals.* Catalysis Today, 2002. **73**(1-2): p. 139-152.

194. Lim, M.H., C.F. Blanford, and A. Stein, *Synthesis and Characterization of a Reactive Vinyl-Functionalized MCM-41: Probing the Internal Pore Structure by a Bromination Reaction.* Journal of the American Chemical Society, 1997. **119**(17): p. 4090-4091.

195. Mercier, L. and T.J. Pinnavaia, *Direct Synthesis of Hybrid Organic-Inorganic Nanoporous Silica by a Neutral Amine Assembly Route: Structure-Function Control by Stoichiometric Incorporation of Organosiloxane Molecules.* Chemistry of Materials, 1999. **12**(1): p. 188-196.

196. Lu, Y., et al., *Evaporation-Induced Self-Assembly of Hybrid Bridged Silsesquioxane Film and Particulate Mesophases with Integral Organic Functionality.* Journal of the American Chemical Society, 2000. **122**(22): p. 5258-5261.

197. Asefa, T., et al., *Periodic mesoporous organosilicas with organic groups inside the channel walls.* Nature, 1999. **402**(6764): p. 867-871.

198. Inagaki, S., et al., *An ordered mesoporous organosilica hybrid material with a crystal-like wall structure.* Nature, 2002. **416**(6878): p. 304-307.

199. Soler-Illia, G.J.d.A.A., et al., *Chemical Strategies To Design Textured Materials: from Microporous and Mesoporous Oxides to Nanonetworks and Hierarchical Structures.* Chemical Reviews, 2002. **102**(11): p. 4093-4138.

200. C. M. Yang, et al., *Spin-on Mesoporous Silica Films with Ultralow Dielectric Constants, Ordered Pore Structures, and Hydrophobic Surfaces.* Advanced Materials, 2001. **13**(14): p. 1099-1102.

201. Chen, J.Y., et al., *Microstructure and Mechanical Properties of Surfactant Templated Nanoporous Silica Thin Films: Effect of Methylsilylation.* Journal of The Electrochemical Society, 2003. **150**(6): p. F123-F127.

202. Ji, X., et al., *Synthesis and Characterization of Functionalized Mesoporous Silica by Aerosol-Assisted Self-Assembly.* Chemistry of Materials, 2006. **18**(9): p. 2265-2274.

203. Feng, X., et al., *Functionalized Monolayers on Ordered Mesoporous Supports.* Science, 1997. **276**(5314): p. 923-926.

204. Vinu, A., K.Z. Hossain, and K. Ariga, *Recent Advances in Functionalization of Mesoporous Silica.* Journal of Nanoscience and Nanotechnology, 2005. **5**: p. 347-371.

205. Zhang, W.H., et al., *Synthesis and Characterization of Bifunctionalized Ordered Mesoporous Materials.* Advanced Functional Materials, 2004. **14**(6): p. 544-552.

206. Stein, A., B.J. Melde, and R.C. Schroden, *Hybrid Inorganic-Organic Mesoporous Silicates/Nanoscopic Reactors Coming of Age.* Advanced Materials, 2000. **12**(19): p. 1403-1419.

# Vita

Ye Hu attended Nankai High School, Tianjin, China. In 1995 he entered Lanzhou University in Gansu Privision, China. He received the degree of Bachelor of Science from Lanzhou University in June, 1999. During a couple of years he had his graduate study in Tsinghua University, Beijing, China. In September, 2003, he entered the Graduate School at The University of Texas at Austin. He obtained his Master Degree in Chemistry from the University of Texas at Austin in December, 2005. He joined the PhD program in the department of Biomedical Engineering at the University of Texas at Austin in 2006 and started working with Dr. Mauro Ferrari in the field of the application of nanotechnology in early diagnostics.

Permanent address: <1947 Creole Dr., Austin, TX 78727>

This dissertation was typed by the author.